Washington University in St. Louis
Washington University Open Scholarship

All Theses and Dissertations (ETDs)

January 2010

The Mechanisms and Roles of Neural Feedback Loops for Visual Processing

Debajit Saha
Washington University in St. Louis

Follow this and additional works at: https://openscholarship.wustl.edu/etd

Recommended Citation
Saha, Debajit, "The Mechanisms and Roles of Neural Feedback Loops for Visual Processing" (2010). *All Theses and Dissertations (ETDs)*. 307.
https://openscholarship.wustl.edu/etd/307

This Dissertation is brought to you for free and open access by Washington University Open Scholarship. It has been accepted for inclusion in All Theses and Dissertations (ETDs) by an authorized administrator of Washington University Open Scholarship. For more information, please contact digital@wumail.wustl.edu.

WASHINGTON UNIVERSITY IN ST. LOUIS
Department of Physics

Dissertation Examination Committee:
Ralf Wessel, Chair
Michael Ariel
Anders E. Carlsson
James G. Miller
Baranidharan Raman
Li Yang

THE MECHANISMS AND ROLES OF NEURAL FEEDBACK LOOPS FOR VISUAL PROCESSING

by

Debajit Saha

A dissertation presented to the
Graduate School of Arts and Sciences
of Washington University in Saint Louis
in partial fulfillment of the
requirements for the degree of
Doctor of Philosophy

December 2010
Saint Louis, Missouri

ABSTRACT OF THE DISSERTATION

The mechanisms and roles of neural feedback loops for visual processing

By

Debajit Saha

Doctor of Philosophy in Physics

Washington University in St. Louis, 2010

Professor Ralf Wessel, Chairperson

Feedback pathways are widely present in various sensory systems transmitting time-delayed and partly-processed information from higher to lower visual centers. Although feedback loops are abundant in visual systems, investigations focusing on the mechanisms and roles of feedback in terms of micro-circuitry and system dynamics have been largely ignored. Here, we investigate the cellular, synaptic and circuit level properties of a cholinergic isthmic neuron (Ipc) to understand the role of isthmotectal feedback loop in visual processing of red-ear turtles, *Trachemys scripta elegans*. Turtle isthmotectal complex contains two distinct nuclei, Ipc and Imc, which interact exclusively with the optic tectum, but are otherwise isolated from other brain areas. The cholinergic Ipc neurons receive topographic glutamatergic inputs from tectal SGP neurons and project back to upper tectal layers in a topographic manner while GABAergic Imc neurons, which also get inputs from the SGP neurons project back non-

topographically to both the tectum and Ipc nucleus. We have used an isolated eye-attached whole-brain preparation for our investigations of turtle isthmotectal feedback loop. We have investigated the cellular properties of the Ipc neurons by whole-cell blind-patch recordings and found that all Ipc neurons exhibit tonic firing responses to somatic current injections that are well-modeled by a leaky integrate-and-fire neuron with spike rate adaptation. Further investigations reveal that the optic nerve stimulations generate balanced excitatory and inhibitory synaptic currents in the Ipc neurons. We have also found that synaptic connection between the Imc to Ipc neuron is inhibitory. The visual response properties of the Ipc neurons to a range of computer-generated stimuli are investigated using extracellular recordings. We have found that the Ipc neurons have a localized excitatory receptive field and show stimulus selectivity and stimulus-size tuning. We also investigate lateral interactions in the Ipc neurons in response to multiple stimuli within the visual field. Finally, we quantify the oscillatory bursts observed in Ipc responses under visual stimulations.

Preface

Publication in progress: Chapter 5

Saha D, Morton D, Ariel M and Wessel R**.** Visual response properties of a cholinergic neuron in turtle nucleus isthmi. Recommended for publication on 07-20-2010 in J Comp Physiol A.

All experiments in this dissertation are done by me. David Morton has designed the visual stimulation technique for extracellular recordings. In chapter 3, the modeling is done with the collaboration of Dihui Lai. In Chapter 4, simulation of synaptic currents is done by David Morton.

ACKNOWLEDGEMENTS

I would like to take this opportunity to express my sincere gratitude to my parents, whose blessings and well-wishes have always been a treasure in my life and keep me going in difficult times.

I would like to acknowledge my advisor Prof. Ralf Wessel, who gave me the opportunity to work in neuroscience and guided me in each and every step of my research. Apart from broad knowledge in an interdisciplinary field, Ralf has the unique ability to communicate with students and to explain complex ideas in a simple manner from different perspectives. It has been a real pleasure to work with him.

I am thankful to Prof. Michael Ariel (Mickey) for the long time collaboration and his help in getting me started on my research. I would also like to thank Dr. Michael Jones and Dr. Michael Brown for their help in my project.

I would like to thank all of my colleagues, especially, Matt, David, Dihui and Jeff, who were of great support in every way during my stay in the group. I would also like to thank previous group members especially, Jing and Adam for showing me the way in lab and for extensive scientific discussions.

Finally, I would like to thank my wife Sudeshna for her support and patience during all these years.

TABLE OF CONTENTS

LIST OF FIGURES AND TABLES

Chapter 1

Chapter 2

Chapter 3

Chapter 4

Chapter 5

Chapter 6

Chapter 7

Chapter 8

Chapter 1

GENERAL INTRODUCTION

Vision is a complex process by which we perceive the world around us. We process different visual information by many different mechanisms such as, interpreting retinal images in their spatiotemporal context (Albright and Stoner 2002; Nieder 2002; Paradiso et al. 2005, 2006; Dellen et al. 2007, 2009), shifting attention (Boynton 2005; Knudsen 2007) and dynamic adaptation of receptive fields (Ringach et al. 1997; Wörgötter et al. 1998; Shapley et al. 2003). The visual information is processed at different levels of our brain, starting from the retina, where photoreceptors first convert the light energy to the electrical impulse, which is transmitted to the retinal ganglion cells (RGC) through the bipolar cells. The RGC axons from each eye coalesce together to form the optic nerve. In primate visual pathway, after the partial cross-over of the two optic nerves at optic chiasm, the largest group of optic fibers travels to the lateral geniculate nucleus (LGN) in thalamus. The neurons in LGN project to primary visual cortex (or V1), which shares projections with higher cortical areas. This pathway is called feedforward pathway in vision comprising of neurons directly involved in transmission of stimuli in the visual field to the higher visual centers (i.e. cortex). Although the brain gathers all visual information entirely from the RGC inputs, the process of signal flow in our brain is not unidirectional. Rather, the feedback pathways which transmit time-delayed and partially processed visual information from higher to lower visual centers dominate the feedforward pathways at different levels of visual processing (Bullier 2006). For example, in

striate cortex, the ascending LGN input terminals are outnumbered by the descending pathway terminals from higher cortical areas. Similarly, the amount of cortical input back to the thalamus is much higher compared to the direct retinal inputs to it. Retina itself consists of a complex network of feedback loops dominated by horizontal cells, which synapses between photoreceptors and bipolar cells. Given such prominence of feedback networks in different levels of central nervous system, it can be safely said that the feedback represents a crucial component in vision (Martin 2002; Tsodyks and Gilbert 2004; Bullier 2006).

In general, two major visual pathways from retina to the telencephalon are present in all land animals (amniotes), i.e., reptiles, birds, and mammals. The lemnothalamic pathway starts from retina, reaches an area of the telencephalon via retino-recipient dorsal thalamic (lemnothalamic) nucleus (Fig. 1.1a). The collothalamic pathway extends from the retina to the retino-recipient midbrain to the dorsal thalamic (collothalamic) nucleus to a different area of the telencephalon (Fig. 1.1a, b). Although these two pathways interact with each other at different levels, in different species, there are distinct differences between these two pathways in strength and functional groups of the RGC inputs represented (Giolli and Towns 1980, Leamey et al. 2008). For example, in carnivores and primates the lemnothalamic pathway is predominant as lateral geniculus receives more RGC synapses than the superior colliculus (SC), which is a retino-recipient midbrain structure in the collothalamic pathway. In reptiles,

birds, and many mammalian species (e.g. mouse, rabbit), the collothalamic pathway is regarded as the primary visual pathway as optic tectum, OT (SC in mammals) receives more RGC synapses than the retinorecipient thalamic nucleus.

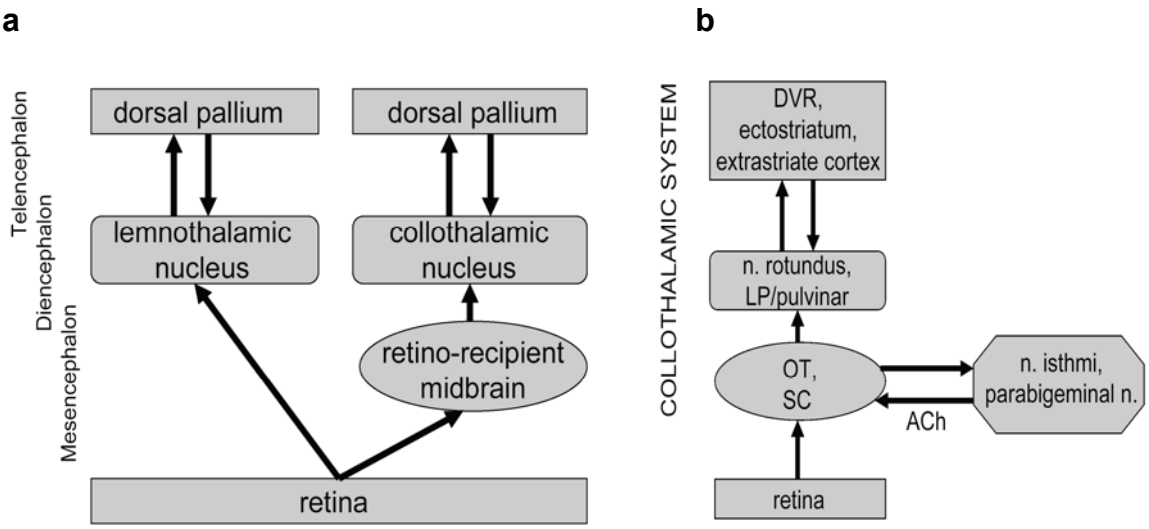

Figure 1.1 (a) Simplified schematic of the lemnothalamic (left) and collothalamic (right) visual pathways from the retina, the mesencephalon (optic tectum, superior colliculus), the diencephalon (dorsal thalamus), to separate areas of the dorsal pallium of the telencephalon. Interactions between the two areas of the dorsal pallium and possible feedback from the dorsal pallium to the retino-recipient midbrain are not shown. Modified after ch. 4 in McIlwain 1996. (b) Simplified schematic of the collothalamic visual pathway with reciprocally connected nucleus isthmi and optic tectum. For clarity, explicit names are listed for brain areas in the mesencephalon, the diencephalon, and the telencephalon for reptiles, birds, and mammals.

In the collothalamic pathway, in all amniotes, i.e. reptiles, birds, and mammals there exists an isthmic complex, which is reciprocally and topographically connected with the optic tectum (bird: Hunt and Kuenzle 1976; Hunt et al. 1977; Gunturkun and Remy 1990; Hellmann and Gunturkun 2001; Toemboel et al. 1995; Wang et al. 2004, 2006; reptiles: Sereno and Ulinski 1987; Powers and Reiner 1993; frog: Gruberg and Udin 1978; cat: Graybiel 1978; Sherk 1979b). The isthmic neurons form feedback loops with the optic tectum and contributes to the visual processing in collothalamic pathway by modulating tectal neurons (Wang et al. 1995; Wang et al. 2000; Winkowski and Gruberg 2002; Dudkin and Gruberg 2003; Wang 2003; Marin et al. 2007). In turtle, the isthmic complex also has the ability to modulate tectal neurons and to play an integral role in visual processing in the collothalamic pathway that starts from the retina, continues to the tectal SGC neurons, which innervate the ipsilateral nucleus rotundus and continues all the way to the dorsal ventricular ridge (DVR) of visual cortex (Reiner 1994; Belekhova et al. 2003).

Before diving into the details of isthmotectal feedback loop, it should be mentioned that the mammalian cortico-thalamic feedback loop is the most common feedback loop in vision research (Fig. 1.2). It has contributed significantly to the cellular and the large-scale circuit level investigations of the feedback circuitry (Steriade 2001; Alitto and Usrey 2003; Basso et al. 2005; Sillito et al. 2006; Sherman and Guillery 2006), but intricate cortico-thalamic and inter-

cortical connections (Fig. 1.2a) (Izhikevich and Edelman 2008) pose serious challenge to address the role of feedback in mammalian cortico-thalamic circuitry. Different attempts are made to address this challenge by maintaining complex circuits in a brain slice (Blumenfeld and McCormick 2000; MacLean et al. 2006) or investigating simpler feedback circuitry in non-mammalian species. Historically, non-mammalian animal models have helped neuroscientists to push forward the frontiers of knowledge when addressing fundamental questions in neuroscience (Marder 2002; Laurent 2006). Here, as an innovative alternative approach that integrates the cellular and circuit level studies of visual feedback loops, we propose to investigate the turtle isthmotectal feedback loop (Fig. 1.3), which shares design features with the mammalian cortico-thalamic loop (Fig. 1.2b, c) in a turtle whole-brain preparation. The eye-attached whole-brain preparation offers both conceptual and technical advantages for the study of isthmotectal circuitry allowing an investigation of the role of feedback in visual processing. Conceptual advantage is the Ipc and Imc neuron's exclusive connectivity with the optic tectum and isolation from all other brain areas (Sereno and Ulinski 1987). Technical advantage is obtaining whole-cell recordings of synaptic currents from Ipc neurons in response to visual stimulations in the contralateral retina in an intact feedback loop within the turtle eye-attached whole-brain preparation. Our study is also motivated by the previous investigations of visual stimulation combined with intracellular, extracellular and optical recordings, and pharmacological manipulations in the turtle eye-attached whole-brain preparation, which provided important insights into central visual

processing (Rosenberg and Ariel 1990, 1991; Fan et al. 1993; Ariel and Fan 1993; Fan et al. 1995; Senseman 1996; Kogo and Ariel 1997; Prechtl et al. 1997; Kogo et al. 1998; Martin et al. 1998; Rosenberg and Ariel 1998; Kogo and Ariel 1999; Senseman 1999; Senseman and Robbins 1999; Ariel and Kogo 2001; Senseman and Robbins 2002; Martin et al. 2003; Robbins and Senseman 2004; Ariel and Kogo 2005; Ariel and Johny 2007).

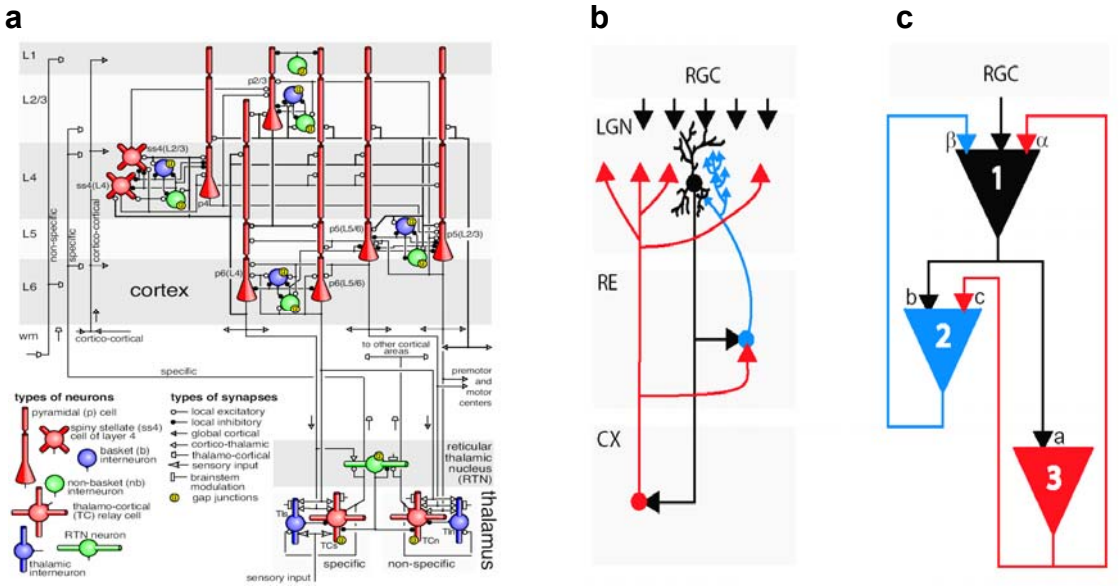

Figure 1.2 The cortico-thalamic feedback loop in mammals. (a) A simplified diagram of the microcircuitry of the cortical laminar structure and thalamic nuclei (Reprinted from Izhikevich and Edelman 2008). (b) A highly simplified schematic of the cortico-thalamic feedback loop in mammals. Note inputs from retinal ganglion cells (RGCs) are located at the top as black arrows. Numerous connections, including the intracortical pathways, are omitted in this schematic. RGC axons project to the thalamic lateral geniculate nucleus (LGN), which projects to the thalamic reticular nucleus (RE) and the cortex (CX), these in turn, feed back to the LGN. The CX also

projects to the RE (Modified after Sillito and Jones 2002). (c) At a higher level of abstraction, the cortico-thalamic feedback loops follow a characteristic topology, which consists of two feedback loops with a non-reciprocal lateral connection between them (Caudill et al. 2009).

The turtle isthmotectal system contains two cytoarchitectonically distinct isthmic nuclei; pars parvocellularis (Ipc) and pars magnocellularis (Imc), which receive sensory information from the ipsilateral optic tectum and project back to it (Sereno and Ulinski 1987; Powers and Reiner 1993). The radial narrow dendrites of the tectal SGP neurons overlap with the retinal axon terminals in superficial tectal layers (Kunzle and Schnyder 1984). The axons of the SGP neurons project to the ipsilateral Ipc and Imc nuclei. The Imc neurons have large, sparsely branched dendritic fields overlapped by local axon collaterals while distally their axons nontopographically innervate the deeper layers of the ipsilateral tectum and also the ipsilateral Ipc nucleus (Sereno and Ulinski 1987). The cholinergic Ipc neurons receive topographic inputs from the SGP neurons and nontopographic inputs from the Imc neurons. The Ipc neurons have medium-sized, elongated somata (~20 μm diameter) and flattened bipolar dendritic fields. The myelinated axons project topographically to the ipsilateral tectum without local axon branches. Each axon terminates as a compact swarm of ~3000 boutons within a cylinder of 150 μm in diameter and 400 μm tall, placed mainly in the upper tectal layers, where it spans less than 1% of the tectal surface (Sereno and Ulinski 1987). The topographically organized columnar Ipc

axon terminals spatially overlap with the RGC axons and the tectal neuron dendrites. Being a surface structure, the Ipc is accessible for whole-cell recordings and is readily identified for electrode placement or local drug/tracer injections.

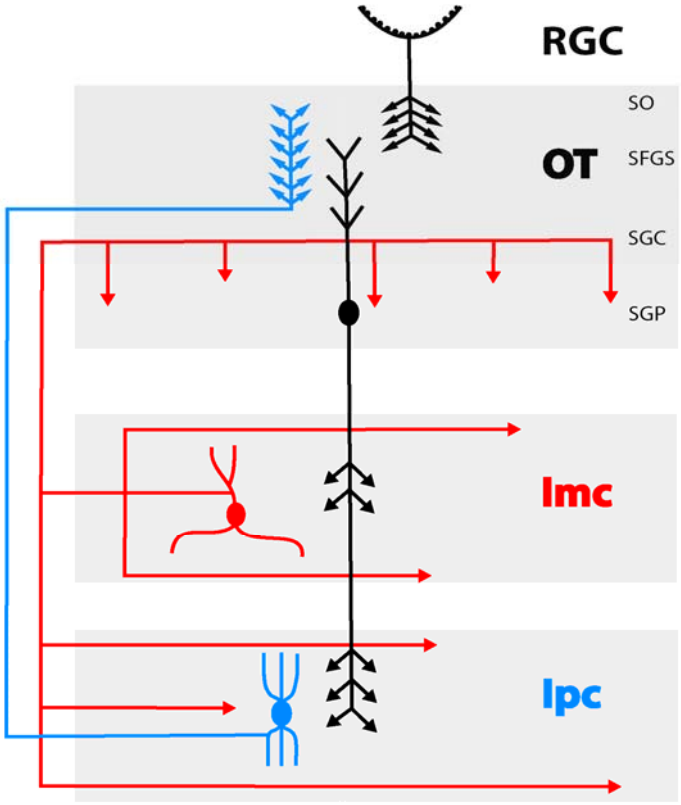

Figure 1.3 Schematic summary of the turtle isthmotectal system. Retinal ganglioin cell (RGC) neurons (black) project to the superficial layers (SO, SFGS) of the optic tectum (OT). Tectal neurons (black) with somata in the stratum griseum periventriculare (SGP) layer receive RGC inputs at their narrow apical dendrites reaching to the stratum fibrosum et griseum superficiale (SFGS) layer. The SGP neurons project to the nucleus isthmi pars parvocellularis (Ipc) and pars magnocellularis (Imc) neurons. The cholinergic Ipc neurons (blue) receive topographic input from SGP

neurons. The Ipc neurons have flattened bipolar dendritic fields and project topographically back to the ipsilateral tectum, where each Ipc axon terminates as a compact swarm of boutons in upper tectal layers. The GABAergic Imc neurons (red) have large, sparsely branched dendritic fields, have local axon collaterals, and project nontopographically to the Ipc and to deeper tectal layers (SGC, SGP).

The turtle isthmotectal circuitry shares many similarities with the birds. Apart from the Ipc and Imc nucleus, birds also have an isthmic nucleus called isthmi pars semilunaris (Slu). The somatodendritic morphology of the bird's Ipc and Imc neurons and the feedback loops they form with the tectal neurons are very similar to the turtle isthmic neurons (Sereno and Ulinski 1987; Wang et al. 2004, 2006). In birds, both the Ipc and Imc neurons receive retinotopic input from the optic tectum. The cholinergic Ipc neurons topographically project back to the tectum, while the Imc neurons feed back to the Ipc nucleus and to the tectum in a nontopographic manner (Wang et al. 2004, 2006). In fish, there is only one type of subnucleus to the isthmic structure, which receives input from the contralateral retina via optic tectum and shares topographic connections with the OT (Sakamoto et al. 1981; Dunn-Meynell and Sharma 1984; Xue et al. 2001). In case of amphibians, the isthmotectal connections vary between different species. In frog, the isthmic structure consists of only one type of neurons (Caudill et al. 2010), but different groups of isthmic neurons project to the contralateral and ipsilateral tectum (Grobstein et al. 1978; Gruberg and Udin 1978; Grobstein and

Comer 1983; Dudkin and Gruberg 1999; Dudkin et al. 2007), while in salamander, the most of the isthmic neurons project bilaterally (Wiggers 1998). In mammals, the superficial layer of the optic tectum (superior colliculus) receives cholinergic innervation from the parabigeminal nucleus (Graybiel 1978; Sherk 1979b; Hall et al. 1989), which is often cited as the homologue of the avian Ipc (Wang et al. 2006; Goddard et al. 2007). The PBN neurons are topographically connected with the ipsilateral superior colliculus (SC) and also project to contralateral SC.

From extensive investigations in numerous species, the isthmic neurons have emerged as a modulator of the tectal visual processing. In birds, the cholinergic (Sorenson et al. 1989; Medina and Reiner 1994) Ipc neurons have been implicated to maintain the spatial attention mechanisms by encoding the spatial location of objects (Maczko et al. 2006), and to gate the ascending collothalamic pathway to the nucleus rotundus (Marin et al. 2007). The role of isthmotectal circuitry with a negative and a positive feedback loop has been hypothesized as winner-take-all mechanism, which regulates sensitivities of the tectal neurons (Wang 2003; Wang et al. 2006; Maczko et al. 2006; Brandt and Wessel 2007). In frog, the nucleus isthmi neurons send cholinergic innervations to both the ipsilateral and contralateral tectum (Gruberg and Udin 1978; Winkowski and Gruberg 2002; Dudkin et al. 2007) and enhance calcium influx into the RGC axon terminals in tectum (Dudkin and Gruberg 2003). A localized electrolytic lesion to the nucleus isthmi causes a scotoma to the prey stimuli in specific areas of the

visual field (Winkowski and Gruberg 2002). In mammals, the parabigeminal nucleus provides the majority of cholinergic input to the superior colliculus (Tokunaga and Otani 1978; Mufson et al. 1986) and is involved in gaze control and spatial attention (Isa 2002; Cui and Malpeli 2003).

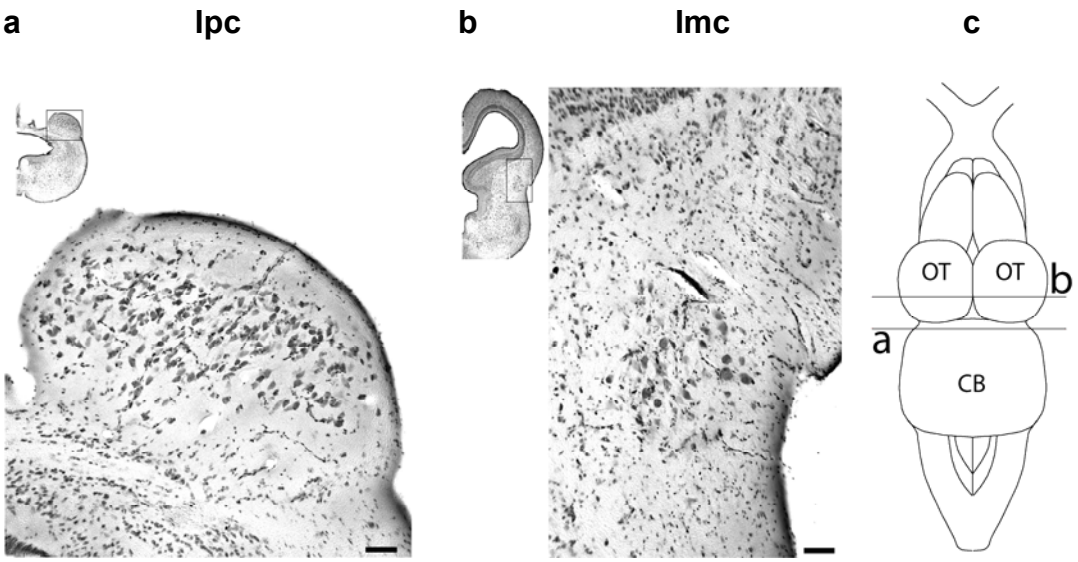

Figure 1.4 Transverse sections of a cresyl-violet-stained turtle brain. The large size and high density of (a) lpc and (b) lmc somata allows blind-patching in the isolated whole-brain preparations with high success rate (section thickness = 50 μm; scale bar = 100 μm). (c) The horizontal lines in the dorsal view indicate the locations of the transverse sections. Images are generated by Jason Weller.

The goal of this dissertation is to understand the mechanisms and the role of the feedback loops in visual processing using the turtle isthmotectal circuitry. To achieve this, both intracellular and extracellular recordings are conducted from

the cholinergic Ipc neurons in an eye-attached whole-brain preparation (Fig. 2.1). We chose to investigate the isthmotectal feedback loop using Ipc neurons because they are the main output neurons projecting back to the optic tectum. Being a surface structure and having close-packed, medium-sized neurons (Fig. 1.4a), the Ipc nucleus also provides an ideal setting for the blind-patch, extracellular and pharmacological investigations.

In **chapter 2** of this dissertation, the general methods used for the different experiments are described. This includes the dissection and recipe for the turtle eye-attached whole-brain preparation, set-up and techniques for the whole-cell blind-patch and extracellular recordings and a detailed description of generation and delivery of the visual stimuli. **Chapter 3** discusses the basic electrophysiological properties of the Ipc neurons. Principal component analysis on various electrophysiological properties of the Ipc neurons confirms that there is only one type of Ipc neuron in turtle Ipc nucleus. A model leaky integrate-and-fire neuron with spike-rate adaptation reproduces the Ipc response properties. **Chapter 4** discusses the synaptic connectivity of the Ipc neurons. Various experiments, including the Ipc responses to visual stimulations in contralateral eye and electrical stimulations of retina, optic nerve, tectal neurons and Imc neurons are performed to investigate the synaptic currents underlying the Ipc response properties. The Ipc neurons respond to the optic nerve stimulation with an excitatory and an inhibitory synaptic current, which are about equal in amplitude but different in time course. We have also found that the synaptic

connection between the Imc to Ipc is inhibitory. **Chapter 5** describes the visual response properties of the Ipc neurons. Extracellular recordings are achieved from the single-unit Ipc neurons responding to a range of computer-generated visual stimuli. We have found that the Ipc neurons respond best to the small moving dark stimuli on white background. We have also found that the excitatory receptive field of the Ipc neuron is small. The Ipc neurons show stimulus-size and speed tuning but no directional sensitivity. **Chapter 6** elaborates how multiple stimuli at different locations in the visual field modify the Ipc response properties. It has been found that a visual stimulus outside the excitatory receptive field (ERF) of the Ipc neuron non-linearly modulates the Ipc responses to a stimulus inside the ERF. In **chapter 7**, we show that the Ipc neurons respond to small stimuli with bursts of spikes. We quantify the Ipc bursting properties for wide-range of computer-generated visual stimuli. Finally, **Chapter 8** poses some open questions and provides future directions for this project.

References

Albright TD, Stoner GR (2002) Contextual influences on visual processing. Annu Rev Neurosci 25: 339–379.

Alitto HJ, Usrey WM (2003) Corticothalamic feedback and sensory processing. Current Opinion in Neurobiology 13: 440-445.

Ariel M, Fan TX (1993) Electrophysiological evidence for a bisynaptic retinocerebellar pathway. J Neurophysiol 69: 1323-1330.

Ariel M, Kogo N (2001) Direction tuning of inhibitory inputs to the turtle accessory optic system. J Neurophysiol 86: 2919-2930.

Ariel M, Kogo N (2005) Shunting inhibition in accessory optic system neurons. J Neurophysiol 93: 1959-1969.

Ariel M, Johny MB (2007) Analysis of quantal size of voltage responses to retinal stimulation in the accessory optic system. Brain Res 1157: 41-55.

Basso MA, Uhlrich D, Bickford ME (2005) Cortical function: A view from the thalamus. Neuron 45: 485-488.

Belekova M, Kenigfest N, Rio JP, Reperant J, Ward R, Vesselkin N, Karamian O (2003) Tectothalamic visual projections in turtles: Theirs cells of origin revealed by tracing methods. J Comp Neurology 457: 37-56.

Blumenfeld H, McCormick DA (2000) Corticothalamic inputs control the pattern of activity generated in thalamocortical networks. J Neurosci 20: 5153-5162.

Boynton GM (2005) Attention and visual perception. Current Opinion in Neurobiology 15: 465-469.

Brandt SF, Wessel R (2007) Winner-take-all selection in a neural system with delayed feedback. Biol Cybernetics 97: 221-228.

Bullier J (2006) What is fed back? In: *23 Problems in Systems Neuroscience*. Ed: Van Hemmen JL, Sejnowski TJ. Oxford University Press. pp.103-132.

Caudill MS, Brandt SF, Nussinov Z, Wessel R (2009) Intricate phase diagram of a prevalent visual circuit reveals universal dynamics, phase transitions, and resonances. Phys Rev E 80: 051923.

Caudill MS, Eggebrecht AT, Gruberg ER, Wessel R (2010) Electrophysiological properties of isthmic neurons in frogs revealed by in vitro and in vivo studies. J Comp Physiol 196: 249-262.

Cui H, Malpeli JG (2003) Activity in the parabigeminal nucleus during eye movements directed at moving and stationary targets. J Neurophysiol 89: 3128-3142.

Dellen BK, Clark JW, Wessel R (2007) The brain's view of the natural world in motion: Computing structure from function using directional Fourier transforms. Int J Mod Phys B 21: 2493-2504.

Dellen BK, Clark JW, Wessel R (2009) Contextual interaction in a generalized energy model of complex cells. Spat Vis 22: 301-24.

Dudkin EA, Gruberg ER (2003) Nucleus isthmi enhances calcium influx into optic nerve fiber terminals in Rana pipiens. Brain Res 969: 44-52.

Dudkin ES, Gruberg ER (1999) Relative number of cells projecting from contralateral and ipsilateral nucleus isthmi to loci in the optic tectum is

dependent on visuotopic location: horseradish peroxidase study in the leopard frog. J Comp Neurol 414: 212-216.

Dudkin EA, Sheffield JB, Gruberg ER (2007) Combining visual information from the two eyes: the relationship between isthmotectal cells that project to ipsilateral and to contralateral optic tectum using fluorescent retrograde labels in the frog, Rana pipiens. J Comp Neurol 502: 38-54.

Dunn-Meynell AA, Sharma SC (1984) Changes in the topographically organized connections between the nucleus isthmi and the optic tectum after partial tectal ablation in adult goldfish. J Comp Neurol 227:497–510.

Fan TX, Rosenberg AF, Ariel M (1993) Visual-response properties of units in the turtle cerebellar granular layer in vitro. J Neurophysiol 69: 1314-1322.

Fan TX, Weber AE, Pickard GE, Faber KM, Ariel M (1995) Visual responses and connectivity in the turtle pretectum. J Neurophysiol 73: 2507-2521.

Giolli RA, Towns LC (1980) A review of axon collateralization in the mammalian system. Brain Behav Evol 17: 364-390.

Goddard CA, Knudsen EI, Huguenard JR (2007) Intrinsic excitability of cholinergic neurons in the rat parabigeminal nucleus. J Neurophysiol 98: 3486-3493.

Graybiel AM (1978) A satellite system of the superior colliculus: the parabigeminal nucleus and its projection to the superficial collicular layers. Brain Res 145: 365-374.

Grobstein P, Comer C (1983) The nucleus isthmi as an intertectal relay for the ipsilateral oculotectal projection in the frog, Rana pipiens. J Compar Neurol 217: 54-74.

Grobstein P, Comer C, Hollyday M, Archer SM (1978)A crossed isthmo-tectal projection in Rana pipiens and its involvement in the ipsilateral visuotectal projection. Brain Research 156: 117-123.

Gruberg ER, Udin SB (1978) Topographic projections between the nucleus isthmi and the tectum of the frog, *Rana pipiens*. J Comp Neurol 179: 487-500.

Gunturkun O, Remy M (1990) The topographical projection of the nucleus isthmi pars parvocellularis (Ipc) onto the tectum opticum in the pigeon. Neurosci Lett 111: 18-22.

Hall WC, Fitzpatrcik D, Klatt LL, Raczkowski D (1989) Cholinergic innervation of the superior colliculus in the cat. J Comp Neurol 287: 495-514.

Hellmann B, Gunturkun O (2001) Structural organization of parallel information processing within the tectofugal visual system of the pigeon. J Comp Neurol 429: 94-112.

Hunt SP, Künzle H (1976) Observations on the projections and intrinsic organization of the pigeon optic tectum: an autoradiographic study based on anterograde and retrograde, axonal and dendritic flow. J Comp Neurol 170: 153-172.

Hunt SP, Streit P, Kunzle H, Cuenod M (1977) Characterization of the pigeon isthmo-tectal pathway by selective uptake and retrograde movement of

radioactive compounds and by Golgi-like horseradish peroxidase labeling. Brain Res 129: 197-212.

Isa T (2002) Intrinsic processing in the mammalian superior colliculus. Curr Opin Neurobiol 12: 668–677.

Izhikevich EM, Edelman GM (2008) Large-scale model of mammalian thalamocortical systems. PNAS 105: 3593-3598.

Knudsen EI (2007) Fundamental components of attention. Annu Rev Neurosci 30: 57-78.

Kogo N, Ariel M (1997) Membrane properties and monosynaptic retinal excitation of neurons in the turtle accessory optic system. J Neurophysiol 78: 614-627.

Kogo N, McGartland Rubio D, Ariel M (1998) Direction tuning of individual retinal inputs to the turtle accessory optic system. J Neurosci 18: 2673-2684.

Kogo N, Ariel M (1999) Response attenuation during coincident afferent excitatory inputs. J Neurophysiol 81: 2945-2955.

Kunzle H, Schnyder H (1984) The isthmus-tegmentum complex in the turtle and rat: a comparative analysis of its interconnections with the optic tectum. Exp Brain Res 56: 509-522.

Laurent G (2006) Shall we even understand the fly's brain? In: 23 problems in systems neuroscience. (VanHemmen JL, Sejnowski TJ, eds), pp. 3-21, Oxford University Press.

Leamey CA, Protti DA, Dreher B (2008) Comparative survey of the mammalian visual system with reference to the mouse. In: (Chalupa LM, Williams RW, eds) Eye, retina, and visual system of the mouse. MIT Press, pp. 35-60.

MacLean JN, Fenstermaker V, Watson BO, Yuste R (2006) A visual thalamocortical slice. Nat Methods 3: 129-34.

Maczko KA, Knudsen PF, Knudsen EI (2006) Auditory and visual space maps in the cholinergic nucleus isthmi pars parvocellularis in the barn owl. J Neurosci 26: 12799-12806.

Marder E (2002) Non-mammalian models for studying neural development and function. Nature 417: 318-321.

Marin G, Salas C, Sentic E, Rojas X, Letelier JC, Mpodozis J (2007) A cholinergic gating mechanism controlled by competitive interactions in the optic tectum of the pigeon. J Neurosci 27: 8112-8121.

Martin KAC (2002) Microcircuits in visual cortex. Current Opinion in Neurobiology 12: 418-425.

Martin J, Kogo N, Ariel M (1998) Morphology of basal optic tract terminals in the turtle, Pseudemys scripta elegans. J Comp Neurol 393: 267-283.

Martin J, Kogo N, Fan TX, Ariel M (2003) Morphology of the turtle accessory optic system. Visual Neurosci 20: 639-649.

McIlwain JT (1996) An introduction to the biology of vision. Cambridge University Press.

Medina L, Reiner A (1994) Distribution of choline acetyltransferase immunoreativity in the pigeon brain. Journal of Comparative Neurology 342: 497-537

Mufson EJ, Martin TL, Mash DC, Wainer BH, Mesulam MM (1986) Cholinergic projections from the parabigeminal nucleus (Ch8) to the superior colliculus in

the mouse: a combined analysis of horseradish peroxidase transport and choline acetyltransferase immunohistochemistry. Brain Res 370: 144–148.

Nieder A (2002) Seeing more than meets the eye: processing of illusory contours in animals. J Comp Physiol A 188: 249-260.

Paradiso M, MacEvoy SP, Blau S (2005) The importance of modulatory input for V1 activity and perception. Progress in Brain Research 149: 257-267.

Paradiso M, Blau S, Huang X, MacEvoy SP, Rossi AF, Shalev G (2006) Lightness, filling-in, and the fundamental role of context in visual perception. Progress in Brain Research 155: 109-123.

Powers AS, Reiner A (1993) The distribution of cholinergic neurons in the central nervous system of turtles. Brain Behav Evol 41: 326-345.

Prechtl JC, Cohen LB, Pesaran B, Mitra PP, Kleinfeld D (1997) Visual stimuli induce waves of electrical activity in turtle cortex. Proc Natl Acad Sci USA 94: 7621-7626.

Reiner A (1994) Laminar distribution of the cells of origin of ascending and descending tectofugal pathways in turtles: implications for the evolution of tectal lamination. Brain Beh Evol 43: 254-292.

Ringach DL, Hawken MJ, Shapley R (1997) Dynamics of orientation tuning in macaque primary visual cortex. Nature 387: 281-284.

Robbins KA, Senseman DM (2004) Extracting wave structure from biological data with application to responses in the turtle visual cortex. J Comput Neurosci 16: 267-298.

Rosenberg AF, Ariel M (1990) Visual-response properties of neurons in turtle basal optic nucleus in vitro. J Neurophysiol 63: 1033-1045.

Rosenberg AF, Ariel M (1991) Electrophysiological evidence for a direct projection of direction-sensitive retinal ganglion cells to the turtle's accessory optic system. J Neurophysiol 65: 1022-1033.

Rosenberg AF, Ariel M (1998) Analysis of direction-tuning curves of neurons in the turtle's accessory optic system. Exp Brain Res 121: 361-370.

Sakamoto N, Ito H, Ueda S (1981) Topographic projections between the nucleus isthmi and the optic tectum in a teleost, Navodon modestus. Brain Res 224: 225–234.

Senseman DM (1996) Correspondence between visually evoked voltage-sensitive dye signals and synaptic activity recorded in cortical pyramidal cells with intracellular microelectrodes. Visual Neurosci 13: 963-977.

Senseman DM (1999) Spatiotemporal structure of depolarization spread in cortical pyramidal cell populations evoked by diffuse retinal light flashes. Vis Neurosci 16: 65-79.

Senseman DM, Robbins KA (1999) Modal behavior of cortical neural networks during visual processing. J Neurosci 19: RC3.

Senseman DM, Robbins KA (2002) High-speed VSD imaging of visually evoked cortical waves: Decomposition into intra- and intercortical wave motions. J Neurophysiol 87: 1499-1514.

Sereno MI, Ulinski PS (1987) Caudal topographic nucleus isthmi and the rostral nontopographic nucleus isthmi in the turtle, *Pseudemys scripta*. J Comp Neurology 261: 319-346.

Shapley R, Hawken M, Ringach DL (2003) Dynamics of orientation selectivity in the primary visual cortex and the importance of cortical inhibition. Neuron 38: 689-699.

Sherk H (1979b) Connections and visual field mapping in cat's tectoparabigeminal circuit. J Neurophysiol 42: 1656-1668.

Sherman SM, Guillery RW (2006) Exploring the thalamus and its role in cortical function. MIT Press.

Sillito AM, Cudeiro J, Jones HE (2006) Always returning: feedback and sensory processing in visual cortex and thalamus. TINS 29: 307-316.

Sillito AM, Jones HE (2002) Corticothalamic interactions in the transfer of visual information. Phil Trans R Soc Lond B 357: 1739-1752.

Sorenson EM, Parkinson D, Dahl JL, & Chiappinelli VA (1989) Immunohistochemical localization of choline acetyltransferase in the chicken mesencephalon. Journal of Comparative Neurology 281: 641-657.

Steriade M (2001) The intact and sliced brain. MIT Press.

Tokunaga A, Otani K (1978). Neuronal organization of the corpus parabigeminum in the rat. Exp Neurol 58: 361–375.

Tombol T, Egedi G, Nemeth A (1995) Some data on connections of neurons of nuclei isthmi of the chicken. J Hirnforsch 36: 501-508.

Tsodyks M, Gilbert C (2004) Neural networks and perceptual learning. Nature 431: 775-781.

Wang SR (2003) The nucleus isthmi and dual modulation of the receptive field of tectal neurons in non-mammals. Brain Research Reviews 41: 13-25.

Wang SR, Wang YC, Frost BJ (1995) Magnocellular and parvocellular divisions of pigeon nucleus isthmi differentially modulate visual responses in the tectum. Exp Brain Res 104: 376-384.

Wang Y, Luksch H, Brecha NC, Karten HJ (2006) Columnar projections from the cholinergic nucleus isthmi to the optic tectum in chicks (*Gallus gallus*): A possible substrate for synchronizing tectal channels. J Comp Neurol 494: 7-35.

Wang Y, Major DE, Karten HJ (2004) Morphology and connections of nucleus isthmi pars magnocellularis in chicks (Gallus gallus). J Comp Neurol 469: 275-297.

Wang Y, Xiao J, Wang SR (2000) Excitatory and inhibitory receptive fields of tectal cells are differentially modified by magnocellular and parvocellular divisions of the pigeon nucleus isthmi. J Comp Physiol A 186: 505-511.

Wiggers W (1998) Isthmotectal connections in plethodontid salamanders. J Comp Neurol 395: 261-272.

Winkowski DE, Gruberg ER (2002) The representation of the ipsilateral eye in nucleus isthmi of the leopard frog, Rana pipiens. Visual Neurosci 19: 669-679.

Wörgötter F, Suder K, Zhao Y, Kerscher N, Eysel UT, Funke K (1998) State-dependent receptive field restructuring in the visual cortex. Nature 396: 165-168.

Xue HG, Yamamoto N, Yoshimoto M, Yang CY, Ito H (2001) Fiber connections of the nucleus isthmi in the carp (Cyprinus carpio) and tilapia (Oreochromis niloticus). Brain Behav Evol 58:185–204.

Chapter 2

GENERAL METHODS

We have used a turtle eye-attached whole-brain preparation to investigate the role of the isthmotectal feedback loop in vision. Both Kriegstein and Ariel (Kriegstein 1987; Rosenberg and Ariel 1988) developed the eye-attached whole-brain preparations for turtles (Fig. 2.1), which have the phenomenal ability to withstand anoxia (Belkin 1963; Sick et al. 1982; Lutz et al. 1985; Suarez 1988). Isolated whole-brain preparations offer the complete control of the bath medium's composition, including the absence of anesthetic, and the absence of vibrations associated with heartbeat and respiration, which facilitates recordings of synaptic currents due to stimulation of various parts of the whole-brain circuitry. These advantages of whole-brain preparation are shared with the brain slice preparation (Yamamoto and McIlwain 1966; Okamoto and Quastel 1973); the method of choice for cellular, synaptic, and local-circuit investigations (Dingledine 1984; Kettenmann and Grantyn 1992; Schurr and Rigor 1995). However, the isolated whole-brain preparation also maintains intact large-scale neuronal circuits (Llinas et al. 1981; Hounsgaard and Nicholson 1990). We have used extrinsic-circuit advantage of the isolated whole-brain preparation to its full extent for the *in vitro* study of central visual processing involving the eye and numerous interconnected brain areas (i.e. tectum, nucleus isthmi).

We have achieved both intracellular and extracellular recordings from the nucleus isthmi pars parvocellularis (Ipc) neurons in a turtle whole-brain

preparation. This chapter introduces the general methods for dissection, different recording and stimulation techniques. More details specific to different experiments will be addressed in the corresponding chapters.

2.1 Dissection and recipe for the turtle eye-attached whole-brain preparation

Adult red-ear turtles (Trachemys scripta elegans, 12-15 cm carapace length) were used in this study. Procedures used in this study were approved by the Washington University Institutional Animal Care and Use Committee and conform to the guidelines of the National Institutes of Health on the Care and Use of Laboratory Animals. Following cryanesthesia (> 15 min of hypothermia in ice water), rapid decapitation and then cannulation was performed on neck vasculature to infuse a cold saline to rinse out cranial blood. Within 20 minutes of decapitation, the telencephalon was removed. The dura surrounding the brain was removed, as was the pia covering lateral mesencephalon. For extracellular recordings, the eye was kept attached to the brainstem but freed from its orbits by cutting the conjunctiva and extraocular muscles. The eye was then hemisected and drained of its vitreous. For intracellular recordings, depending on the experiment, either the eye-cup or the optic nerve was kept attached to the brain stem. The preparation was then transferred to the superfusion chamber positioned on an air table with the eye-cup beneath a focusing lens. The preparation was bathed in physiological media (in mM; 85 NaCl, 2 KCl, 2 $MgCl_2$,

45 $NaHCO_3$, 20 D-glucose, 3 $CaCl_2$ bubbled with 95% O_2 and 5% CO_2), adjusted to pH 7.4 at room temperature.

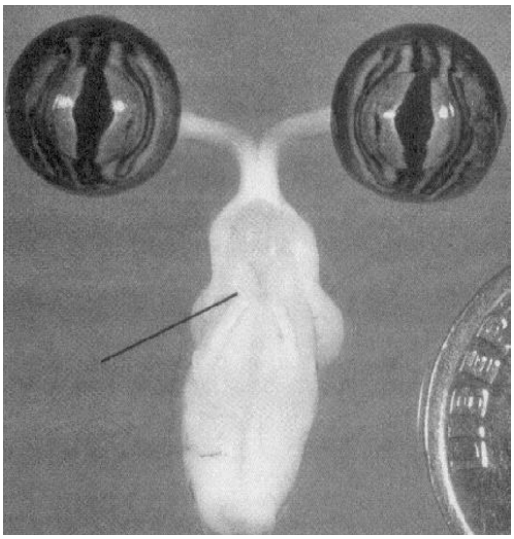

Figure 2.1 The turtle eye-attached whole-brain preparation. Ventral surface of *in vitro* turtle brain, eyes attached, telencephalon removed preparation placed next to a dime (18 mm diameter; Rosenberg and Ariel 1990). The black line points to the basal optic nucleus below the optic tectum (OT). The anterior half of each eye was removed prior to recording.

2.2 Set-up and techniques for the blind-patch whole-cell recordings

For blind-patch whole-cell recordings from nucleus isthmi par parvocellularis (Ipc) neurons, patch pipettes were fabricated on a Flaming-Brown horizontal puller (P-97, Sutter Instruments) from Corning #7052 glass capillary tubing (OD 1.5 mm, ID 0.86 mm) to yield 5 to 8 MΩ pipette resistance. The pipette solution for ruptured patch recordings contained (in mM) 117 $KMeSO_4$, 5 KCl, 5 NaCl, 1.2 $MgCl_2$, 10 HEPES, 5 EGTA; pH 7.3; with osmolarity 260 mOsMol. Pipette

solutions were filtered before use. Electrodes were advanced through the Ipc nucleus with a motorized micromanipulator (MP-285, Sutter Instruments) while maintaining a constant positive pressure. Electrode resistance was monitored continuously by applying short current pulses (Axoclamp 900 amplifier; -1.0 nA, 10 ms duration, 10 Hz). An increase of the resulting voltage pulse height (an increase in series resistance) was observed as the pipette tip approached a cell membrane. The pipette was advanced until the series resistance increased by about 10 MΩ. Current was then reduced to -0.1 nA and the positive pressure was reversed to a small negative pressure by pulling gently on a syringe plunger. This gentle suction was applied until the pipette formed a GΩ seal. Additional brief suction was applied to rupture the patch of membrane within the pipette. The pipette capacitance was compensated by the amplifier's circuitry and the access resistance was monitored. Analog data were low-pass filtered (4-pole Butterworth) at 1 kHz, digitized at 10 kHz, stored and analyzed on a PC equipped with a PCI-MIO-16E-4 and LabView software.

2.3 Electrical and optical stimulations for the whole-cell recordings

Electrical stimulations of the tectum and the retinal ganglion cell (RGC) axons were achieved by concentric, bipolar tungsten electrodes (tip diameter = 4 μm; core diameter = 76 μm). Current pulses of (100 - 200 μA) 0.5 ms duration were used for the stimulation.

Optical stimulations were achieved by computer-controlled LEDs (white). The light was projected to a specific location on the retina via a single optic fiber of 200 μm diameter, which generated a spot of light of similar dimension.

Optic nerve stimulations were achieved by a suction electrode (A-M systems) whose glass tip was fabricated such a way that it fitted the optic nerve tightly. Current pulses of 0.5 ms duration were used for the stimulation.

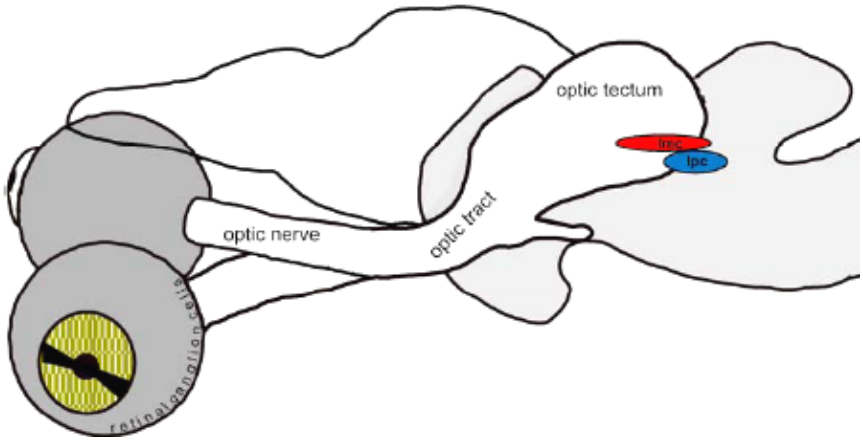

Figure 2.2 Side-view of the turtle eye-attached whole-brain preparation. Different parts of collothalamic visual pathway are labeled. The anterior half of each eye is removed prior to recording. This preparation allows spatiotemporal visual stimulation of the retina in the eyecup and electrical stimulation in tectum or optic tract while recording extracellularly or intracellularly from cholinergic lpc neurons (labeled in blue). Location of another isthmic nuclei; pars magnocellularis (lmc) shown in the figure (labeled in red).

2.4 Set-up and techniques for the extracellular recording

Extracellular recordings from the Ipc neurons were achieved by tungsten microelectrodes (A-M Systems, parylene-C insulated, 250 µm core diameter, 12 deg tapered tip) of 1 MΩ impedance (measured at 1 kHz, 0.1 nA *p-p* current). Since the Ipc nucleus is a surface structure, its location was identified by a characteristic protrusion just caudal of the optic tectum (Fig. 2.3). To find a responsive recording site, the microelectrode was advanced into the Ipc nucleus (100 - 400 µm) smoothly, using a hydraulic drive (FHC 50-12-9 Manual Drum Drive Unit) while the search stimulus (see SECTION 2.5.2) was focused on the retina of the contralateral eye-cup. Recordings were either made from a multiunit recording site (SNR > 4:1) or a single-unit recording site. The voltage traces were obtained using a differential AC amplifier (A-M Systems, Model 1800). The signal was passed through a 300 - 5000 Hz analog band pass filter and then sampled at 10 kHz (PCI-MIO-16E-4) using a LabView-controlled data acquisition system (National Instruments). Recordings were continuously monitored using an audio monitor (AM Systems 3300) and an oscilloscope (Tektronix TDS 210).

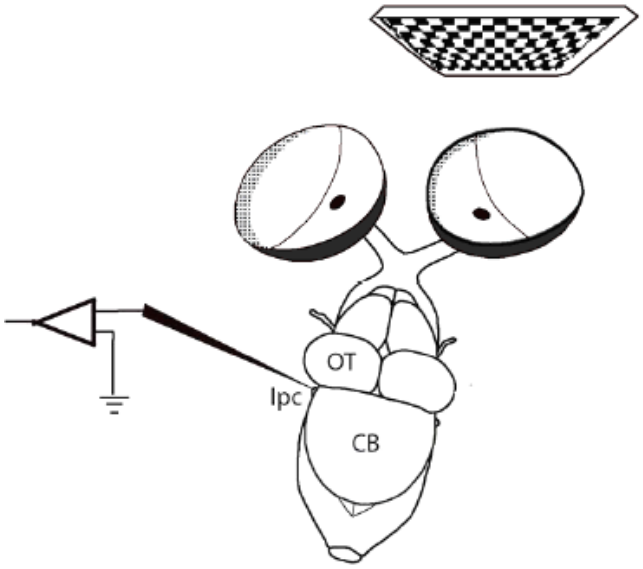

Figure 2.3 Schematic of a dorsal view of the turtle whole-brain preparation with the hemisected eye-cups attached and the telencephalon removed. The intracellular recording electrode is shown in the picture. Abbreviations: Ipc, nucleus isthmi pars parvocellularis; CB, cerebellum. Computer-generated visual stimuli are presented on a monitor (checker board) and are projected with appropriate optics (not shown) onto the eye-cup retina.

2.5 Visual stimulation technique for extracellular recordings

Visual stimuli were created by a computer and delivered with a LCD monitor (Samsung 19", 1440x900 pixels, contrast ratio = 20000:1, response time = 2 ms). The image of the monitor was projected onto the retinal surface of the hemisected eye-cup with a converging lens system. A monitor pixel corresponded to 7 μm on the retina or ~0.08^{o} of visual angle (Northmore and Granda 1991; Ariel and Kogo 2001). Stimuli were created using *psychopy*, an

open-source psychophysics module written for the Python programming language (Peirce 2008).

2.5.1 Eye-cup layout Software tools were written to allow the experimenter to characterize the projection of the computer screen onto the retina. A computer game pad was used to control the measurements of size and position of the eye-cup interactively, relative to the monitor. The eye-cup parameters, including the position and orientation of the visual streak, and the size and position of the optic disk were documented. An image based on these parameters (Fig. 2.4 inset) overlaid on the eye-cup preparation (in the recording chamber) when projected through the focusing system.

2.5.2 Search stimulus The search stimulus consisted of 5 - 8 black spots of different sizes (2 – 8^{o}) moving pseudo-randomly on a white background inside the eye-cup with different directions and speeds (2 – 5^{o}/s) (Fig. 2.4). The spots moved in a straight line until they reached the edge of the eye-cup region whereupon they randomly changed direction but not speed or size. Unless specified elsewhere, the default computer screen background was white in a darkened room yet, to provide reference, a dim image of the eye-cup (< 7% opacity) was viewable behind the stimulus.

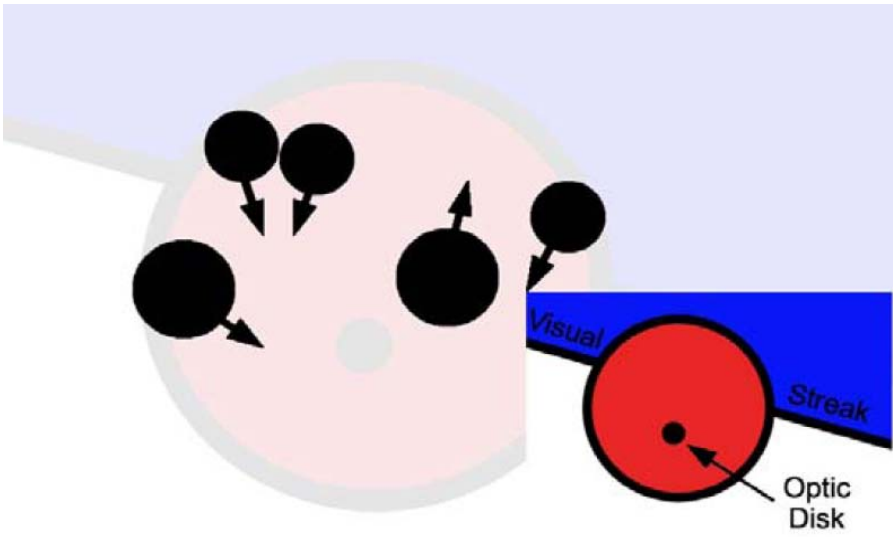

Figure 2.4 The monitor-to-eye-cup projection and the presentation of visual stimuli. (a) A search stimulus consisting of 5 - 8 black spots of different sizes (2 – 8^{o}) moving pseudo randomly on white background with different speeds (2 – 5^{o}/s) and directions in a straight line until they reach the edge of the eye-cup whereupon they randomly change direction. A semitransparent image of the eye-cup is projected beneath the stimulus to provide reference. *Inset:* The tool used to define the size and position of the eye-cup, the position and orientation of the visual streak, and the size and position of the optic disk relative to the monitor. The image is of high contrast so that the user can see the image projected onto the retina. Typical values for the eye-cup diameter and optic disk diameter are 800 and 100 pixels, respectively, so that each pixel is a fraction of a degree of visual angle.

2.5.3 Stimulation coordinate set-up To define the stimulation coordinate system, we monitored neural activity for a black spot moving on the screen,

starting outside the eye-cup region. The movement and size of the spot was controlled by a computer mouse. As the spot moved towards the eye-cup center, single/multi unit responses were audibly detected at some locations with the use of an audio monitor. The spot locations and sizes were saved at the onset of a response by clicking the mouse. After multiple such identifications of responses, an image of all the response-triggering spots overlaid on each other was generated (Fig. 2.5). This image was used as a guide to define a stimulation coordinate system that was about twice the size of the active area and oriented parallel to the visual streak (white square in Fig. 2.5 inset). All experimental stimuli were subsequently scaled and rotated using this normalized stimulation coordinate system, giving us the ability to generate a whole set of stimuli which can be presented independently of the particulars of each monitor-to-eye-cup projection setup. The nasal retina or temporal visual field parallel to the visual streak was defined 0^{o} (180^{o}) in the right (left) eye. The superior and inferior visual fields of both eyes were defined as 90^{o} and 270^{o} respectively.

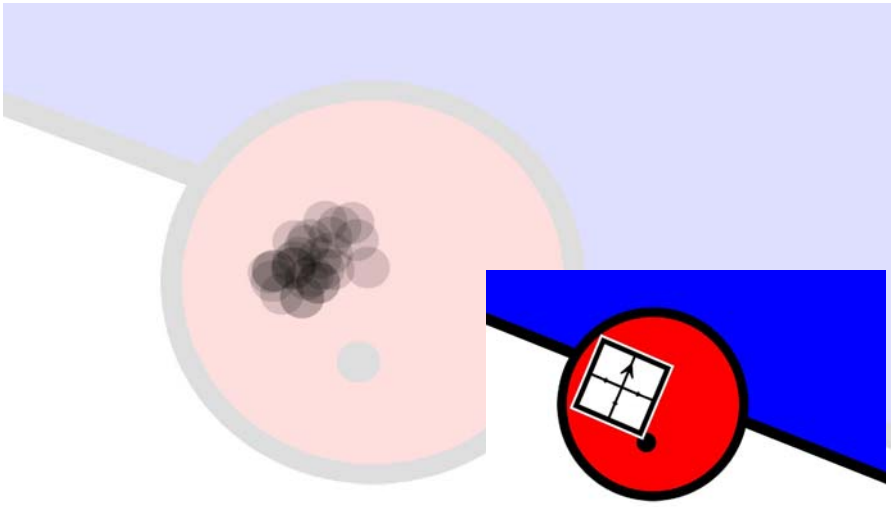

Figure 2.5 The stimulation coordinate system is traced out with a moving spot. The spot moves from outside the eye-cup towards the eye-cup center. The spot location is saved at the onset of a response. After multiple such savings of spot locations, an image of all the spots overlaid on each other is generated. *Inset:* The trace program markings determine the position, size and orientation of the stimulation coordinate system. Subsequent stimuli are all drawn translated, scaled, and rotated into this coordinate system.

2.5.4 Visual stimuli application: Various stimuli, both static and moving were shown from a pool of computer generated stimuli. During an experiment, stimuli were shown time-locked with the data acquisition. The data acquisition system sent a 5-V trigger pulse to the stimulus computer's parallel port, triggering the display of the stimulus. With the video card (ASUS EN8600GT, 256 MB), the *psychopy* codes maintained sub-millisecond frame-rendering precision. Detailed description of the visual stimuli will be provided in an experiment specific manner in later chapters.

2.6 References

Ariel M, Kogo N (2001) Direction tuning of inhibitory inputs to the turtle accessory optic system. J Neurophysiol 86: 2919-2930.

Belkin DA (1963) Anoxia: Tolerance in reptiles. Science 139: 492-493.

Dingledine R (1984) Brain slices. Springer.

Hounsgaard J, Nicholson C (1990) The isolated turtle brain and the physiology of neuronal circuits. In: Jahnsen H (ed.) Preparations of vertebrate central nervous system in vitro. Wiley p. 155-181.

Kettenmann H, Grantyn R (1992) Practical electrophysiological methods: A guide for in vitro studies in vertebrate neurobiology. Wiley.

Kriegstein AR (1987) Synaptic responses of cortical pyramidal neurons to light stimulation in the isolated turtle visual system. J Neurosci 7: 2488-2492.

Llinas R, Yarom Y, Sugimori M (1981) Isolated mammalian brain in vitro: new technique for analysis of electrical activity of neuronal circuit function. Federation Proc 40: 2240-2245.

Lutz PL, Rosenthal M, Sick TJ (1985) Living without oxygen: turtle brain as a model of anaerobic metabolism. Mol Physiol 8: 411-525.

Northmore DP, Granda AM (1991) Ocular dimensions and schematic eyes of freshwater and sea turtles. Vis Neurosci 7: 627-635.

Okamoto K, Quastel JH (1973) Spontaneous action potentials in isolated guinea-pig cerebellar slices: Effects of amino acids and conditions of affecting sodium and water up-take. Proc R Soc London B 184: 83-90.

Peirce JW (2008) Generating Stimuli for Neuroscience Using PsychoPy. Front Neuroinformatics 2:10.

Rosenberg AF, Ariel M (1988) Cells in the turtle's basal optic nucleus are direction selective over a broad velocity range. Soc Neurosci Abstr 14: 990.

Rosenberg AF, Ariel M (1990) Visual-response properties of neurons in turtle basal optic nucleus in vitro. J Neurophysiol 63: 1033-1045.

Schurr A, Rigor BM (1995) Brain slices in basic and clinical research. CRC.

Sick TJ, Rosenthal M, Lamanna JC, Lutz PB (1982) Brain potassium ion homeostasis, anoxia and metabolic inhibition in turtles and rats. Am J Physiol 243: R281-288.

Suarez RK (1988) Thinking with and without oxygen: energy metabolism in vertebrate brains. Can J Zool 66: 1041-1045.

Yamamoto C, McIlwain H (1966) Electrical activities in thin sections from the mammalian brain maintained in chemically-defined media in vitro. J Neurochem 13: 1333-1343.

Chapter 3

ELECTROPHYSIOLOGICAL PROPERTIES OF A CHOLINERGIC NEURON IN TURTLE NUCLEUS ISTHMI

3.1 Abstract

The nucleus isthmi pars parvocellularis (Ipc), which shares reciprocal topographic projections with ipsilateral optic tectum, forms the cholinergic division of turtle isthmic complex. Electrophysiological properties of Ipc neurons to somatic current injections were investigated using whole-cell blind-patch recordings in a whole-brain preparation. All Ipc neurons responded to depolarizing current injections with tonic firing and spike-rate adaptation. The spontaneous firing rate was low for all cells. All neurons showed an h-current at large hyperpolarizing current injections. A principal component analysis was done on various parameters obtained from cellular electrophysiology to test any possible electrophysiological distinction between different Ipc neurons. No evidence of distinct electrophysiological classes of Ipc neurons was found, which is consistent with the somatodendritic and axonal morphology of turtle Ipc neurons. Finally, guided by experimental observations, a model leaky integrate-and-fire neuron with spike-rate adaptation was constructed.

3.2 Introduction

The nucleus isthmic complex is a midbrain structure that shares reciprocal connections with the optic tectum in non-mammalian vertebrates such as reptiles, birds and amphibians (Hunt and Künzle 1976; Hunt et al. 1977; Gruberg and Udin 1978; Sereno and Ulinski 1987; Powers and Reiner 1993; Dudkin and Gruberg 1999; Wang et al. 2004, 2006). There are two distinct subclasses in the isthmic complex of birds and reptiles (Wang et al. 2004, 2006; Sereno and Ulinski 1987) that presumably modulate tectal neurons differentially with their two morphologically and biochemically distinct feedback projections to the tectum (Wang et al. 1995; Wang et al. 2000; Winkowski and Gruberg 2002; Dudkin and Gruberg 2003; Wang 2003; Marin et al. 2007). One provides narrow topographic cholinergic inputs back to tectal neurons while the other provides broad GABAergic inhibitions. According to the revised nomenclature for turtle isthmic nuclei (Powers and Reiner 1993), which is consistent with that used in the avian isthmotectal system, we refer to these two isthmic nuclei as the pars parvocellularis (Ipc) and the pars magnocellularis (Imc). In turtle, the cholinergic Ipc neurons have medium-sized, elongated somata (~20 μm diameter) and flattened bipolar dendritic fields. The myelinated axons project topographically to the ipsilateral tectum without local axon branches. Each axon terminates as a compact swarm of about 3000 boutons within a cylinder with 150 μm diameter and 400 μm height located mainly in the upper tectal layers (Sereno and Ulinski 1987). In turtle, there is no morphological distinction between different Ipc neurons, but for neurons in bird Ipc nucleus, which have many similarities to the

turtle Ipc neurons, there is evidence of two types of Ipc neurons categorized by their somatodendritic and axonal morphology (Wang et al. 2006). Although the functional significance of these two types of neurons is still unknown, any potential subdivision within cholinergic Ipc nucleus is interesting because of their ability to modulate tectal neurons and in turn, the higher visual pathway.

Here, we study the cellular properties of the turtle Ipc neurons responding to somatic current injections and answer the question regarding whether there are any electrophysiological subclasses of Ipc neurons in the turtle nucleus isthmi. We have quantified various electrophysiological properties like spike shape, passive membrane properties, somatic current injection response profile and spike-rate adaptation responses for various Ipc neurons. We have used a principal component analysis to quantify any clustering of Ipc neurons depending on the response properties investigated. We have not found any evidence of distinct electrophysiological classes of Ipc neurons. We have also constructed an experimentally constrained leaky integrate-and-fire model neuron with spike-rate adaptation for turtle Ipc neurons.

3.3 Methods

3.3.1 Experiments

The surgery and the intracellular recordings from the Ipc neurons (Fig. 3.1) were performed as described in the Chapter 2 (see SECTION 2.1, 2.2). 32 adult red-

ear turtles (12-15 cm carapace length) were used in this study. Glass patch pipettes of 5 to 8 MΩ resistance were used for the recordings.

a **b**

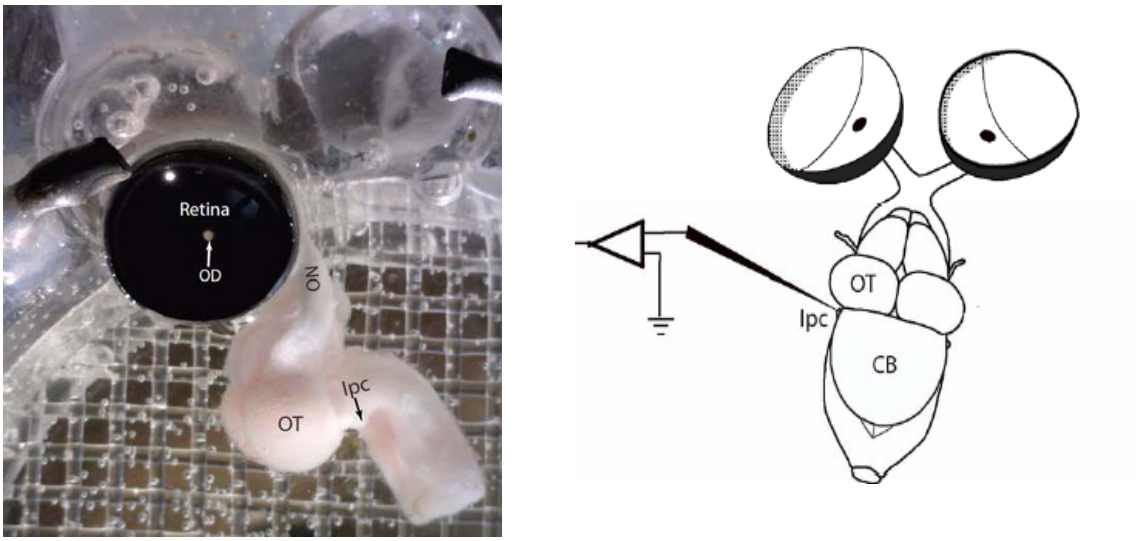

Figure 3.1 The turtle eye-attached whole-brain preparation and location of the lpc nucleus. (a) Lateral view of the turtle preparation with the telencephalon removed and the hemisected eye-cup in the recording chamber. lpc nucleus could be identified with the surface landmark of a protrusion just caudal to the optic tectum (OT). Location of the retina, optic disc (OD) and optic nerve (ON) are also shown in the picture. (b) Schematic of a dorsal view of the turtle whole-brain preparation with the hemisected eye-cups attached and the telencephalon removed. The intracellular recording electrode is shown in the picture. Schematic is obtained by courtesy of Dr. Michael Ariel.

Intracellular recordings were obtained from 40 cells (32 animals). The recording time varied from 30 min. to 1 hour. Somatic current injections of 0.5 s (for 19

cells) or 1 s (21 cells) durations were used to characterize the lpc cellular properties (Fig. 3.2a). The resting membrane potential E_r (mV) was measured after 1 min. of the whole-cell patch. Input impedance R_m (MΩ) was calculated from the steady-state value of the membrane potential responding to small (20 to 50 pA) hyperpolarizing current injection of 1 s duration. The membrane time constant τ_m (ms) was determined by fitting an exponential to the hyperpolarizing voltage trace. Since many lpc neurons were spontaneously spiking, rheobase current (lowest current injection that elicited at least one spike) was not a meaningful parameter. Rather, the spike shape and first spike latency were characterized by the lowest current injection (0.1 nA for all cells) applied during the experiment. The first spike latency T_1 (ms) for the lowest injection current was determined by the time difference between the onset of the current pulse and the peak voltage deflection of the first action potential (AP). The first spike amplitude A_1 (mV) was the voltage difference between the peak voltage of the first AP and the peak voltage of after-hyperpolarization. The half-width W_1 (ms) of the first AP was the width of the action potential at half of its amplitude (A_1).

The changes in firing rates with different injection currents were characterized by frequency vs. current (*f-I*) plots (Fig. 3.2c). To determine the *f-I* plot for each cell the injection current amplitude was increased from 0.1 nA to at least 0.5 nA with 0.1 nA increments. Both 0.5 s and 1 s current pulses were used. For each injection current *I* (nA) the total number of spikes during the injection period was calculated and converted to firing rate *f* (Hz). A straight line was fit to the *f-I* plot

and the slope $m_{f\text{-}I}$ (Hz/nA) was determined. The spontaneous firing rate f_{spont} (Hz) was experimentally constrained during the *f-I* fit. Cells with 0.5 s and 1 s current injections were analyzed and clustered separately. To determine the spike-rate adaptation, interspike intervals (ISI) were calculated for 0.5 nA current injection (both 0.5 s and 1 s duration) and plotted against post stimulus time (Fig. 3.2b). To quantify the time constant for spike-rate adaptation τ_{SRA} (ms) and steady-state values $ISI_{steady\text{-}state}$ (ms), the time course of ISI was fit with an exponential decay function. The h-current was quantified for -0.2 nA current injections (n=17 cells) of 0.5 s duration. The difference of membrane potential just before and 500 ms after the h-current activation ΔV_h (mV) was quantified as the measure of h-current.

3.3.2 Principal component analysis (PCA)

To determine whether all lpc neurons have similar electrophysiological characteristics, principal component analysis was performed. This analysis would identify separate clusters of lpc neurons if there were existence of multiple populations. First, each measured electrophysiological quantities were normalized for multiple observations by,

$$x_{Norm} = \frac{x_i - \bar{x}}{\Delta\bar{x}} \qquad (1)$$

Where x_i was a single measurement of one quantity, $\bar{x}$ was the average of that quantity for all the cells, $\Delta\bar{x}$ was the standard deviation and x_{Norm} was the normalized measurement. These normalized parameter sets allowed each

quantity to contribute equally to the likeness and differences of multiple lpc neurons, regardless of their numerical values. The PCA analysis was done separately for cells with 0.5 s (n = 17 cells) and 1 s (n = 21 cells) injections. The merit of doing this was to show whether the duration of current injection biases the electrophysiological observations. The correlation matrix consisted of 10 parameters (all but ΔV_h) for the 1 s injections and 9 parameters (all but R_m and τ_m) for the 0.5 s injections. The eigenvalues and the eigenvectors of the correlation matrices were determined using MATLAB 6.5 (Mathworks, Natick, USA) and the measured quantities with the largest eigenvalues were projected onto the principal component planes.

3.3.3 Leaky integrate-and-fire model

To construct an experimentally constrained model of turtle lpc neurons, we used a leaky integrate-and-fire neuron with spike-rate adaptation. When the membrane potential is below the threshold V_θ, the dynamics of the membrane potential V of the model neuron evolves according to the differential equation,

$$\tau_m \frac{dV}{dt} = E_r - V - R_m (I_{SRA} - I_e) \qquad \text{if } V < V_\theta \tag{2}$$

where τ_m is the membrane time constant, E_r is the resting membrane potential, R_m is the membrane resistance, I_{SRA} is the spike-rate adaptation current and I_e is the injection current. The spike-rate adaptation current is represented by,

$$I_{SRA} = g_{SRA}(t)(V - E_{SRA}) \tag{3}$$

where E_{SRA} is the adaptation reversal potential and $g_{SRA}(t)$ is the time-varying adaptation conductance, which varies in between spikes according to the equation,

$$\tau_{SRA} \frac{dg_{SRA}}{dt} = -g_{SRA} \tag{4}$$

When a spike occurs, the adaptation conductance is modified according to the equation,

$$g_{SRA}(t^+) \rightarrow g_{SRA}(t^-) + \Delta g_{SRA} \tag{5}$$

3.4 Results

3.4.1 Cellular properties

We performed blind whole-cell patch recordings from a total of 40 lpc neurons (32 animals) and analyzed cellular properties of those neurons by somatic current injections (Fig. 3.2). The average resting membrane potential was -58 ± 5 mV (mean ± SD, n = 40), the average input resistance was 371 ± 108 MΩ (n = 21) and the average membrane time constant was 77± 22 ms (n = 21). The input resistance and membrane time constant were measured from 1 s long, small hyperpolarizing (-20 to -50 pA) somatic current injections. The spike features were quantified for the smallest depolarizing injection current (0.1 nA). The amplitude A_1 of the first AP was 89 ± 15 mV (n = 40), the half-width W_1 was 0.5 ± 0.1 ms (n = 40) and the first spike latency T_1 was 51 ± 35 ms (n = 40). All recorded neurons responded to hyperpolarizing somatic current injection with a sag (Fig. 3.2a), which is typical in the presence of an h-current (Kamondi and Reiner 1991; Mercuri et al. 1995; Pape 1996). The h-current voltage sag,

quantified by the parameter ΔV_h for -0.2 nA current injection, had large variation between cells (16 ± 7 mV, n = 28). The spontaneous activity was small for all the cells and varied between 0 to 8 Hz (n = 40). All lpc neurons showed tonic firing in response to depolarizing somatic current injections (both 0.5 s and 1 s duration). The injection current vs. firing rate (*f-I*) profiles for all the cells were linear with slope m = 103 ± 38 Hz/nA (n = 40). Spike-rate adaptation reached a steady-state after the first 100 ms of the current injections for all cells (Fig. 3.2b). The time constant of spike-rate adaptation at 0.5 nA injection current was 37 ± 10 ms (n = 40). From the first ISI, we infer that lpc neurons may transiently reach an instantaneous firing rate up to 300 Hz (Fig. 3.2c).

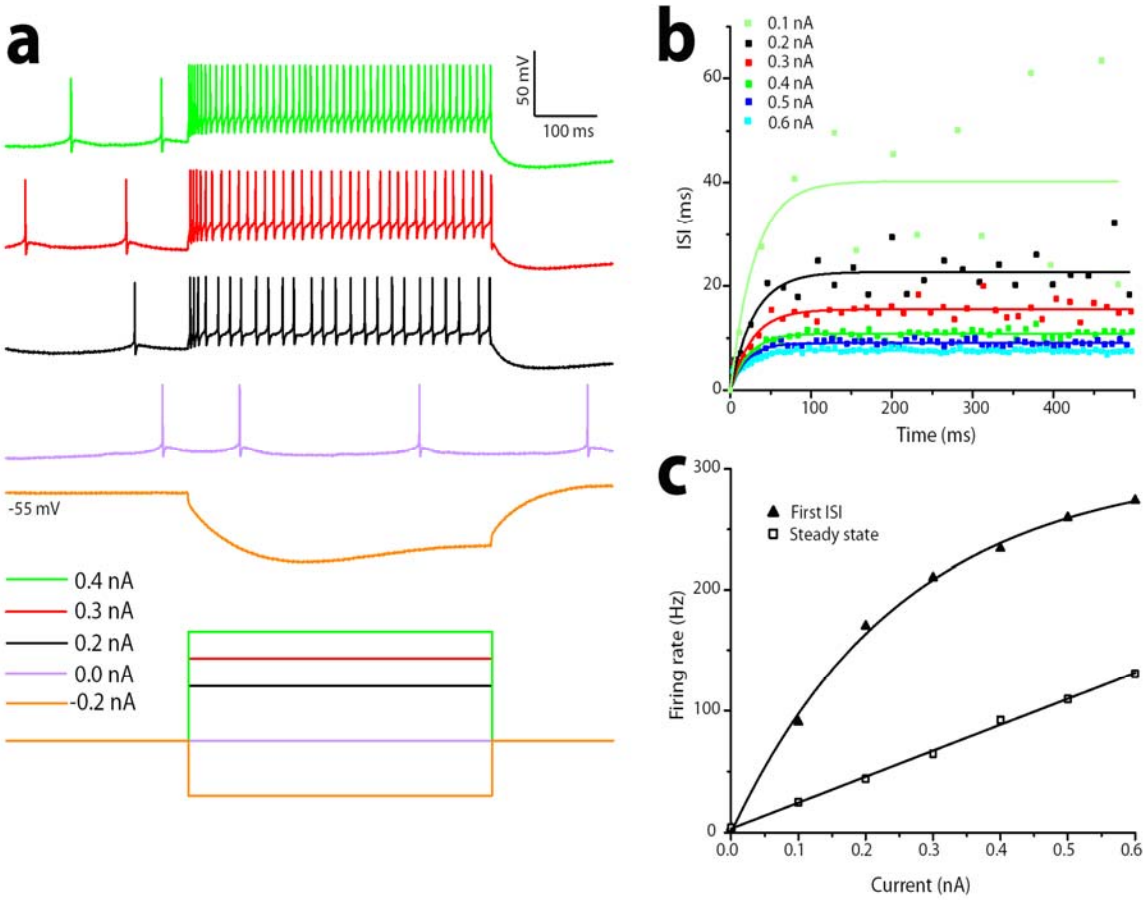

Figure 3.2 Electrophysiological properties of an lpc neuron. (a) lpc responses to current injections of different amplitudes (rectangular pulse, 500ms). The resting membrane potential was -55 mV. The cell showed spontaneous spiking at zero current. (b) The change of interspike intervals (ISI, squares), Δ, with time after current onset for different current amplitudes. The curves were obtained by fitting the data points with an exponential function, $\Delta(t) = \delta(1 - e^{-t/\tau})$, where *t* is the time after current onset, τ is a time constant reflecting the spike-rate adaptation, and δ is the steady-state ISI (i.e. the inverse of the steady-state firing rate). The spike-rate adaptation time constant τ decreases from 30 to 17 ms with increasing current amplitude I. (c) Firing rates as a function of injected current amplitude based on the first ISI (filled triangles) and based on the steady-state ISI (values of fitting parameter δ from (b), open squares). The curve for the steady-state was obtained by fitting a straight line, $f_{ss}(I) = mI + f_{sp}$, to the data points. Here I is the injected current amplitude, m = 213 Hz/nA, $f_{sp} = 3$ Hz **is the spontaneous firing rate, and** R^2 = 0.99**. The curve for first ISI was obtained by fitting the exponential, $f_1(I) = f_{\max}(1 - e^{-I/I_0})$, to the data points. Here I is the injected current amplitude,** $f_{\max}$ = 303 Hz **is the maximum firing rate,** I_0 = 0.26 nA**, and** R^2 = 0.99**.**

3.4.2 Principal component analysis

Although the somatodendritic morphology indicates only one population of Ipc neurons in turtle, there is evidence of two types of neurons in bird Ipc nucleus, which is very similar to turtle Ipc nucleus. Since no electrophysiology has been done in turtle Ipc neurons to date, first, we tested whether similar somatodendritic morphology leads to only one type of electrophysiological subclass in turtle Ipc neurons. We recorded from 40 Ipc neurons from 50 to 400 μm deep in the Ipc nucleus, covering both rostral and caudal part of the nucleus. The cellular properties were studied using both 0.5 s and 1 s current pulses. For 1 s injections, passive membrane properties (resting membrane potential E_r, impedance R_m, time constant τ_m), spike shape properties (amplitude A_1, width W_1, latency T_1), current-frequency response profile parameters (slope $m_{f\text{-}I}$, spontaneous rate f_{spont}) and spike-rate adaptation quantities (time constant τ_{SRA}, steady-state rate $ISI_{steady\text{-}state}$) were measured (a total of 10 parameters, see METHOD for details). To determine whether the measurements of these 10 parameters from 21 different cells can be categorized into one or more populations based on their cellular properties, we performed principal component analysis (Jolliffe 1986). Each variable for multiple observations was normalized first (Eq. (1)). Then the eigenvalues of the correlation matrix were determined (Fig. 3.3A left). The first two eigenvalues accounted for 91% of the data set's cumulative variance. Therefore, only the two principal component vectors with largest eigenvalues were chosen to represent the results, reducing the parameter space to two dimensions. All the observed quantities were projected onto these

two principal components (Fig. 3.3A right). We found that the principal component values were scattered about the mean values (zero for normalized variables) of all the cells and no evidence of distinct populations could be found. We also performed the principal component analysis on the 19 cells with 0.5 s current injections. The correlation matrix composed of 9 variables, which included all variables used for the 1 s injections except for membrane impedance R_m and time constant τ_m. These two quantities could not be calculated from the data set because of the absence of lower (< 50 pA) hyperpolarizing current injections. The parameter quantifying the h-current at 0.2 nA (ΔV_h) was added to the data set (see METHOD). The principal component analysis was done with standardized variables same way as of 1 s injections. All the data were projected onto the two dimensional principal component space with the two largest eigenvalues, which accounted for 83% of all parameters' total variance (Fig. 3.3 B). In this case also, the values were scatted around their mean and no discrete clusters were readily apparent in the reduced principal component space.

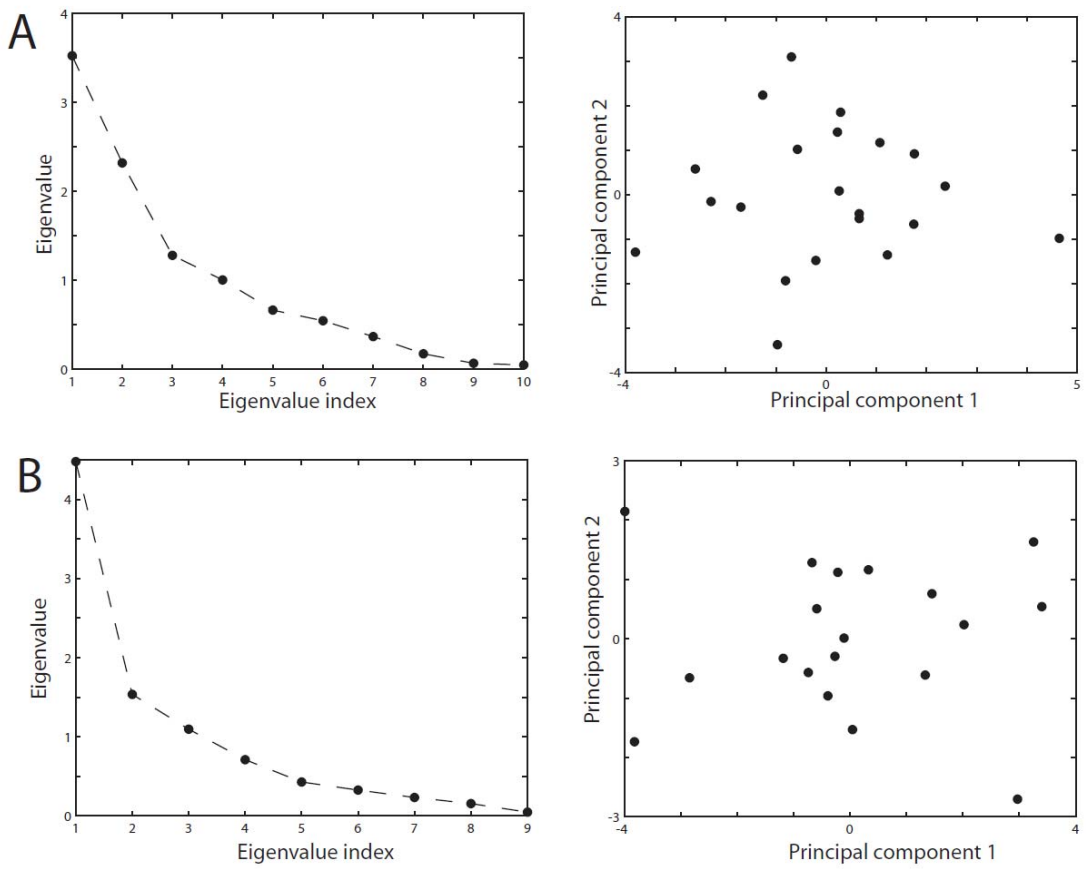

Figure 3.3 Principal component analysis of electrophysiological properties of lpc neurons calculated from responses to somatic current injections. (A) left, eigenvalues determined by PCA for the 21 cells with 10 parameters each from 1 s current injections. Right, projection of the measurements on the principal component plane with the two largest eigenvalues. No discrete clusters appear for the 21 lpc neurons in the two-dimensional principal component space. (B) left, eigenvalues determined by the PCA of the correlation matrix of 9 parameters from the 19 cells with 0.5 s current injection. Right, projection of normalized measurements to the principal

component axis with two largest eigenvalues. Again, no clustering seems to appear for the 19 lpc neurons in the principal component plane.

3.4.3 Determine experimentally constrained leaky integrate-and-fire model parameters

The fact that the lpc neurons responses to somatic current injections were remarkably linear and regular (no bursts or obvious spike pattern), suggested that turtle lpc neurons, just like avian lpc neurons, could be simulated with leaky integrate-and-fire model neurons with an added spike-rate adaptation current (Shao et al. 2009). The parameters were constrained by comparing simulated lpc responses (Eq. (2)) to the experimentally obtained lpc neuron's electrophysiological properties in response to depolarizing somatic current injections (Fig. 3.2). Because of spike-rate adaptation (Eq. (3) to (5)), the model neuron responded to the onset of current pulse with a shorter interspike interval (ISI) (Fig. 3.4a, c). The ISI increased over the duration of the pulse and reached a steady-state value within few hundred ms.

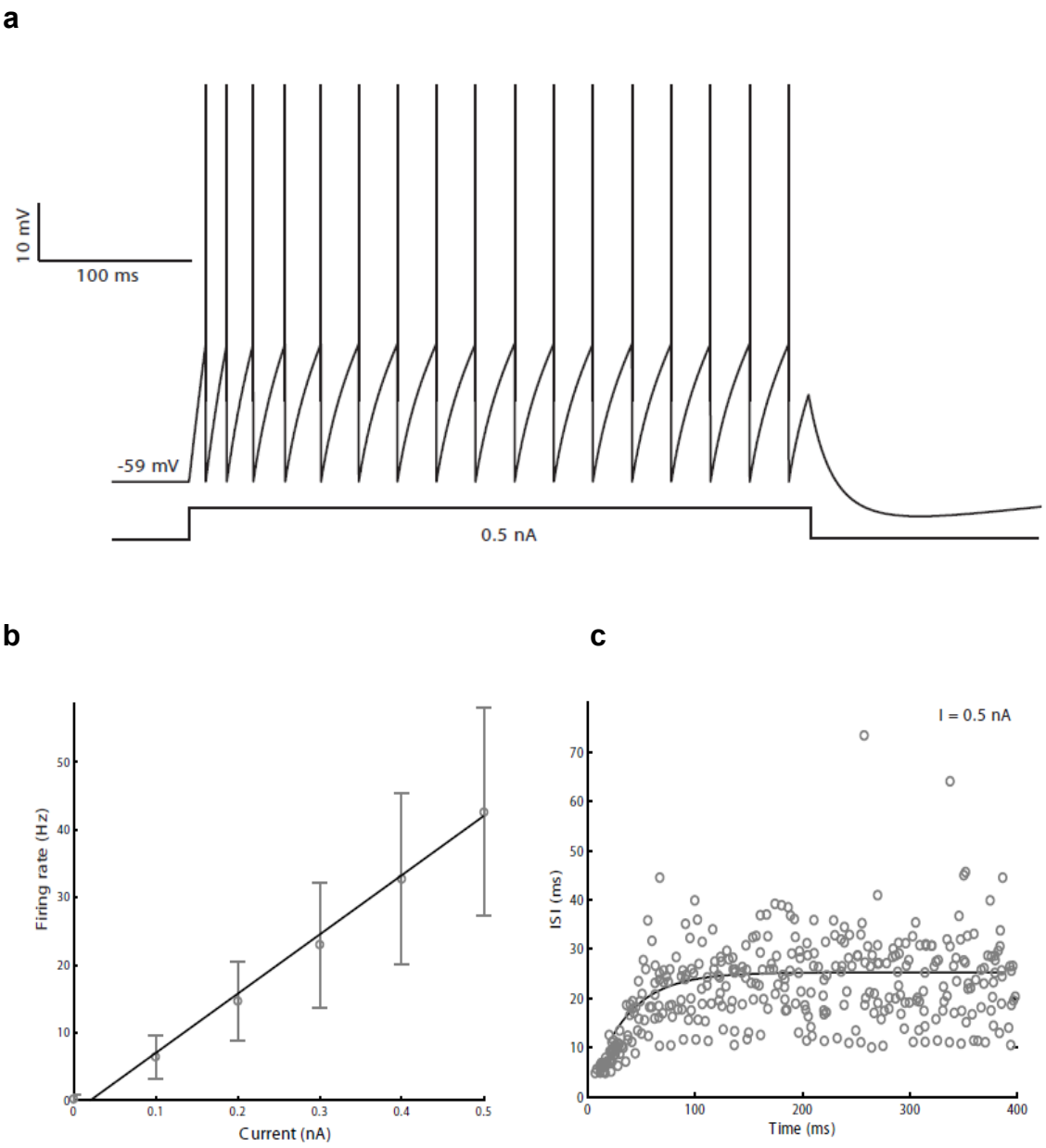

Figure 3.4 Cellular properties of leaky integrate-and-fire model neuron. (a) The simulated spike train of an lpc neuron responding to a 0.5 nA somatic current injection. (b) The fitted f-I plot of the model neuron to the experimental data. The circles indicate the experimentally obtained average firing rate and the error bars represent SD (n = 21). (c) The fitting of simulated ISI curve to the experimental results obtained for 0.5 nA

current injections. The ISI curve obtained from the model neuron satisfying the equation, $ISI(t) = A(1 - \exp(-t / B))$**.The gray circles represent the ISI values obtained from 21 Ipc neurons for 0.5 nA current injections.**

To derive the simulated *f-I* plot for the model neuron, we calculated the average firing rate for different currents by dividing the total number of spikes by the duration of the current injection. We then fit a linear function through the average firing rates obtained from simulated spike trains (Fig. 3.4c). The ISIs were calculated from simulated spike trains elicited by 0.5 nA current injection and an exponential function was fit to the result (Fig. 3.4c). All cellular parameters, a total of 8 (Eq. (2) to (5)), were adjusted within their experimentally constrained boundaries until the simulated *f-I* plot and ISI profile for 0.5 nA current injections matched the experimental data (Fig. 3.4b, c) obtained from all Ipc neurons (n = 21).

Model Parameters	τ_m *(ms)*	R_m (MΩ)	E_r *(mV)*	V_θ *(mV)*	V_{reset} *(mV)*	τ_{sra} *(ms)*	Δg_{sra} *(nS)*	E_{sra} *(mV)*
Values	78	372	-59	-35	-59	60	4.6	-70

Table 3.1 Single neuron parameters for an Ipc model neuron. $\tau_m =$ **membrane time constant,** $R_m =$ **membrane input resistance,** $E_r =$ **resting membrane potential,** $V_\theta =$ **threshold for spiking,** $V_{reset} =$ **reset voltage,** $\tau_{sra} =$

spike-rate adaptation time constant, $\Delta g_{sra} =$ **spike-rate adaptation conductance increment,** $E_{sra} =$ **spike-rate adaptation reversal potential.**

3.5 Discussion

Here we have shown that the turtle Ipc neurons respond to depolarizing somatic current injections with tonic firing. The spiking pattern shows spike-rate adaptation for the first hundred ms of current injection and reaches a steady-state firing rate within 0.5 s of the current pulse onset. We have found the presence of h-currents in Ipc neurons for large hyperpolarizing current injections. We have recorded various electrophysiological properties quantifying spike shape, firing pattern and passive membrane properties for several Ipc neurons and performed PCA analysis to quantify any possible presence of multiple populations of neurons in the turtle Ipc nucleus. We have found no evidence of distinct clusters of Ipc neurons, which is consistent with the somatodendritic morphology of the Ipc neurons. The remarkably regular and linear firing pattern of Ipc neurons motivated us to construct an experimentally constrained leaky integrate-and-fire model with spike-rate adaptation for Ipc neurons.

Spike-rate adaptation to somatic current injection is a distinctive feature of turtle Ipc neurons, which is also present in bird and frog isthmic neurons (Shao et al. 2009, Caudill et al. 2010). Potassium currents with slow inactivation might play a role in this Ipc response property as they often mediate the spike-rate adaptation in different neurons (Lewis et al. 1986; Brown et al. 1990; Storm 1990;

Brownstone 2006). The phenomenological model of leaky integrate-and-fire neuron also uses a spike-rate adaptation current to provide a good approximation to the turtle Ipc neuron's electrophysiological properties.

Injection of large negative current (>0.1 nA) resulted in a graded hyperpolarization that produced a sag towards resting membrane potential (Fig. 3.2a), which is a typical characteristic of h-current (I_h). In some cases, this inward current produced strong depolarization that resulted in a rebound spike (data not shown). The sag towards resting membrane potential is described as an inward rectification (Pape 1996) and in many central neurons postulated as a result of time and voltage dependent membrane conductance mediated by the mixture of potassium and sodium currents. The I_h for the Ipc neurons activated around -70 to -80 mV, which is below the resting membrane potential of Ipc neurons and is consistent with the threshold for I_h activation in other types of neurons (Kamondi and Reiner 1991; Mercuri et al. 1995; Fu et al. 1997). The I_h is known to be a pacemaker current and provides periodic depolarization during generation of rhythmic oscillatory activity (DiFrancesco 1981, 1986; McCormick and Pape 1990). It has also been hypothesized as a regulator of the spontaneous activity in neurons (Fu et al. 1997).

The spontaneous firing in turtle Ipc neurons is similar to that in bird Ipc neurons (Marin et al. 2005; Maczko et al. 2006). The spontaneous firing rate is low (0 – 8 Hz) for turtle Ipc neurons. The parabigeminal nucleus (PBN), which is often

referred as the mammalian homolog of Ipc, also shows similar spontaneous firing in rats (Goddard et al. 2007). However, the spontaneous firing rate in the cat PBN is significantly higher (Sherk 1979a; Cui and Malpeli 2003). Although the functional significance of the spontaneous activity of the isthmic neurons is unknown, it has been postulated that it may help isthmic neurons respond quickly to sensory inputs (Sherk 1979a). This spontaneous activity might help Ipc neurons deliver a low level of acetylcholine (ACh) continuously to the tectum. The cholinergic Ipc neurons have already been implicated to modulate tectal neurons (Wang et al. 1995; Wang et al. 2000; Wang 2003) and control spatial attention by encoding spatial location of novel stimuli (Maczko et al. 2006). This low spontaneous firing rate is also common in other cholinergic neurons (Wilson 2005; Arrigoni et al. 2006).

3.6 References

Arrigoni E, Chamberlin NL, Saper CB, McCarley RW (2006) Adenosine inhibits basal forebrain cholinergic and noncholinergic neurons in vitro. Neuroscience 140: 403–413.

Brown DA, Gähwiler BH, Griffith WH, Halliwell JV (1990) Membrane currents in hippocampal neurons. Progress in Brain Research 83: 141-160.

Brownstone RM (2006) Beginning at the end: repetitive firing properties in the final common pathway. Progress in Neurobiology 78: 156-172.

Caudill MS, Eggebrecht AT, Gruberg ER, Wessel R (2010) Electrophysiological properties of isthmic neurons in frogs revealed by in vitro and in vivo studies. J Comp Physiol A 196: 249-262.

Cui H, Malpeli JG (2003) Activity in the parabigeminal nucleus during eye movements directed at moving and stationary targets. J Neurophysiol 89: 3128-3142.

Difrancesco D (1981) A study of the ionic nature of the pace-maker current in calf Purkinje fibers. J. Physiol. (Lond.) 314: 377–393.

Difrancesco D (1986) Characterization of single pacemaker channels in cardiac sino-atrial node cells. Nature 324: 470–473.

Dudkin EA, Gruberg ER (2003) Nucleus isthmi enhances calcium influx into optic nerve fiber terminals in Rana pipiens. Brain Res 969: 44-52.

Dudkin ES, Gruberg ER (1999) Relative number of cells projecting from contralateral and ipsilateral nucleus isthmi to loci in the optic tectum is

dependent on visuotopic location: horseradish peroxidase study in the leopard frog. J. Comp. Neurol 414: 212-216.

Fu XW, Brezden BL, Wu SH (1997) Hyperpolarization-activated inward current in neurons of the rat's dorsal nucleus of the lateral lemniscus in vitro. J Neurophysiol 78: 2235-2245.

Goddard CA, Knudsen EI, Huguenard JR (2007) Intrinsic excitability of cholinergic neurons in the rat parabigeminal nucleus. J Neurophysiol 98: 3486-3493.

Gruberg ER, Udin SB (1978) Topographic projections between the nucleus isthmi and the tectum of the frog, *Rana pipiens*. J Comp Neurol 179: 487-500.

Hunt SP, Künzle H (1976) Observations on the projections and intrinsic organization of the pigeon optic tectum: an autoradiographic study based on anterograde and retrograde, axonal and dendritic flow. J Comp Neurol 170: 153-172.

Hunt SP, Streit P, Kunzle H, Cuenod M (1977) Characterization of the pigeon isthmo-tectal pathway by selective uptake and retrograde movement of radioactive compounds and by Golgi-like horseradish peroxidase labeling. Brain Res 129: 197-212.

Jolliffe IT (1986) Principal component analysis. Springer, New York.

Kamondi, A, Reiner PB (1991) Hyperpolarization-activated inward current in histaminergic tuberomammillary neurons of the rat hypothalamus. J. Neurophysiol. 66: 1902–1911.

Lewis DV, Huguenard JR, Anderson WW, & Wilson WA (1986) Membrane currents underlying bursting pacemaker activity and spike frequency adaptation in invertebrates. Advances in Neurology 44: 235-261.

Maczko KA, Knudsen PF, Knudsen EI (2006) Auditory and visual space maps in the cholinergic nucleus isthmi pars parvocellularis in the barn owl. J Neurosci 26: 12799-12806.

Marin G, Salas C, Sentic E, Rojas X, Letelier JC, Mpodozis J (2007) A cholinergic gating mechanism controlled by competitive interactions in the optic tectum of the pigeon. J Neurosci 27: 8112-8121.

Marín G, Mpodozis J, Sentis E, Ossandón T, Letelier JC (2005) Oscillatory bursts in the optic tectum of birds represent re-entrant signals from the nucleus isthmi pars parvocellularis. J Neurosci 25: 7081-7089.

Mccormick DA, Pape HC (1990)Properties of a hyperpolarization- activated cation current and its role in rhythmic oscillation in thalamic relay neurons. J. Physiol. (Lond.) 431: 291–318.

Mercuri NB, Bonci A, Calabresi P, Stefani A, Bernardi G (1995) Properties of the hyperpolarization-activated cation current I_h in rat midbrain dopaminergic neurons. Eur. J. Neurosci. 7: 462–469.

Pape HC (1996) Queer current and pacemaker: the hyperpolarization-activated cation current in neurons. Annu. Rev. Physiol. 58: 299–327.

Powers AS, Reiner A (1993) The distribution of cholinergic neurons in the central nervous system of turtles. Brain Behav Evol 41: 326-345.

Saha D, Ariel M, Wessel R (2008) Dynamics of excitatory and inhibitory synaptic currents in a visual feedback loop in turtle. SfN Abstract.

Sereno MI, Ulinski PS (1987) Caudal topographic nucleus isthmi and the rostral nontopographic nucleus isthmi in the turtle, *Pseudemys scripta*. J Comp Neurology 261: 319-346.

Shao J, Lai D, Meyer U, Luksch H, Wessel R (2009) Generating oscillatory bursts from a network of regular spiking neurons without inhibition. J Comput Neurosci 27: 591-606.

Sherk H. A comparison of visual-response properties in cat's parabigeminal nucleus and superior colliculus. J Neurophysiol 42: 1640-1655, 1979a.

Storm JF (1990) Potassium currents in hippocampal pyramidal cells. *Progress in Brain Research* 83: 161-187.

Wang SR (2003) The nucleus isthmi and dual modulation of the receptive field of tectal neurons in non-mammals. Brain Research Reviews 41: 13-25.

Wang SR, Wang YC, Frost BJ (1995) Magnocellular and parvocellular divisions of pigeon nucleus isthmi differentially modulate visual responses in the tectum. Exp Brain Res 104: 376-384.

Wang Y, Luksch H, Brecha NC, Karten HJ (2006) Columnar projections from the cholinergic nucleus isthmi to the optic tectum in chicks (*Gallus gallus*): A possible substrate for synchronizing tectal channels. J Comp Neurol 494:7-35.

Wang Y, Major DE, Karten HJ (2004) Morphology and connections of nucleus isthmi pars magnocellularis in chicks (Gallus gallus). J Comp Neurol 469: 275-297.

Wang Y, Xiao J, Wang SR (2000) Excitatory and inhibitory receptive fields of tectal cells are differentially modified by magnocellular and parvocellular divisions of the pigeon nucleus isthmi. J Comp Physiol A 186: 505-511.

Wilson CJ (2005) The mechanism of intrinsic amplification of hyperpolarizations and spontaneous bursting in striatal cholinergic interneurons. Neuron 45: 575–585.

Winkowski DE, Gruberg ER (2002) The representation of the ipsilateral eye in nucleus isthmi of the leopard frog, Rana pipiens. Visual Neurosci 19: 669-679.

Chapter 4

SYNAPTIC CONNECTIVITY

IN TURTLE ISTHMOTECTAL SYSTEM

4.1 Abstract

In three-component turtle isthmotectal system, the nucleus isthmi pars parvocellularis (Ipc) neurons receive excitatory glutamatergic inputs from tectal neurons and GABAergic inhibitory inputs from the nucleus isthmi pars magnocellularis (Imc) neurons. The interaction of local excitation through topographic tectal-Ipc connection and broad inhibition due to nontopographic Imc to Ipc projections makes Ipc ideally suited to investigate the balance between two opposing synaptic currents. Visual stimulation and the retinal ganglion cell (RGC) axon stimulation of the contralateral retina revealed a complex combination of multiple synaptic currents in Ipc. Electrical stimulation of optic nerve yielded two synaptic currents, one excitatory and one inhibitory, which were about equal in amplitude but different in time course. We also found that the synaptic connection from Imc to Ipc is inhibitory. Overall, this investigation revealed how two synaptic currents of opposite amplitude might shape the Ipc response properties that in turn, influence tectal processing. A piecewise investigation of the isthmotectal circuitry also shed light on the sources of these synaptic currents.

4.2 Introduction

The turtle Ipc neurons are well suited for establishing general principles of changing balance of excitatory and inhibitory synaptic currents as a mechanism for visual processing since the Ipc neurons receive both topographic glutamatergic (excitatory) inputs from the SGP neurons and largely nontopographic GABAergic (inhibitory) inputs from the Imc neurons. It is the changing balance of excitatory and inhibitory synaptic currents that provides plausible biophysical mechanisms for central visual processing, including gain modulation (Chance et al. 2002), the shifts from drivers to modulators (Abbott and Chance 2005), direction selectivity (Priebe and Ferster 2005), invariance of orientation tuning to changes in stimulus contrast (Ferster and Miller 2000; Hirsch et al. 2003; Marino et al. 2005), and invariance of contrast sensitivity to response gain (Cano et al. 2006), to name a few.

Here, we take the advantage of the turtle whole-brain preparation to investigate the synaptic connectivity of the cholinergic Ipc neuron within the three-component isthmotectal system (Fig. 4.1d) and also to explore the responses of those neurons to electrical stimulation of optic nerve and visual stimulation of RGCs. The turtle isthmic complex contains two cytoarchitectonically distinct isthmic nuclei, Ipc and Imc (Fig. 4.1d), which receive sensory information from the ipsilateral optic tectum (Sereno and Ulinski 1987; Powers and Reiner 1993). RGC axons terminate in the superficial layers of the tectum (Fig. 4.1d), where they innervate the radial, narrow dendrites of the tectal stratum griseum

periventriculare (SGP) neurons (Fig. 4.1a, d). The axons of the SGP neurons project to the Ipc and Imc nuclei. In the Imc nucleus, neurons have large, sparsely branched dendritic fields overlapped by local axon collaterals. The axons of the Imc neurons nontopographically project to both the deeper layers of the tectum and to the Ipc nucleus (Fig. 4.1c, d) (Sereno and Ulinski 1987). In the Ipc nucleus, neurons have medium-sized, elongated somata, flattened bipolar dendritic fields, and axons that project topographically back to the tectum without any local axon collaterals (Fig. 4.1b, d). Each Ipc axon terminates as a compact swarm of boutons within a cylinder of about 150 μm in diameter and 400 μm tall, placed mainly in the upper tectal layers, where it spans less than one percent of the tectal surface. The topographically-organized, columnar Ipc axon terminals spatially overlap with the RGC axons and the SGP neuron dendrites.

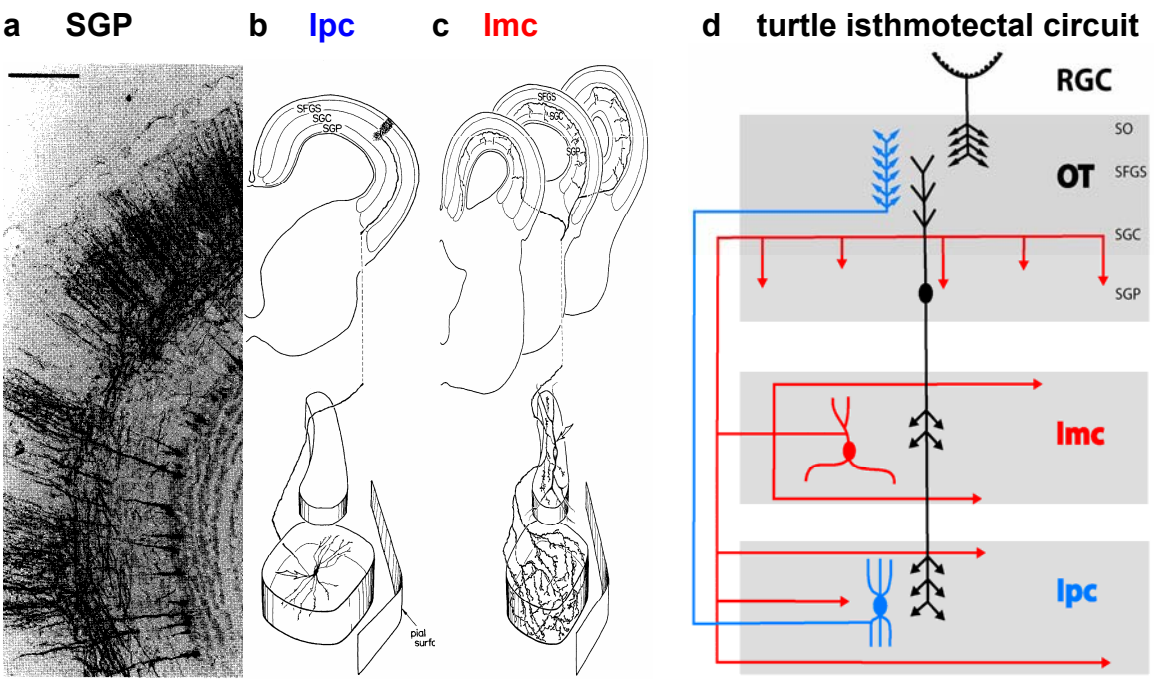

Figure 4.1: The isthmotectal feedback loop in turtle. (a) Neurons in the optic tectum (OT) with somata in the stratum griseum periventriculare (SGP) receive retinal ganglion cell (RGC) axon inputs at their narrow apical dendrites reaching to the stratum fibrosum et griseum superficiale (SFGS). The glutamatergic SGP neurons (black in (d)) project to the two isthmic nuclei: pars parvocellularis (Ipc) and pars magnocellularis (Imc) (scale bar = 200 µm; Kunzle and Schnyder 1984). (b) The cholinergic Ipc neurons (blue in (d)) have flattened bipolar dendrites, and project topographically to the ipsilateral tectum, where each Ipc axon terminates as a compact swarm of boutons in upper tectal layers (Sereno and Ulinski 1987). (c) The GABAergic Imc neurons (red in (d)) have large, sparsely branched dendritic fields, have local axon collaterals, and project nontopographically to the Ipc and to deeper tectal layers (SGC, SGP) (Sereno and Ulinski 1987). In (b) and (c), the isthmic nuclei have been enlarged relative to the tectum for clarity. (d) Schematic summary of the anatomical information described in (a) – (c).

To elucidate the interactions of excitatory and inhibitory synaptic currents that mediate the visual response properties of the Ipc neurons, we have recorded intracellularly from the Ipc neurons while stimulating the optic nerve. We have also recorded the Ipc responses to electrical stimulation of the retina and visual stimulation of the contralateral eye. To investigate the mechanisms of generation

of the Ipc response properties to these stimulations, synaptic connectivity between Imc → Ipc and tectal neurons →Ipc were studied.

4.3 Methods

29 red-ear turtles were used for this study. The surgery was performed as described in Chapter 2 (see SECTION 2.1). Depending on the experiment, either one eye-cup or only the optic nerve was left attached to the brainstem preparation. Blind-patch whole-cell recordings (See SECTION 2.2) were achieved for 37 Ipc neurons and responses to stimulation of various parts of retina → tectum → Ipc circuitry were obtained. Optical stimulation of the contralateral eye of the recorded Ipc neurons was achieved with computer-controlled LEDs (white) projecting onto the retina via a single optic fiber of 200 μm in diameter. Electrical stimulation of RGC axons in retina, surface tectal stimulation and deep tectal Imc axon stimulations were achieved by concentric, bipolar tungsten electrodes (tip diameter = 4 μm; core diameter = 76 μm). Current pulses of (100 - 200 μA) 0.5 ms duration were used in these stimulations. Optic nerve stimulation was generated by a glass tip suction electrode (A-M systems), which was fabricated so that it fit the optic nerve tightly. Brief current pulses of 0.5 ms durations were applied to a suction electrode placed around the contralateral optic nerve while recording intracellularly from an Ipc neuron.

4.4 Results

4.4.1 Electrical stimulation of RGC axons in retina generate complex response patterns in Ipc neurons

To quantify the Ipc neurons' responses to RGC stimulation, we recorded intracellularly from 3 Ipc neurons while electrically stimulating the RGC axons at the surface of the contralateral eye-cup. For the 3 units studied, one or two locations close to the optic disc of the retina was stimulated (Fig. 4.2a). The Ipc responses exhibited a complex combination of both excitatory and inhibitory currents. The inhibitory response time course was long (200 – 400 ms) while the excitation was relatively short (Fig. 4.2b). The excitatory response also displayed a greater variability in latency.

a **b**

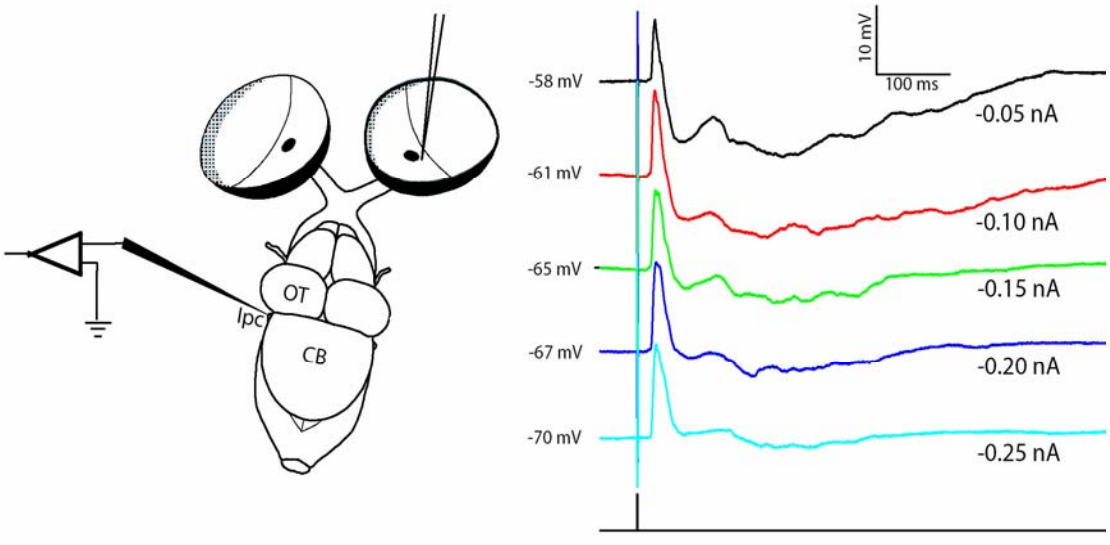

Figure 4.2: Ipc responses to local electrical RGC axon stimulations. (a) Schematic of a dorsal view of the turtle whole-brain preparation with the attached eye-cup for electrical RGC stimulation and whole-cell recordings

from lpc neurons via blind patching. (b) Responses of an lpc neuron at different holding currents to local electrical stimulation of RGCs in the contralateral retina. For clarity, the different color traces are offset and the corresponding resting membrane potentials are indicated at the left of each voltage trace.

4.4.2 Visual responses of lpc neurons

We investigated the lpc responses to simple visual stimulation (i.e. white light spot of ~200 μm diameter) of the retina, which resulted in a combination of excitatory and inhibitory synaptic currents. When different parts of retina were probed by the light spot (Fig. 4.3a), the lpc subthreshold membrane potential responses extended well beyond the area of the visual space where visual stimuli triggered spikes (Fig. 4.3b). Thus the visual stimuli almost anywhere within visual space could modulate the lpc responses both inside and outside the classical receptive field.

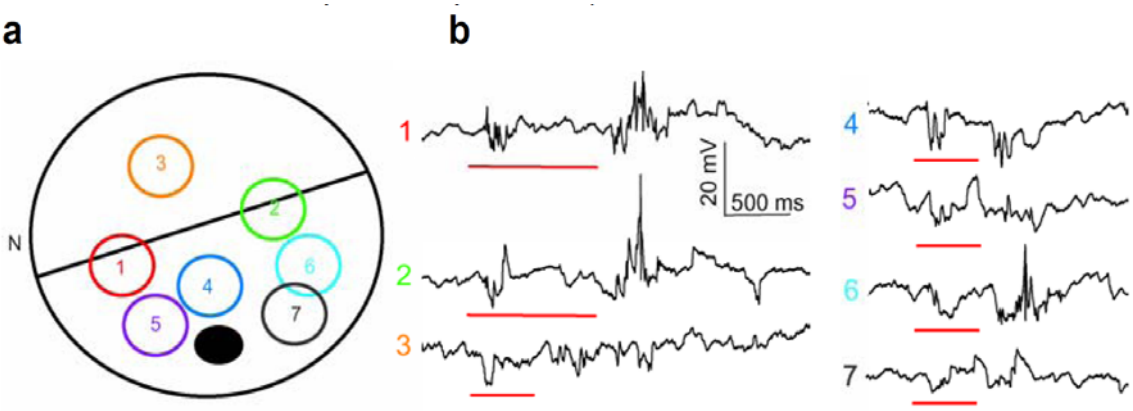

Figure 4.3: Ipc responses to small spots of light flashed onto the retina at different locations. (a) Locations of light spots (200 μm diameter) in the contralateral eye corresponding to the voltage traces in (b). The black line represents the visual streak. The black spot represents the optic disc in the eye. (b) Ipc membrane potential (whole-cell recording) for visual stimulation at different locations of the retina. The red line under each plot corresponds to the stimulus onset and duration. The numbers (color coded) at the left hand side of each plot correspond to the location of light spot shown in (a).

We recorded from 14 Ipc neurons while stimulating the retina with a small white light spot (Fig. 4.4a). Although the responses were quite complex and not fully quantified, there were patterns that worth notifying. Almost all Ipc neurons responded to both the onset and offset of the flashing stimuli (Fig. 4.4b). The response latency varied between few hundred milliseconds. For all the units studied, the Ipc responses were predominantly inhibitory with a longer time course. Excitatory responses were brief and occurred in many cases multiple times with widely varying latencies. When the synaptic currents due to optical stimulation were investigated using voltage-clamp technique (Fig. 4.4b), it resulted in predominantly inhibitory currents with lots of structure in the current response profile, indicating possible presence of multiple currents shaping the Ipc visual response properties.

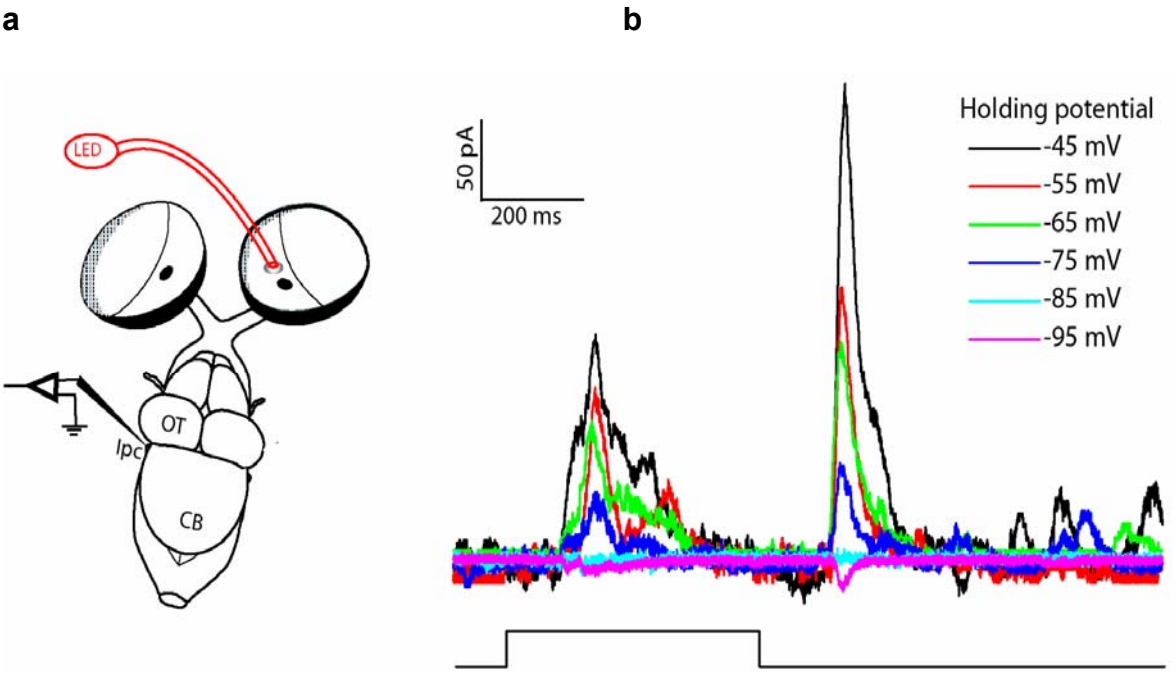

Figure 4.4: Synaptic currents in an lpc neuron in response to a small flash of light. (a) Schematic of a dorsal view of the turtle whole-brain preparation with the attached eye-cup and whole-cell recordings from an lpc neuron via blind patching. A flash of light of 500 ms duration is generated with a computer-controlled LED. The light is projected to specific location on the retina via a single optic fiber of 200 µm diameter which generates a spot of light of similar dimension. (b) Synaptic currents recorded in voltage clamp for different holding potentials. Each trace is an average of 3 trials and smoothed by averaging within a 0.5 ms sliding window. For this stimulus location, the recorded lpc neuron received inhibitory current, which is an outward current that makes membrane potential more negative (hyperpolarized). For this stimulation, the lpc neuron apparently gets input from an ON pathway and an OFF pathway.

4.4.3 Balanced excitation and inhibition in Ipc due to optic nerve stimulation

To gain insight into the complex response properties of Ipc neurons to visual and retinal stimulation, we investigated the Ipc responses to electrical stimulation of the optic nerve. By stimulating the optic nerve, we stimulated all the visually responsive neurons in the upstream pathway including the SGP neurons in tectum, which in turn, excited the Ipc neurons. The advantage of using this technique was to avoid the complex processing of visual images in turtle retina to gain insight into the role of isthmotectal connections in generating the observed excitatory and inhibitory synaptic currents in Ipc neurons. The excitatory pathway to the Ipc neurons originates from the tectal SGP neurons and the inhibitory pathway originates in the isthmic Imc neurons. These two input neurons to the Ipc are further distinguished by the structure of their dendrites and thus their expected receptive fields (Fig. 4.1) (Sereno and Ulinski 1987). In conclusion, the cholinergic Ipc neurons receive topographic glutamatergic inputs from the SGP neurons and largely nontopographic GABAergic inputs from the Imc neurons. The turtle Ipc neuron is thus well suited for establishing general principles of how balanced excitatory and inhibitory synaptic currents may act as a mechanism for visual processing.

We recorded from 14 Ipc neurons responding to the optic nerve stimulation. All neurons responded with a combination of excitatory and inhibitory post synaptic potentials. The inhibition was long (100 – 300 ms) while the short excitatory impulses appeared with variable latencies.

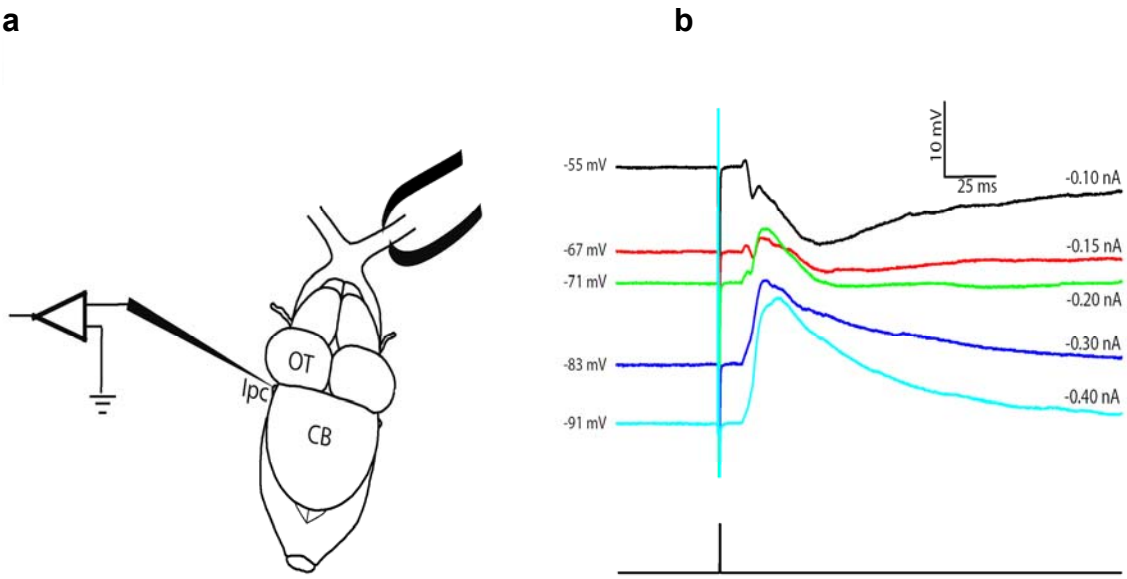

Figure 4.5: Responses of an Ipc neuron to contralateral optic nerve stimulation for different holding currents. (a) Schematic of a dorsal view of the turtle whole-brain preparation with the attached optic nerve inside a suction electrode (top right) for electrical stimulation. We achieve whole-cell recordings from Ipc (electrode shown) neurons via blind patching. (b) Single-pulse optic nerve electrical stimulation resulted in a brief depolarization followed by a long hyperpolarization. Recordings were obtained for different holding currents. Each trace represents an average of three trials.

To estimate the two synaptic currents from the measured lpc voltage responses to optic nerve stimulation (Fig. 4.5b), we constructed a conductance based point model of an lpc neuron with passive ion channels and two synapses, mediated by GABA and glutamate. The simplest model satisfied the equations: $\tau_m \frac{dV}{dt} = I_L + I_{hold} + I_{Glut} + I_{GABA}$ with the leak current, $I_L = g_L(V - E_L)$. The synaptic currents were $I_{Glut} = g_{Glut}(t)(V - E_{Glut})$ and $I_{GABA} = g_{GABA}(t)(V - E_{GABA})$, where the time course of the synaptic conductance change was modeled by the alpha function $g(t) = \bar{g}\frac{t-\Delta}{\tau}\exp(-(t-\Delta-\tau)/\tau)$, such that the conductance $g(t)$ equals the maximum conductance, $g(\Delta+\tau) = \bar{g}$, at time τ after the onset time Δ. The set of coupled equations was solved using SCIPY ordinary differential equation solver function (*odeint*) and verified with NEURON simulation package.

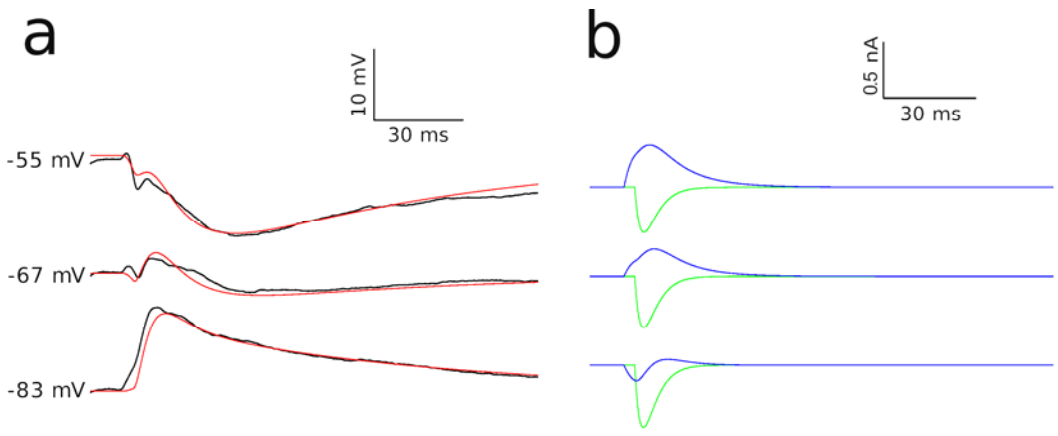

Figure 4.6 Model simulation of the synaptic currents underlying the recorded lpc responses to contralateral optic nerve stimulations. (a) Recorded (black) (same as in Fig. 4.5b) and simulated (red) voltage

responses. Single-pulse optic nerve stimulation resulted in a brief depolarization followed by a long hyperpolarization. Recordings were obtained for different holding currents. Each trace represents an average of three trials. (b) The two synaptic currents with reversal potential at -79 mV (blue) and 10 mV (green) that generate the corresponding simulated voltage responses in (a). Because of the large membrane time constant, the duration of the voltage response is much longer than the duration of the synaptic current.

A subset of model parameters was determined independently. From the voltage response to hyperpolarizing current injection (-0.02 nA) into the Ipc soma (e.g. Fig. 3.2a) we estimated the leak conductance $g_L = 3\,\text{nS}$ and the membrane time constant $\tau_m = 90\,\text{ms}$. The reversal potential $E_{GABA} = -79\,\text{mV}$ was estimated from the Ipc response to Imc stimulation (Fig. 4.7b). The reversal potential for the glutamate synapse was assumed to be $E_{Glut} = 10\,\text{mV}$. All other parameters were varied, following standard fitting procedures, such that one set of parameters would best fit the voltage responses for all 5 holding currents (Fig. 4.5b), of which 3 representative examples are shown in Fig. 4.6a. The resulting parameter values are $\Delta_{Glut} = 14.5\,\text{ms}$, $\tau_{Glut} = 3$ ms, and $\bar{g}_{Glut} = 0.006\,\mu\text{S}$ for the Glutamate synapse and $\Delta_{GABA} = 11\,\text{ms}$, $\tau_{GABA} = 8.5$ ms, and $\bar{g}_{GABA} = 0.0175\,\mu\text{S}$ for the GABA synapse. This simulation showed that near rest (e.g. -55 mV) the two synaptic currents were approximately equal in amplitude and were of opposite signs. It is largely the difference in time course that resulted in a nonzero (but small) net

current, which caused the voltage response; a classic example of balanced excitation and inhibition.

4.4.4 The Imc to Ipc synaptic connection is inhibitory

Crucial for our understanding of the functioning of the isthmotectal loop is knowledge about the Imc-to-Ipc synaptic connections. Imc neurons receive broad tectal input and innervate the Ipc nucleus, and thus are well-suited to provide large-field inhibition to Ipc neurons. To test this possibility, we conducted whole-cell blind-patch recordings from the Ipc neurons while stimulating the Imc axons in the deep tectal layers. A stimulus electrode (red vertical line, Fig. 4.7a) was lowered into deep tectal SGC layers (~500 μm below the surface) to stimulate Imc axons antidromically. The resulting Imc spikes traveled from the optic tectum to the Imc and continued to the Ipc. Because of the broad and dense Imc projection pattern, a recorded Ipc neuron (blue dot) had a high probability of receiving synaptic inputs from the stimulated Imc axons (see Fig. 4.7a). To avoid direct axon stimulation of the recorded Ipc neuron or SGP neurons, the topography of Ipc-tectum projection was taken into account (Sereno and Ulinski 1987) and recordings were made from the dorso-lateral part of the Ipc nucleus while stimulating the rostro-medial tectum. Our recordings of Ipc voltage responses (n = 9 cells) revealed large and long-lasting (200 - 400 ms) inhibition in response to Imc axon stimulation. In one cell, the deep tectal stimulation showed long inhibition along with short excitation, which is consistent with stimulation of both GABAergic Imc and glutamatergic SGP neurons in deep

tectal layers. To determine the source of this inhibitory current, current-clamp experiments were conducted (Fig. 4.7b). The inhibitory post synaptic potential due to Imc stimulation reversed around -79 mV (Fig. 4.7b, bottom). To verify pharmacologically whether this inhibitory current was generated by GABA, we applied bicuculline (50 µM) to the bath medium. This resulted in a long-lasting spiking activity in the Ipc neuron (Fig. 4.7c), which might be the result of blockade of all inhibitory currents in tectum. Intracellular picrotoxin application (n = 2 cells) was also inconclusive as the cells stopped spiking within 15 min. of patching (data not shown).

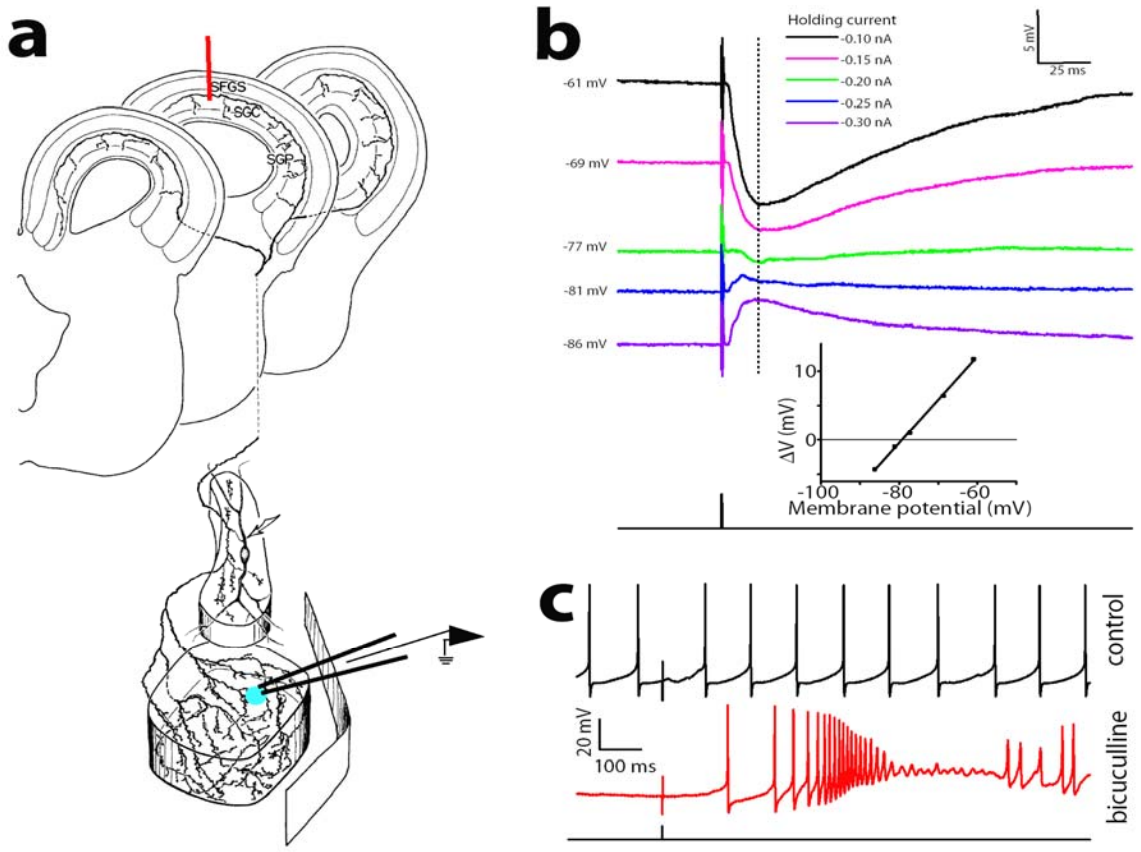

Figure 4.7: Synaptic response of an Ipc neuron to Imc axon stimulation. (a) The GABAergic Imc neuron axon splits into two major branches. One branch projects nontopographically to the Ipc nucleus. The other branch

projects nontopographically to tectal layers SGC and SGP (Sereno and Ulinski 1987). The two isthmic nuclei have been enlarged relative to the tectum for clarity. The axon split and the broad projection pattern allows for Imc stimulation via its axons in the tectum. A stimulus electrode (red vertical line; concentric bipolar tungsten electrode, tip diameter = 4 μm; core diameter = 76 μm) is lowered into deep tectal SGC layers (500 μm) for antidromic electrical stimulation of Imc axons. The generated Imc spikes travel from the OT to the Imc and continue into the Ipc nucleus. Because of the broad and dense Imc projection pattern, a recorded Ipc neuron (blue dot) has a high chance to receive synaptic inputs from the stimulated Imc axons. (b) Single pulse stimulation (0.5 ms, 200 μA) resulted in a long-lasting postsynaptic potential (PSP). Recordings were obtained for five different holding currents corresponding to membrane potentials between -61 and -86 mV. Each trace represents an average of three trials. The vertical dotted line (18 ms after the stimulus pulse) represents the time at which the membrane potential was measured. Inset: The peak amplitude of the PSP, ΔV, was measured as the difference between the membrane potential at the holding current and the membrane potential at 18 ms after the stimulus pulse. The PSP peak amplitude increases linearly with increasing membrane potential and reverses sign at -79 mV. (c) For a different Ipc neuron that was spontaneously spiking the Imc axon stimulation via the tectal electrode caused an IPSP and an increase in the interspike interval (control). Approximately 5 minutes after switching to

perfusion with 50 μM bicuculline the response to tectal stimulation changed to delayed and long-lasting spike activity.

4.4.5 Synaptic currents in Ipc neurons due to Imc and tectal neuron stimulation

To gain insight into the synaptic currents underlying the Ipc response properties, voltage-clamp recordings were made while stimulating deep tectal Imc axons and surface tectal neurons. Anatomical studies have shown that the RGC inputs terminate in the superficial layer of the tectum and overlap with SGP neuron dendrites (Fig. 4.1a, d). Stimulation of superficial tectal neurons allowed us to directly stimulate the SGP to Ipc pathway. Since SGP neurons excite both Imc and Ipc neurons, this surface tectal stimulation resulted in both excitatory and inhibitory currents in Ipc, as expected. To stimulate the inhibitory pathway separately, Imc stimulation was done in the same way as mentioned in SECTION 4.4.4 (Fig. 4.7a). The goal of this experiment was to test both SGP to Ipc and Imc to Ipc pathway, separately and obtain the synaptic currents generated in Ipc due to these stimulations, which might help understand the role of excitation and inhibition in Ipc visual response properties.

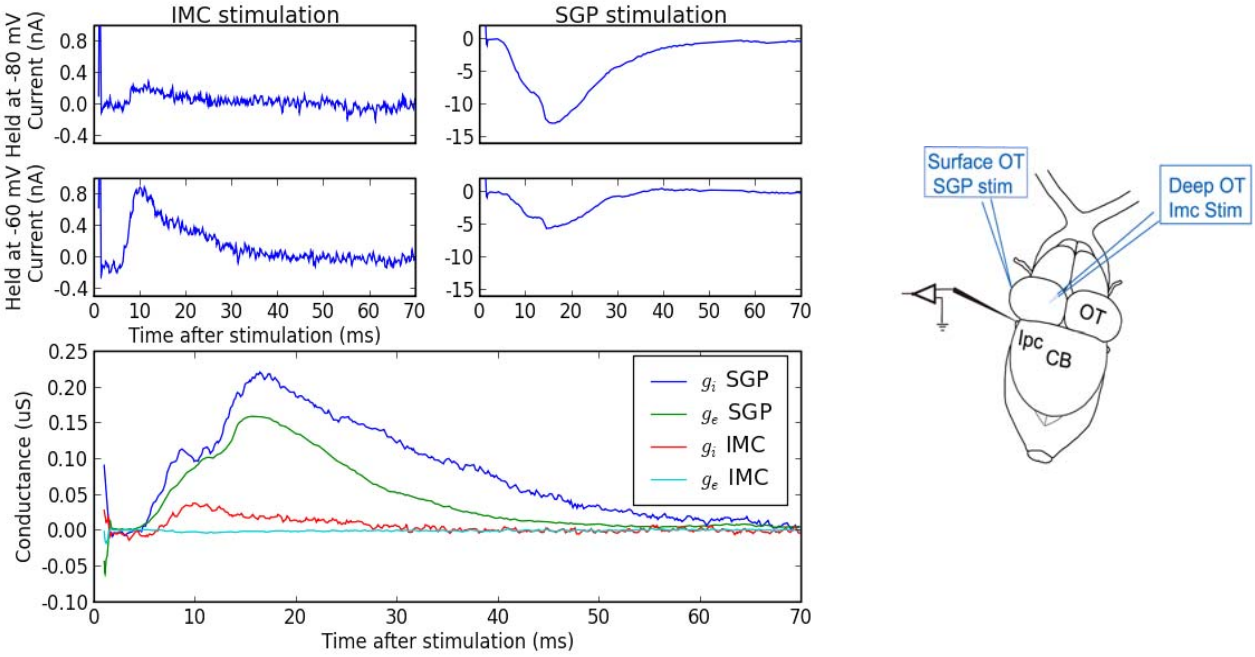

Figure 4.8: Synaptic currents recorded at Ipc due to deep tectal (Imc → Ipc) and surface tectal (SGP → Ipc) stimulation. *Right*, Schematic of stimulation. Deep tectal (500 µm from pial surface) electrode stimulates Imc axon in tectum, which in turn, inhibits Ipc. Surface electrode stimulates SGP neuron in tectum. *Top left, (4 panels)*, synaptic currents due to Imc and SGP stimulation at two different holding potential. Outward current represents an inhibitory current. *Bottom left*, Synaptic conductances underlying these currents. Reversal potential for inhibitory current and excitatory currents are -79 mV and 0 mV respectively.

In this analysis, the resulting synaptic currents in the Ipc neuron due to the Imc and SGP neuron stimulations were assumed to be a combination of an excitatory and an inhibitory current, which summed to give the total synaptic current,

$$I_{total}(t) = g_e(t)(V(t) - E_e) + g_i(t)(V(t) - E_i)$$

where $I_{total}(t)$ is the total synaptic current at time *t*, and $g_e(t)$, $g_i(t)$ represent the synaptic conductance and E_e, E_i represent the reversal potentials for excitatory and inhibitory currents, respectively. To find the conductances for individual synaptic currents, this equation was fit to the total synaptic currents at two holding potentials for both stimulations. The excitatory and inhibitory synaptic conductances for SGP stimulation (g_eSGP, g_iSGP respectively) turned out to be slightly different in time course. The Imc synaptic conductance was mainly inhibitory (g_eIMC) and shorter in time scale compared to the SGP stimulation (Fig. 4.8). According to isthmotectal connections (Fig. 4.1d), Imc neurons are likely candidate for generation of the inhibitory currents either directly (Imc→Ipc) or indirectly (SGP→Imc→Ipc) in both the stimulations. In the two different stimulation paradigms, the difference in inhibitory current (g_iIMC, g_iSGP, Fig. 4.8) may be attributed to the different numbers of activated Imc neurons, which in turn produce different amount of inhibition in the Ipc neuron.

4.5 Discussion

4.5.1 Balance excitation and inhibition

We have found that the Ipc responses to visual stimulation is quite complex. Intracellular recordings from the Ipc neurons revealed interplay of excitatory and inhibitory synaptic inputs in response to white stationary flashes anywhere in the visual field (Fig. 4.3). This indicates that the response of an Ipc neuron could be influenced by inputs far outside its classical receptive field. Since turtle retina

itself is able to do complex processing of visual inputs (Bowling 1980, Granda 1989), the results obtained by visual stimulation is difficult to interpret. An approach was taken to test the retina → tectum → Ipc circuitry piecewise by electrically stimulating the optic nerve, which eliminated the complexity introduced by retina. The optic nerve stimulation revealed interplay of two synaptic inputs in the Ipc neurons. The generation of a small net current through the difference of two much larger synaptic currents of similar amplitudes but opposite signs has been a long-standing puzzle in neuroscience. The mechanisms to shift this balance of synaptic excitation and inhibition include differential activity of the presynaptic neurons, differential timing of the inputs (Wehr and Zador 2003; Wilent and Contreras 2005; Gabernet et al. 2005; Cruikshank et al. 2007; Hull and Scanziani 2007), and differential synaptic dynamics (Higley and Contreras 2006; Klyachko and Stevens 2006). Here, we have found that the Ipc response pattern to optic nerve stimulation can be generated with just two synapses, mediated by GABA and glutamate (Fig. 4.6), which is consistent with the anatomy of the turtle isthmotectal circuitry (Fig. 4.1d). Although, the two synaptic currents turned out to be almost equal in amplitude, their different time-course resulted in the observed response in Ipc neurons. The observation that the inhibition occurs before the excitation is surprising, given that the synaptic inhibition arrives from Imc is delayed by an additional synapse. One possibility is that the SGP neurons respond with pairs of spikes and the Ipc neuron responds weakly to the first spike and stronger to the second spike, whereas the Imc neuron immediately responds with a spike, which in turn arrives

at the Ipc neuron before the arrival of the second SGP spike. Another possibility is that the tectal projections to the Ipc and Imc nuclei are mediated by two different populations of SGP neurons, one slow and another fast, respectively.

4.5.2 Possible role of Imc in creating the Ipc response properties

Ipc responses to visual stimulation or optic nerve stimulation resulted in both excitatory and inhibitory synaptic currents. To find the likely source of the inhibition, we tested the Imc to Ipc synaptic connection. We have found that the Imc to Ipc synaptic connection is inhibitory and the reversal potential of inhibitory post synaptic potential (IPSP) is consistent with a GABAergic synapse (Fig. 4.7b). The Imc neurons receive input from the SGP neurons and project nontopographically to the whole Ipc nucleus as well as to deep tectal layers (Sereno and Ulinski 1987). Considering these features of the isthmotectal circuitry, one explanation of the Ipc response properties is as follows. The retinotopic inputs coming from RGCs to a tectal SGP neurons generate activity which spreads laterally in the SGP layer through gap junctions. With more SGP activity, connected Imc neurons which inhibit the whole Ipc nucleus overwhelm the excitation from the SGP cells since this excitation is localized (Fig. 4.9). Thus, even a small stimulus in the visual field should result in excitatory and inhibitory currents in the Ipc neurons, which would control the Ipc activity within a narrow temporal window. As the stimulus grows larger, more and more Imc neurons are activated and thereby generating stronger inhibition resulting in little or no Ipc spiking responses to whole-field stimuli. The Imc neurons have thick,

myelinated axons (4-6 μm in diameter) (Serino and Ulinski 1987), which can generate very high conduction speed and overcome one synaptic delay and reach lpc faster than direct excitatory input from SGP neurons. Thus, the GABAergic lmc neurons in turtle have the ability to inhibit the lpc neurons when excited simultaneously by the SGP neurons in visual pathway.

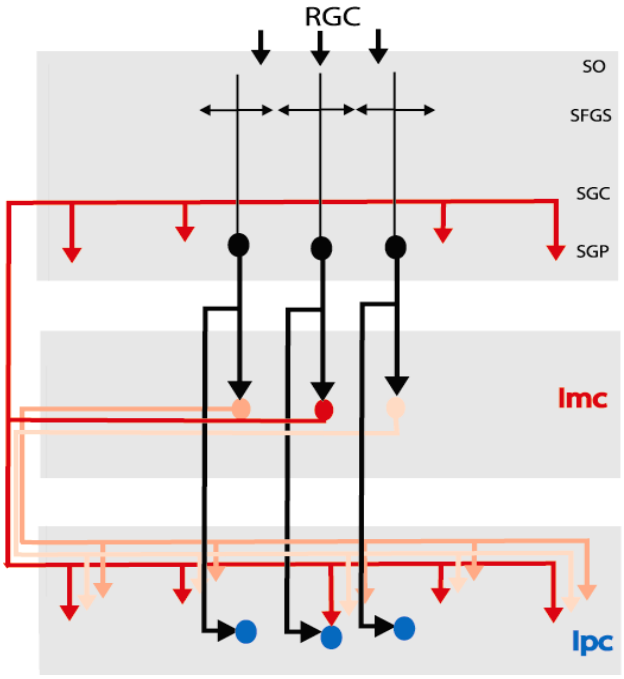

Figure 4.9: Illustration of a possible mechanism of inhibition in lpc neurons by the lmc neurons. SGP neurons (black) receive RGC inputs in their apical dendrite in superficial layer (SO). SGP neurons form dendro-dendritic synapses in SFGS layer (horizontal black arrow) and gap junctions (not shown), which can spread the SGP activity horizontally. Thus any stimuli, however small, stimulate multiple SGP neurons and in turn activate large number of lmc neurons (3 neurons with different shades of red), which inhibit every lpc neuron (blue) through their broad nontopographic projection.

In birds, it has been suggested that long distance suppression in the Ipc neurons is mostly mediated by the Imc neurons (Marin et al. 2007). Other studies show that the Imc neurons in birds have elongated excitatory receptive fields, much larger than the circular Ipc ERFs (Li et al. 2007), which makes broad field Imc neurons ideally suited to generate inhibition in the Ipc neurons. Similarly, tectal processing may also contribute to the Ipc neuron's response properties.

4.6 References

Abbott LF, Chance FS (2005) Drivers and modulators from push-pull and balanced synaptic input. Progress in Brain Res 149: 147-155.

Bowling DB (1980) Light responses of ganglion cells in the retina of the turtle. J Physiol 299: 173-196.

Cano M, Bezdudnaya T, Swadlow HA, Alonso JM (2006) Brain state and contrast sensitivity in the awake visual thalamus. Nature Neurosci 9: 1240-1242.

Chance FS, Abbott LF, Reyes AD (2002) Gain modulation from background synaptic input. Neuron 35: 773-782.

Cruikshank SJ, Lewis TJ, Connors BW (2007) Synaptic basis for intense thalamocortical activation of feedforward inhibitory cells in neocortex. Nature Neurosci 10: 462-468.

Ferster D, Miller K (2000) Neural mechanisms of orientation selectivity in the visual cortex. Annu Rev Neurosci 23: 441-471.

Gabernet L, Jadhav SP, Feldman DE, Carandini M, Scanziani M (2005) Somatosensory integration controlled by dynamic thalamocortical feed-forward inhibition. Neuron 48: 315-327.

Granda AM, Fulbrook JE (1989) Classification of turtle retinal ganglion cells. J Neurophysiol 62: 723-737.

Hirsch JA, Martinez LM, Pillai C, Alonso JM, Wang Q, Sommer FT (2003) Functionally distinct inhibitory neurons at the first stage of visual cortical processing. Nature Neurosci 6: 1300-1306.

Higley MJ, Contreras D (2006) Balanced excitation and inhibition determine spike timing during frequency adaptation. J Neurosci 26: 448-457.

Hull C, Scanziani M (2007) It's about time for thalamocortical circuits. Nature Neurosci 10: 400-402.

Izhikevich EM, Edelman GM (2008) Large-scale model of mammalian thalamocortical systems. PNAS 105: 3593-3598.

Klyachko VA, Stevens CF (2006) Excitatory and feed-forward inhibitory hippocampal synapses work synergistically as an adaptive filter of natural spike trains. PLoS Biol 4: 1187-1200.

Kunzle H, Schnyder H (1984) The isthmus-tegmentum complex in the turtle and rat: a comparative analysis of its interconnections with the optic tectum. Exp Brain Res 56: 509-522.

Li DP, Xiao Q, Wang SR (2007) Feedforward construction of the receptive field and orientation selectivity of visual neurons in the pigeon. Cereb Cortex 17: 885-893.

Marin G, Salas C, Sentic E, Rojas X, Letelier JC, Mpodozis J (2007) A cholinergic gating mechanism controlled by competitive interactions in the optic tectum of the pigeon. J Neurosci 27: 8112-8121.

Marino J, Schummers J, Lyon DC, Schwabe L, Beck O, Wiesing P, Obermayer K, Sur M (2005) Invariant computations in local cortical networks with balanced excitation and inhibition. Nature Neurosci 8: 194-201.

Powers AS, Reiner A (1993) The distribution of cholinergic neurons in the central nervous system of turtles. Brain Behav Evol 41: 326-345.

Priebe NJ, Ferster D (2005) Direction selectivity of excitation and inhibition in simple cells of the cat primary visual cortex. Neuron 45: 133-145.

Sereno MI, Ulinski PS (1987) Caudal topographic nucleus isthmi and the rostral nontopographic nucleus isthmi in the turtle, *Pseudemys scripta*. J Comp Neurology 261: 319-346.

Wang Y, Luksch H, Brecha NC, Karten HJ (2006) Columnar projections from the cholinergic nucleus isthmi to the optic tectum in chicks (*Gallus gallus*): A possible substrate for synchronizing tectal channels. J Comp Neurol 494: 7-35.

Wang Y, Major DE, Karten HJ (2004) Morphology and connections of nucleus isthmi pars magnocellularis in chicks (Gallus gallus). J Comp Neurol 469: 275-297.

Wehr M, Zador AM (2003) Balanced inhibition underlies tuning and sharpens spike timing in auditory cortex. Nature 426: 442-446.

Wilent WB, Contreras D (2005) Dynamics of excitation and inhibition underlying stimulus selectivity in rat somatosensory cortex. Nat Neurosci 8: 1364-1370.

Chapter 5

VISUAL RESPONSE PROPERTIES OF A CHOLINERGIC NEURON IN TURTLE NUCLEUS ISTHMI

5.1 Abstract

The optic tectum (superior colliculus) holds a central position within the major visual pathway of most vertebrate species and is reciprocally connected with the nucleus isthmi. Isthmic activity modulates tectal visual processing, yet a systematic investigation of isthmic visual response properties is still lacking. Here, we recorded spikes from individual nucleus isthmi pars parvocellularis (Ipc) neurons in the turtle eye-attached whole-brain preparation in response to a range of computer-generated visual stimuli. Ipc neurons responded to a variety of moving or flashing stimuli as long as those stimuli were small. In the spectrum of visual stimuli tested, a small moving spot of negative contrast (dark spot on bright background) elicited the strongest response, whereas a whole-field sinusoidal drifting grating elicited the weakest response. When mapped with a moving spot, the excitatory receptive field was of circular Gaussian shape with an average half-width of less than 3 deg. We found no evidence for directional sensitivity. For moving spots of varying sizes, the measured Ipc response-size profile was reproduced by the linear Difference-of-Gaussian model, which is consistent with the superposition of a narrow excitatory center and a broad surround inhibition. Intracellular Ipc recordings revealed a strong inhibitory connection from the nucleus isthmi pars magnocellularis (Imc), which has the anatomical feature to provide a broad inhibitory projection. The recorded Ipc response properties,

together with the Ipc modulatory role in tectal visual processing, suggest that the columns of Ipc axon terminals in turtle optic tectum bias tectal visual responses to small dark changing features in visual scenes.

5.2 Introduction

The nucleus isthmi (parabigeminal nucleus) is a visually responsive midbrain structure in vertebrates (Sherk 1978, 1979a; Yan and Wang 1986; Northmore 1991; Wang and Frost 1991; Wiggers and Roth 1991; Cui and Malpeli 2003; Northmore and Gallagher 2003; Gallagher and Northmore 2006; Maczko et al. 2006; Li et al. 2007; Caudill et al. 2010) that influences visual processing by direct modulation of tectal circuits (Wang et al. 1995; Wang et al. 2000; Wang 2003; Winkowski and Gruberg 2002; Dudkin and Gruberg 2003; Marin et al. 2007). This modulation is mediated by reciprocal connections between nucleus isthmi and optic tectum (Graybiel 1978; Gruberg and Udin 1978; Sereno and Ulinski 1987; Powers and Reiner 1993; Wang et al. 2004, 2006).

The turtle magnocelleular isthmic complex contains two cytoarchitectonically distinct isthmic nuclei (Fig. 4.1d), which receive sensory information from the ipsilateral optic tectum (Sereno and Ulinski 1987; Powers and Reiner 1993). Consistent with the nomenclature used in the avian isthmotectal system (Wang et al. 2004, 2006), we refer to the two isthmic nuclei as the pars parvocellularis (Ipc) and the pars magnocellularis (Imc). Retinal ganglion cell (RGC) axons terminate in the superficial layers of the tectum (Fig. 4.1a), where they innervate

the radial, narrow dendrites of the tectal stratum griseum periventriculare (SGP) neurons (Schechter and Ulinski 1979). The axons of SGP neurons project to the Ipc and Imc nuclei (Kunzle and Schnyder 1984). In the Imc nucleus, neurons have large, sparsely branched dendritic fields overlapped by local axon collaterals. The axons of Imc neurons nontopographically project to both the deeper layers of the tectum and to the Ipc nucleus (Sereno and Ulinski 1987). In the Ipc nucleus, neurons have medium-sized, elongated somata, flattened bipolar dendritic fields, and axons that project topographically back to the tectum. Each Ipc axon terminates as a compact swarm of boutons within a cylinder about 150 μm in diameter and 400 μm tall, placed mainly in the upper tectal layers, where it spans less than one percent of the tectal surface (Sereno and Ulinski 1987). The topographically-organized, columnar Ipc axon terminals spatially overlap with the RGC axons and the SGP neuron dendrites.

Cholinergic isthmic neurons (turtle: Desan et al. 1984; Powers and Reiner 1993; frog: Gruberg and Udin 1978; Winkowski and Gruberg 2002; Dudkin et al. 2007; bird: Sorenson et al. 1989; Medina and Reiner 1994; mammal: Graybiel 1978; Sherk 1979b; Hall et al. 1989) provide a major source of acetylcholine (ACh) to the optic tectum (superior colliculus). Although the cholinergic neurons are hypothesized to be modulators of tectal activity (Goddard et al. 2007), the information represented in the spatiotemporal pattern of ACh release is largely unknown. In general, the extensive studies of cholinergic modulation in the brain have focused largely on the postsynaptic effect of ACh release (McCormick

1993; Metherate 2004; Lucas-Meunier et al. 2003, 2009). Cholinergic Ipc neurons, being visually responsive and reciprocally connected exclusively to the tectum, are an ideal system to study both spatiotemporal pattern of ACh release and its postsynaptic effect on tectal neurons. While this study does not address postsynaptic effects of ACh in optic tectum, an understanding of the visual responses of Ipc neurons is a necessary first step in the direction of correlating visual stimulation with spatiotemporal ACh release.

To investigate the visual response properties of the Ipc, we conducted extracellular recordings from Ipc neurons during visual stimulation in the contralateral retina (Fig. 5.1) in a turtle eye-attached whole-brain preparation (Kriegstein 1987; Rosenberg and Ariel 1990). We presented a wide variety of visual stimuli (see METHODS) and found that the Ipc responds strongly to small stimuli preferably dark compared to the background. Ipc responses to static stimuli show significant temporal adaptation. For dynamic stimuli the Ipc responses are tuned to stimulus size and speed, with no directional preference.

5.3 Methods

5.3.1 Set-up and techniques for extracellular recording and visual stimulation

Extracellular recordings from the Ipc neurons were achieved in an eye-attached whole-brain preparation. 9 adult red-ear turtles (Trachemys scripta elegans, 12-15 cm carapace length) were used in this study. Following the surgery (see

SECTION 2.1), the preparation was transferred to the superfusion chamber positioned on an air table with the eye-cup beneath a focusing lens. The preparation was bathed in physiological media (in mM; 85 NaCl, 2 KCl, 2 $MgCl_2$, 45 $NaHCO_3$, 20 D-glucose, 3 $CaCl_2$ bubbled with 95% O_2 and 5% CO_2), adjusted to pH 7.4 at room temperature.

Extracellular recordings from Ipc neurons were achieved with tungsten microelectrodes of 1 MΩ impedance (see details in SECTION 2.4). Since the Ipc nucleus is a surface structure, its location was identified by a characteristic protrusion just caudal of the optic tectum (Fig. 5.1). To find a responsive recording site, the microelectrode was advanced smoothly into the Ipc nucleus while the search stimulus (multiple small moving black spots, see SECTION 2.5.2) was focused on the retina of the contralateral eye-cup. Visual stimuli were created by a computer and delivered with an LCD monitor (see SECTION 2.5), which was projected onto the retinal surface of the hemisected eye-cup with a converging lens system (Fig. 5.1). A monitor pixel corresponded to 7 μm on the retina or ~0.08^{o} of visual angle (Northmore and Granda 1991; Ariel and Kogo 2001). Stimuli were created using *psychopy*, an open-source psychophysics module written for the Python programming language (Peirce 2008). Software tools were written to allow the experimenter to characterize the projection of the computer screen onto the retina. A computer game pad was used to control the measurements of size and position of the eye-cup interactively, relative to the monitor. The eye-cup parameters, including the position and orientation of the

visual streak, and the size and position of the optic disk were documented. An image based on these parameters (Fig. 5.1, bottom inset) overlaid on the eye-cup preparation (in the recording chamber) when projected through the focusing system. The next step was to set the stimulation coordinate system such that the visual stimuli could be presented independently of the particulars of each monitor-to-eye-cup projection setup. We achieved this by finding the responsive area of an lpc neuron to a small moving black spot stimulus and then setting the stimulus coordinate (see SECTION 2.5.3), which was about twice the size of the active area and oriented parallel to the visual streak (white square in Fig. 5.1, bottom inset). All experimental stimuli were subsequently scaled and rotated using this normalized stimulation coordinate system, which was set same way for all the experiments. The nasal retina or temporal visual field parallel to the visual streak was defined 0^o (180^o) in the right (left) eye. The superior and inferior visual fields were defined as 90^o and 270^o, respectively in both eyes. During an experiment, stimuli were shown time-locked with the data acquisition (see SECTION 2.5.4). The *psychopy* codes maintained sub-millisecond frame-rendering precision. Interstimulus intervals of at least 30 s were maintained between different sets of stimuli. The voltage traces were passed through a 300 - 5000 Hz analog band pass filter and then sampled at 10 kHz using a LabView-controlled data acquisition system.

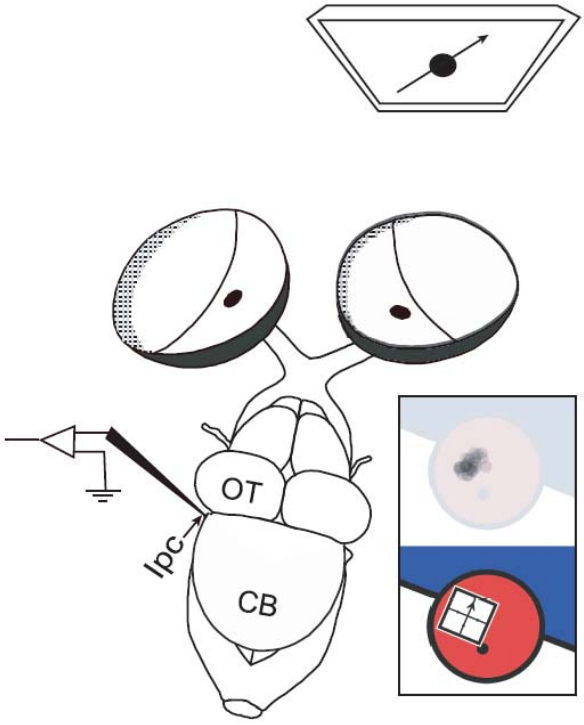

Figure 5.1 Schematic drawing of a dorsal view of the turtle whole-brain preparation with the eye-cups attached and the telencephalon removed. Computer-generated visual stimuli are presented on a monitor (moving black spot) and are projected with appropriate optics (not shown) onto the retinal eye-cup. Surface landmarks guide the placement of microelectrodes for extracellular and blind-patch whole-cell recordings from lpc. Inset: The monitor-to-eye-cup projection and the presentation of visual stimuli. Top, evaluating a responsive area in the visual field with small moving spot stimuli. Bottom, defining a stimulation coordinate system (white square) covering the entire responsive area.

5.3.2 Visual stimulation protocol

To study the Ipc visual response properties to different stimuli, 7 different types of stimuli were used. S1) Black moving spot on white background – A small spot of diameter 6 - 8^{o} moved at about 6 - 8^{o}/s radially through the center of the stimulation coordinates in 8 directions (0, 45, …, 315 degrees relative to the visual streak) pseudo randomly. There was ≥ 500 ms wait between different directions being presented within the stimulus set. S2) White moving spot on black background – This set of stimuli was identical to stimulus S1 except that the contrast was inverted. S3) Black leading edge on white background – A bar moved along its long axis so that only the leading edge crossed the screen. The short axis was the same size as the diameter of spots in stimuli S1 and S2, likewise for the speed. S4) Randomly changing check pattern – The stimulation coordinate system was divided into a 4x4 grid, and each grid space pseudo-randomly displayed white or black with equal probability. Each grid space (check) was about 8 deg square. All 16 checks were updated every 10 frames (168 ms). This stimulus was displayed for 25 seconds. S5) Drifting sinusoidal grating – A grating was displayed with motion perpendicular to the visual streak. The spatial frequency was 0.02 cycles/deg, and the temporal frequency was 1 Hz. The stimulus was displayed for 25 seconds. S6) Flashing black spot on white background – A small spot of diameter 6 - 8^{o} was displayed for 5 seconds in the center of the stimulation coordinate system. S7) Whole screen flash from white to black – The entire screen was set to display black for 5 seconds. Note

that except for S2, the computer screen background was white before and after the trials of stimuli.

5.3.3 Extracellular data analysis

To determine the number of active units at the recording site, sample recordings were analyzed with *waveclus*, a spike-sorting algorithm based on spike detection and sorting using wavelets and superparamagnetic clustering (Quiroga et al. 2004). Single-units were isolated using criteria that included a well-defined spike shape with no kinks in the standard deviation of all classified spikes and a refractory period of 2 ms in the interspike interval distribution. Only single-unit responses were used for the analysis. For each experiment we obtained recordings for at least 3 trials, with exceptions noted in the figure captions.

5.3.4 Difference-of-Gaussians analysis The stimulus size-response profile of Ipc neurons were analyzed using the Difference-of-Gaussians (DOG) model (Rodieck 1965; DeAngelis et al. 1994; Sceniak et al. 1999), which assumes the linear and independent sum of two concentric Gaussians, excitatory and inhibitory, yielding the net response to the stimulus. We used moving spots (stimulus S1) of different sizes to study the stimulus size tuning of Ipc neurons. The assumption was made that only the spot's leading edge is generating the Ipc response. With this assumption, for a linear sweep of a moving spot of radius *s*, the net response *R(s)* follows the relation,

$$R(s) = R_0 + K_e \int_{-a/2}^{a/2} e^{-(2x/a)^2} dx \int_{-s}^{s} e^{-(2y/a)^2} dy - K_i \int_{-b/2}^{b/2} e^{-(2x/b)^2} dx \int_{-s}^{s} e^{-(2y/b)^2} dy$$

where the parameters K_e and K_i represent the strength of excitatory and inhibitory receptive fields, respectively, while *a* and *b* represent the spatial extent of excitatory and inhibitory Gaussian receptive fields. The baseline activity R_0 is assumed to be zero due to low (< 1 Hz) spontaneous activity of Ipc units. Notice that the equation is equivalent to one commonly used for flashing spot stimuli of different radius with an additional constant multiplication factor due to the integration of the whole Gaussian profile along one direction.

5.4 Results

5.4.1 Stimulus selectivity

To evaluate to what extent Ipc visual response properties are stimulus specific, we recorded extracellular single-unit responses while showing different stimuli in a pseudo random order to the contralateral eye of the recorded Ipc neuron. A continuously illuminated white screen elicited almost no response (mean = 0.1 Hz, SD = 0.2 Hz, n = 8 units). However, a dark spot (diameter 6 – 8^o) on a white screen moving through the center of the excitatory receptive field of an Ipc neuron at a speed of 6 – 8^o/s elicited strong spiking responses (Fig. 5.2a, 5.4; spike count 23 – 72, n = 5 units).

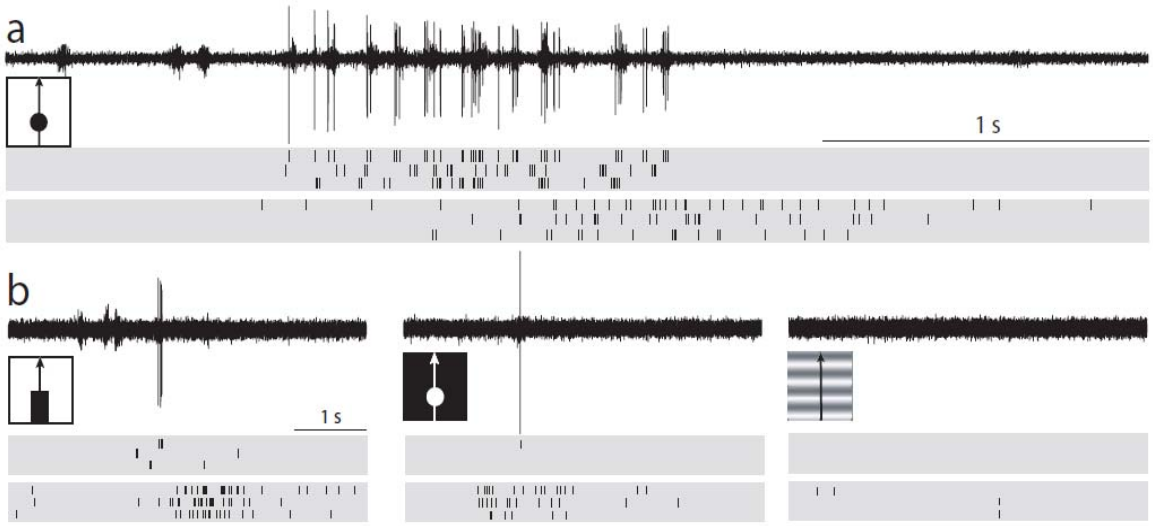

Figure 5.2 Stimulus-selective visual responses of lpc neurons. (a) Responses of two lpc single-units to a black spot moving perpendicular to the visual streak. Schematic of the stimulus is shown at the left of the respective voltage trace. The square box represents the stimulation coordinate system, which covers the entire responsive area of the unit and is aligned parallel to the visual streak. The direction of stimulus movement is indicated by the arrow. Top to bottom, raw voltage trace of one unit, raster of three trials of that unit and raster for another unit. The gray boxes indicate the duration of stimulus movement. Spot diameter: 7°, 8°; speed: 7°/s, 8°/s respectively, for two units. (b) Responses to other moving stimuli for the same units shown in (a). From left to right, moving leading edge, moving white spot (same dimension and speed as of black spot in 3a) and drifting sine grating (spatial frequency 0.02 cycles/deg, temporal frequency 1 Hz).

For all stimuli and lpc units tested, responses are quantified as the average spike count during the first 5 s of stimulus presentation (Fig. 5.3). The lpc response was somewhat reduced when the dark spot was replaced by a moving leading edge of similar width and speed (spike count 17 – 52, n = 4 units) or when a white spot moved on a dark background (spike count 2 – 31, n = 5 units) (Fig. 5.2b, 5.3). Among the tested moving stimuli, the whole-field sinusoidal drifting grating (stimulus S5) elicited the weakest response (spike count 0 – 5, n = 5 units; Fig. 5.2b, 5.3). For stationary stimuli, lpc neurons responded to a whole-field random checkerboard stimulus (spike count 1 – 29, n = 5; Fig. 5.3) and to a small dark spot flashed at the center of the receptive field (spike count 2 – 50, n = 5 units; Fig. 5.4). lpc neurons responded little to whole-field diffuse illumination changes from white to black (spike count 0 – 5, n = 5; data not shown). In conclusion, lpc neurons respond to a variety of moving or flashing stimuli as long as they are small.

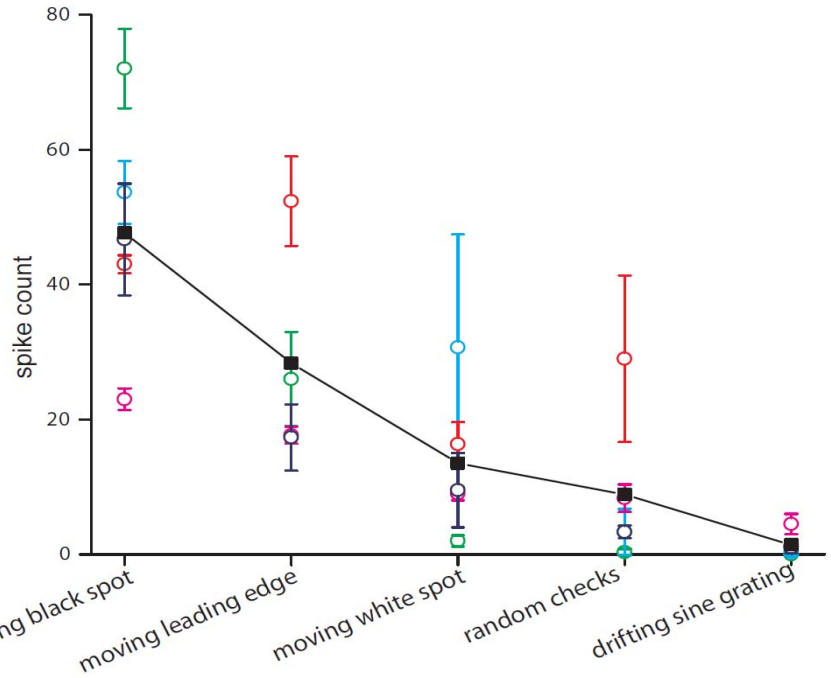

Figure 5.3 Population study of single-unit lpc responses to spatiotemporally changing stimuli. Presented are 5 single-units, collected from 5 sites of 4 different brains. Responses for lpc neurons to different stimuli are quantified by the average spike count, which is the number of spikes for the first 5 s after stimulus onset and averaged over multiple trials. Small moving stimuli; black spot, black leading edge and white spot are presented in the stimulus coordinate system of each unit (S1, S3, S2 respectively, see METHODS). Spot diameter, edge width and speed are kept constant for one unit but varied slightly from unit to unit (spot diameter/edge width 6 - 8°, speed 6 - 8°/s). For each unit the maximum value of average spike count along any one direction (out of 8) is plotted for each small moving stimulus. The cyan unit was not tested for leading edge stimuli. Error bars represent SD for multiple trials (m = 2 for white

moving spot stimulus of blue and magenta units, m = 3 for all others). For broad spatiotemporally changing stimuli; random flashing checkerboard and drifting sine grating (S4, S5), the average spike counts are plotted with the SD values. The black squares indicate the average response of all single-units for any given stimulus. The green and red circles indicate the lpc units shown in Fig. 5.2.

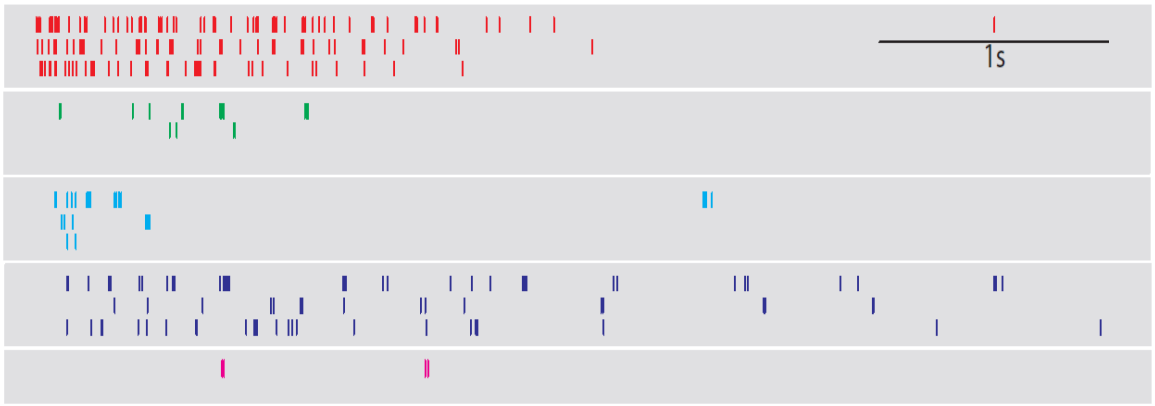

Figure 5.4 Adaptation of lpc single-unit responses to a stationary flash (stimulus S6, see METHODS). Spike raster (m = 3, except bottom unit where m = 2) of 5 lpc single-unit responses (same as in Fig. 5.2) are shown. Flashing spot size kept constant for one unit but varied slightly (6 - 8^{o}) from unit to unit. The gray boxes indicate the onset and duration of the stimuli.

5.4.2 Excitatory receptive field (ERF) structure

We used the results obtained with the small moving black spot (stimulus S1) to elucidate the excitatory receptive field structure of lpc neurons. An analysis was developed to measure the gross structure of the ERF even when the location of

the ERF center was only estimated during stimulus presentation. Single-unit Ipc responses were collected in response to a small black moving spot (stimulus S1). For each direction, peristimulus time histograms, PSTHs (bin 200 ms, smoothed by 400 ms window) were calculated. The delay due to response latency for each unit was adjusted by overlaying the PSTHs of opposite directions. This delay varied between 100 - 300 ms (n = 5 units), which was consistent with the response delay obtained from flashing small dark spots at the center of the receptive field of recorded units. The PSTHs were averaged over multiple trials and translated into 2D spatial coordinates in accordance with the stimulus. These data suggested a 2D Gaussian shape. By taking slices of a 2D Gaussian surface and comparing to the spike histograms, we were able to fit 2D Gaussian to each unit. A genetic algorithm (Druckmann et al. 2008) was utilized to determine the best position, height, and widths and orientation angle of the 2D Gaussian functions, by minimizing the squared difference between the 2D Gaussian function and the data (Fig. 5.5, top panels, red: average rate; pink: SD; black: Gaussian fit). This method enabled us to reproduce the ERF structure (Fig. 5.5, bottom panels) even if the spot missed the exact center (e.g. Fig. 5.5, unit A).

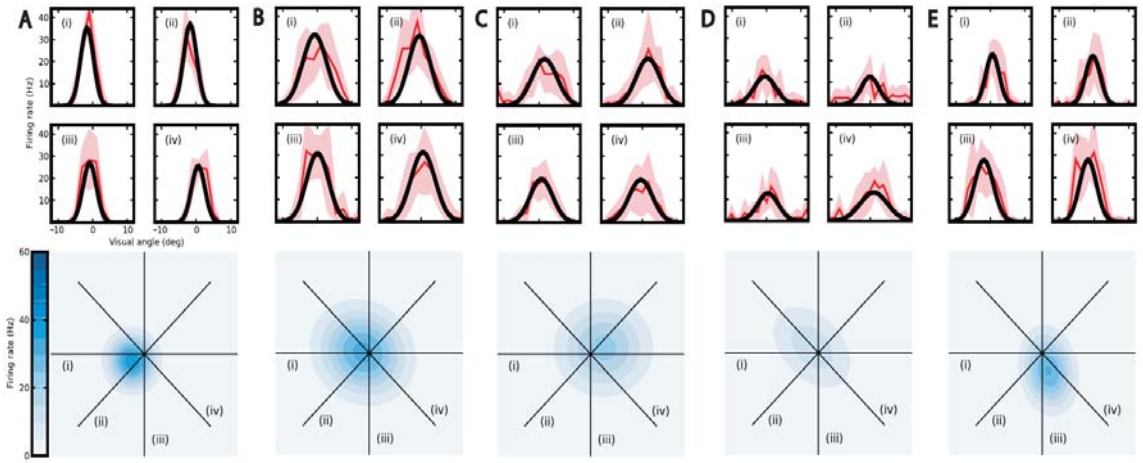

Figure 5.5 Two-dimensional shape of the excitatory receptive field, presented for 5 lpc units (out of the nine analyzed). For each unit, top 4 panels show the average firing rate (red line) with SD (m = 3, pink) along 4 directions, indicated by Roman numbers. The black line in each panel represents the 2D Gaussian fitting along that direction (see METHODS). The bottom plot (blue) shows the location and size of the Gaussian fit (the contour plot windows are all 22^{o} square). The scale bar represents the firing rate. All 5 units are shown in the same scale.

For the 9 units analyzed, the half-widths (half-width 1: Avg. 2.4^{o}, SD 0.6; half-width 2: Avg. 2.9^{o}, SD 0.8) of the 2D Gaussian fits (Fig. 5.5, bottom panels) did not differ significantly. This indicates that lpc neurons have spatially restricted excitatory receptive fields with circular structure.

5.4.3 Stimulus-response profile

We studied the Ipc responses to different sizes of black moving spots (Fig. 5.6a). For each spot size, the stimulus moved in 8 directions (stimulus S1) through the center of the stimulus coordinate system tracing the Ipc excitatory receptive field. The firing rates along all 8 directions were calculated by dividing the total spike count along one direction by half of the stimulus duration. To avoid any artifact due to missing the center of the Ipc ERF along any one direction, the maximum value of average firing rates among 8 directions was chosen to represent the corresponding spot size. Spot size zero corresponded to the average response to the white screen. Ipc single-unit responses (n = 4) followed a classic response-size profile that increased up to a certain spot size then asymptotically decreased to a certain value with increasing of spot size. For the 4 units tested, the Ipc showed a strong spiking response for a spot of radius of about 3^o - 5^o of visual angle (Fig. 5.6b). The response decreased considerably for increased spot radius (> 5^o) for three out of four units (except the blue unit, Fig. 5.6b). For the 4 units studied, the firing rate decrease with increasing spot size was independent of direction of stimulus movement. To quantify this response-size profile, we fitted the phenomenological Difference-of-Gaussian model with four independent variables (see METHODS) to these data (lines in Fig. 5.6b). For 3 units, the half-widths of the fitted excitatory and inhibitory receptive fields varied between 1^o - 2^o and 3^o - 5^o respectively. This estimate of the excitatory receptive field half-width is consistent with the results obtained using the previous analysis (Fig. 5.5). The unit with the largest ERF (5^o; blue unit of Fig. 5.6b) also has the

weakest surround inhibition. Overall the excitatory receptive field turned out to be narrower and stronger than the overlapping wider and weaker inhibitory receptive field for all 4 units (Fig. 5.6c).

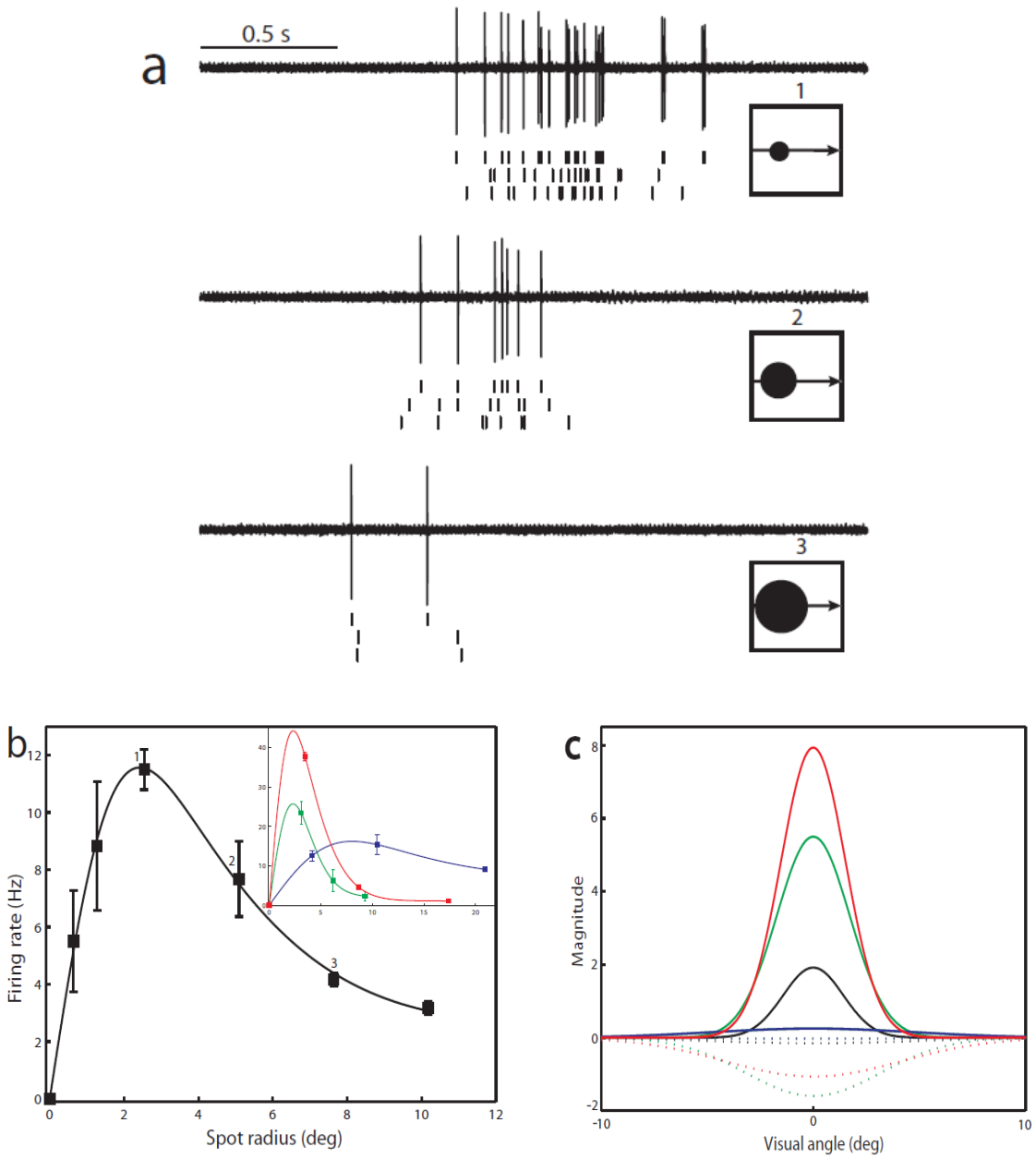

Figure 5.6 lpc responses vary with the size of a small moving black stimuli. (a) The lpc responses are shown for different spot radii of 2.5°, 5° and 7.5° as the spot moves 9.5°/s along the visual streak through the estimated center of the lpc excitatory receptive field. For each spot size, one raw voltage trace and 3 raster plots are shown. The spot size is scaled to the stimulus coordinate system (square box) in the drawn stimuli. (b) The response-size profile is shown for the same unit. A difference of Gaussian model is fitted to the result. Numbers indicate the average firing rate corresponding to spot radius shown in (a). Inset Population study of single-unit lpc responses (3 units) are shown for varying spot radius and fitted with Difference of Gaussian model. Error bars indicate the standard deviation between multiple trials (m = 3). Speed kept constant for each unit but ranged from 5.5 to 9.5°/s. (c) The excitatory (solid) and inhibitory (dotted) Gaussians fitted to the response-size profiles of the units in (b) from the Difference of Gaussian model (same color-coded).

5.4.4 Direction tuning

To investigate the potential directional sensitivity of lpc neurons, a small black moving spot (stimulus S1) was used as it elicited the strongest firing in lpc neurons. Directional preferences to movement along each radial axis were calculated using directional sensitivity index (DSI).

$$DSI = \frac{R_{\max} - R_{\min}}{R_{\max} + R_{\min}}$$

Where R_{max} and R_{min} are the higher and lower average firing rate respectively that was recorded during the linear sweeps of stimulus (stimulus S1) along two opposite directions. By convention, units are classified as directional sensitive, when $R_{max} \geq 2R_{min}$ (i.e. DSI ≥ 0.33) (Rosenberg and Ariel 1991; Sato et al. 1995). Opposite directions (such as 0^o, 180^o etc) were evaluated together as directional pairs. Since the spot moved along 8 directions with 45^o separations, each unit produced 4 directional pairs. The higher firing rate in a directional pair was called R_{max} and lower firing rate was called R_{min}. The DSI index was calculated for total of 36 directional pairs (n = 9 units, Fig. 5.7). We found that the DSI of all but one of the pairs fell below the criterion of 0.33, and thus were not considered directional sensitive. The absolute values of R_{max} and R_{min} were plotted for each unit. The distribution, though above the $R_{max} = R_{min}$ line by definition, did not exceed the DSI criterion line of $R_{max} = 2R_{min}$, indicating no directional tuning (Fig. 5.7, inset).

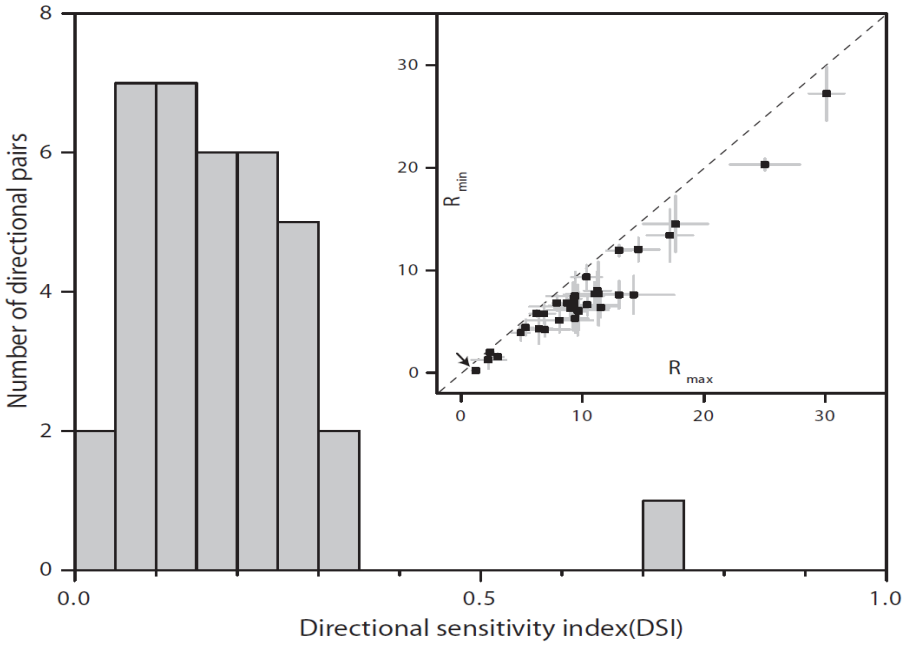

Figure 5.7 Histogram distribution of the directional sensitivity index (DSI, see METHODS) is plotted for 36 directional pairs from 9 lpc single-units (9 recording sites, 8 brains). The spot diameter and speed are kept constant for multiple trials in each unit but varied slightly between different units (diameter 5 - 9^{o}, speed 6 -10^{o}/s using stimulus S1). DSI index of all but one pair falls below 0.33. Inset: R_{max} and R_{min} for all the directional pairs are plotted with their absolute value of firing rate (Hz) with SD (gray bars). R_{max} and R_{min} represent the average value of the higher and lower firing rates over multiple trials (n = 3) for each directional pair. The dotted line represents $R_{max} = R_{min}$. The arrow indicates the directional pair with lowest firing rate that has a DSI just above the criterion.

5.4.5 Speed tuning

Speed tuning of lpc units were also investigated with small moving spot (stimulus S1). A medium sized spot (8° - 9° of visual angle) that elicited strong spiking activity was moved with different speeds across the RF. For the 2 units studied, speeds up to a certain value elicited similar responses (8 -15^{o}/s in Fig. 5.8a, 3-7^{o}/s in Fig. 5.8b), whereas the response decreased for higher speed (27^{o}/s in Fig. 5.8a, 17^{o}/s in Fig. 5.8b). For higher speeds, both units responded with a larger delay compared to the response latency for slower speeds. Speed analyses were done for all 8 different directions of motion for each unit. The results were independent of the direction of spot movement.

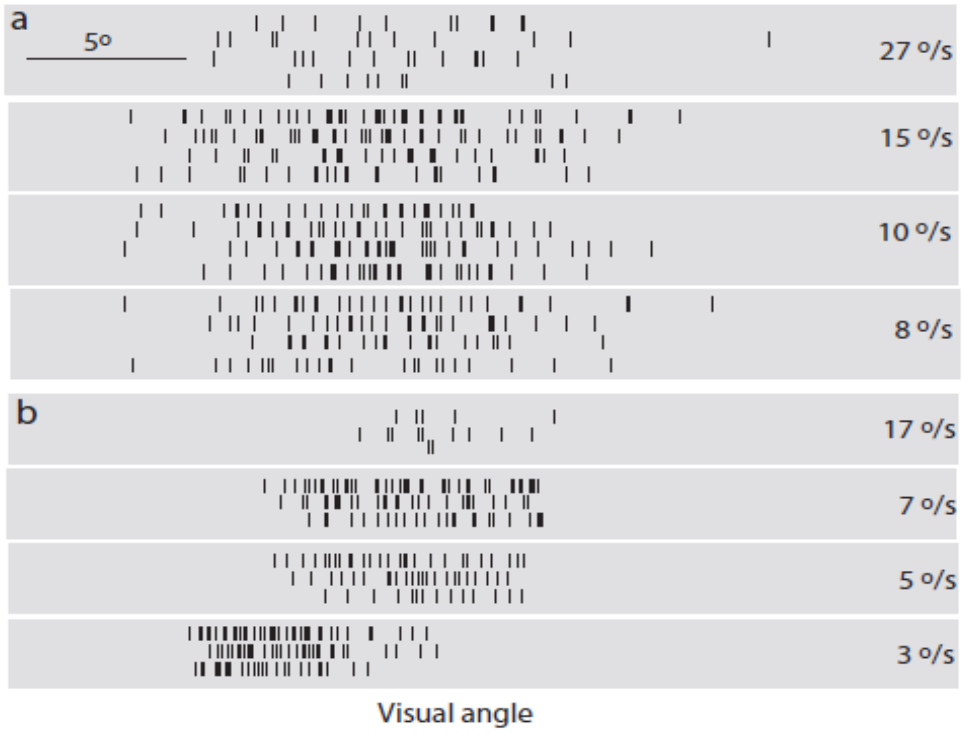

Figure 5.8 Variation of lpc response with different speeds of small black moving stimuli (stimulus S1, see METHODS). Spikes are plotted at the position they occurred in the receptive field for different speeds with a response latency of 300 ms. Each gray box represents 30° of visual angle. Shown are each cell's strongest response among all 8 directions presented. (a) Raster of 4 trials are shown for a moving spot of diameter 9° with different speed values (mentioned at the far right). For different speeds the average spike count and SD values are (format: Speed, Mean ± SD); 27°/s, 11 ± 1.6; 15°/s, 36 ± 8.9; 10°/s, 37.2 ± 3.7; 8°/s, 28.8 ± 3.9. (b) Raster of 3 trials are shown for a different unit for a spot (diameter 8°) moving with different speeds (similar to 5.8a). The mean and SD values of

spike count for different speeds are 17°/s, 5.3 ± 3.5; 7°/s, 32.7 ± 11.6; 5°/s, 22.3 ± 6.7; 3°/s, 34.7 ± 9.3.

5.5 Discussion

We show that turtle Ipc neurons have a localized excitatory receptive field with surround inhibition, a preference for small stimuli, as well as significant adaptation to static stimuli. Here, we compare our findings with those from other animals, discuss possible mechanisms based on our results, the underlying circuitry of the system, and provide an outlook for the role of Ipc cholinergic feedback for tectal visual processing in turtle.

5.5.1 Comparison with other Ipc neurons

The small moving stimuli generate vigorous spiking responses in turtle Ipc (Fig. 5.2) as well as in isthmic neurons of many species (Pigeon: Yan and Wang 1986; Wang and Frost 1991; Marin et al. 2005; Li et al. 2007; Marin et al. 2007; owl: Maczko et al. 2006; fish: Gallagher and Northmore 2006; cat: Sherk 1979a). The spontaneous firing rates of turtle Ipc neurons and pigeon's nucleus isthmi cells are found to be low (Wang and Frost 1991) compared to the high spontaneous activity of PBN neurons (Sherk 1979a; Cui and Malpeli 2003; Goddard et al. 2007). We have found that the turtle Ipc neurons are not directionally sensitive (Fig. 5.7), which is consistent with weakly directional-sensitive pigeon Ipc

neurons (Wang and Frost 1991; Li et al. 2007) and cat PBN neurons (Sherk 1979a).

5.5.2 Excitatory receptive field structure

The turtle Ipc excitatory receptive field is shaped in the pathway from retina, to tectum, to Ipc. The radial narrow dendrites of the tectal SGP neurons overlap with retinal axon terminals in superficial tectal layers (Kunzle and Schnyder 1984). In turn, axons from the SGP neurons project to the ipsilateral Ipc nucleus in a topographic fashion. The SGP apical radial dendrites form dendrodendritic synapses within the SFGS layer (Schechter and Ulinski 1979), thus providing the hardware for the lateral spread of local retinal inputs and suggesting broad Ipc receptive fields. Yet, our recordings reveal circular excitatory Ipc receptive fields of Gaussian shape with an average half-width just below 3 deg (Fig. 5.5). Cat parabigeminal neurons (PBN) have a similar excitatory receptive field with a little less than 3 deg in diameter (Sherk 1979a). In contrast, pigeon Ipc neurons have circular excitatory receptive fields with diameters in the range from 10 to 20 deg (Li et al. 2007; Marin et al. 2005, 2007) and the excitatory receptive fields of frog nucleus isthmi neurons are even larger (Winkowski and Gruberg 2002; Caudill et al. 2010).

5.5.3 Response-size profile

To determine the inhibitory receptive field structure of Ipc neurons, we investigated the Ipc response-size profile using different spot sizes (Fig. 5.6).

Based on a Difference-of-Gaussian analysis the inhibitory receptive field turned out to be weaker and about twice as big as the excitatory receptive field of Ipc neurons. This stimulus size tuning, which is the result of a surround inhibition, is found in cat PBN (Sherk 1979a), bird Ipc (Wang and Frost 1991) and tectal (Mysore 2010) neurons. Similar response-size profile can also be observed in LGN (Alitto and Usrey 2003; Sillito and Jones 2002) and cortical VI neurons (Sceniak et al. 1999). In the turtle isthmotectal system, the GABAergic Imc neuron is a likely candidate for the generation of this inhibitory surround through its broad projection to the Ipc nucleus. Consistent with this hypothesis, we have found that the Imc to Ipc synaptic connection is inhibitory (Fig. 4.7b). In addition, retinal and tectal processing (Bowling 1980, Granda 1989) may contribute to the Ipc's visual response properties. Our study cannot separate these influences from the role of Imc neurons in providing inhibition onto Ipc neurons.

5.5.4 Cholinergic modulation by Ipc

The feedback pathway from nucleus isthmi to tectum in turtle consists of (Fig. 1.3) narrow, topographic, cholinergic projection to multiple tectal layers from Ipc neurons and broad, inhibitory projection from Imc neurons to deep tectal layers (Sereno and Ulinski 1987). This anatomical connection underscores the fact that the cholinergic feedback mediated by Ipc neurons at one tectal locus faces competition with feedback produced at other tectal loci via long distance suppression by Imc neurons. These interactions might provide spatially specific

modulation of tectal circuitry and mediate mechanisms of visual processing in the collothalamic pathway in different species (Gruberg et al. 2006).

Cholinergic Ipc projection will also play an important role in upstream visual processing in the collothalamic pathway. Large-field neurons in the SGC layer of the turtle tectum project to the nucleus rotundus in a nontopographic manner, forming a key element of tectofugal pathway (Reiner 1994; Belekhova et al. 2003). The tectal SGC neurons' dendritic branches extend into the superficial retinorecipient tectal layers (SFGS). The topographically organized columnar Ipc axon terminals spatially overlap with the RGC axons and the SGC dendrites. Thus the release of ACh from Ipc axon terminals across several tectal layers provides ample potential for spatially specific cholinergic modulation of retino-tectal synaptic transmission and in turn the ascending visual pathway. This conjecture is supported by the observations that isthmic activity enhances calcium influx into the optic nerve fiber terminals in frog (Dudkin and Gruberg 2003) and by findings that the local inactivation of the Ipc nucleus prevents visual responses in the spatially corresponding ascending RGC-SGC visual pathway to the nucleus rotundus in birds (Marin et al. 2007). Clearly, a deeper understanding of the Ipc visual responses will be a prerequisite for gaining insight into the role of spatiotemporal ACh release for visual processing in the optic tectum or superior colliculus.

5.6 References

Alitto HJ, Usrey WM (2003) Corticothalamic feedback and sensory processing. Curr Opin Neurobiol 13:440-445.

Ariel M, Kogo N (2001) Direction tuning of inhibitory inputs to the turtle accessory optic system. J Neurophysiol 86:2919-2930.

Bowling DB (1980) Light responses of ganglion cells in the retina of the turtle. J Physiol 299:173-196.

Belekova M, Kenigfest N, Rio JP, Reperant J, Ward R, Vesselkin N, Karamian O (2003) Tectothalamic visual projections in turtles: Theirs cells of origin revealed by tracing methods. J Comp Neurology 457:37-56.

Caudill MS, Eggebrecht AT, Gruberg ER, Wessel R (2010) Electrophysiological properties of isthmic neurons in frogs revealed by in vitro and in vivo studies. J Comp Physiol A 196:249-262.

Cui H, Malpeli JG (2003) Activity in the parabigeminal nucleus during eye movements directed at moving and stationary targets. J Neurophysiol 89:3128-3142.

DeAngelis GC, Freeman RD, Ohzawa I (1994) Length and width tuning of neurons in the cat's primary visual cortex. J. Neurophysiol 71:347–374.

Desan PH, Gruberg ER, Eckenstein F (1984) A cholinergic projection from the nucleus isthmi to the optic tectum in turtle and frog. Proc Soc Neurosci 10:575 (Abstract).

Druckmann S, Berger TK, Hill S, Schürmann F, Markram H, Segev I (2008) Evaluating automated parameter constraining procedures of neuron models by experimental and surrogate data. Biol Cybern 99:371-379.

Dudkin EA, Gruberg ER (2003) Nucleus isthmi enhances calcium influx into optic nerve fiber terminals in Rana pipiens. Brain Res 969:44-52.

Dudkin, EA, Sheffield JB, Gruberg ER (2007) Combining visual information from the two eyes: the relationship between isthmotectal cells that project to ipsilateral and to contralateral optic tectum using fluorescent retrograde labels in the frog, Rana pipiens. J Comp Neurol 502:38-54.

Gallagher SP, Northmore DP (2006) Responses of the teleostean nucleus isthmi to looming objects and other moving stimuli. Vis Neurosci 23:209-219.

Goddard CA, Knudsen EI, Huguenard JR (2007) Intrinsic excitability of cholinergic neurons in the rat parabigeminal nucleus. J Neurophysiol 98:3486-3493.

Granda AM, Fulbrook JE (1989) Classification of turtle retinal ganglion cells. J Neurophysiol 62:723-737.

Graybiel AM (1978) A satellite system of the superior colliculus: the parabigeminal nucleus and its projection to the superficial collicular layers. Brain Res 145:365-374.

Gruberg ER, Dudkin EA, Wang Y, Marin G, Salas C, Sentis E, Letelier JC, Mpodozis J, Malpeli J, Cui H, Ma R, Northmore D, Udin S (2006) Influencing and interpreting visual input: The role of a visual feedback system. J Neurosci 26:10368-10371.

Gruberg ER, Udin SB (1978) Topographic projections between the nucleus isthmi and the tectum of the frog, Rana pipiens. J Comp Neurol 179:487-500.

Hall WC, Fitzpatrcik D, Klatt LL, Raczkowski D (1989) Cholinergic innervation of the superior colliculus in the cat. J Comp Neurol 287:495-514.

Kriegstein AR (1987) Synaptic responses of cortical pyramidal neurons to light stimulation in the isolated turtle visual system. J Neurosci 7:2488-2492.

Kunzle H, Schnyder H (1984) The isthmus-tegmentum complex in the turtle and rat: a comparative analysis of its interconnections with the optic tectum. Exp Brain Res 56:509-522.

Li DP, Xiao Q, Wang SR (2007) Feedforward construction of the receptive field and orientation selectivity of visual neurons in the pigeon. Cereb Cortex 17:885-893.

Lucas-Meunier E, Fossier P, Baux G, Amar M (2003) Cholinergic modulation of the cortical neuronal network. Eur J Physiol 446:17-29.

Lucas-Meunier E, Monier C, Amar M, Baux G, Fregnac Y, Fossier P. (2009) Involvement of nicotinic and muscarinic receptors in the endogenous cholinergic modulation of the balance between excitation and inhibition in the young rat visual cortex. Cereb Cortex 19:2411-2427.

Marín G, Salas C, Sentis E, Rojas X, Letelier JC, Mpodozis JA (2007) cholinergic gating mechanism controlled by competitive interactions in the optic tectum of the pigeon. J Neurosci 27:8112-8121.

Marín G, Mpodozis J, Sentis E, Ossandón T, Letelier JC (2005) Oscillatory bursts in the optic tectum of birds represent re-entrant signals from the nucleus isthmi pars parvocellularis. J Neurosci 25:7081-7089.

Maczko KA, Knudsen PF, Knudsen EI (2006) Auditory and visual space maps in the cholinergic nucleus isthmi pars parvocellularis of the barn owl. J Neurosci 26:12799-12806.

McCormick DA (1993) Actions of acetylcholine in the cerebral cortex and thalamus and implications for functions. Prog Brain Res 98:303-308.

Medina L, Reiner A (1994) Distribution of choline acetyltransferase immunoreactivity in the pigeon brain. J Comp Neurol 342:497-537.

Metherate R (2004) Nicotinic acetylcholine receptors in sensory cortex. Learning & Memory 11:50-59.

Mysore SP, Asadollahi A, Knudsen EI (2010) Global inhibition and stimulus competition in the owl optic tectum. J Neurosci 30:1727-1738.

Northmore DP, Granda AM (1991) Ocular dimensions and schematic eyes of freshwater and sea turtles. Vis Neurosci 7:627-635.

Northmore DP, Gallagher SP (2003) Functional relationship between nucleus isthmi and tectum in teleosts: synchrony but no topography. Vis Neurosci 20:335-348.

Northmore DP (1991) Visual responses of nucleus isthmi in a teleost fish (Lepomis macrochirus). Vision Res 31:525-535.

Peirce JW (2008) Generating Stimuli for Neuroscience Using PsychoPy. Front Neuroinformatics 2:10.

Powers AS, Reiner A (1993) The distribution of cholinergic neurons in the central nervous system of turtles. Brain Behav Evol 41:326-345.

Quiroga RQ, Nadasdy Z, Ben-Shaul Y (2004) Unsupervised spike detection and sorting with wavelets and superparamagnetic clustering. Neural Comput 16:1661-1687.

Rodieck RW (1965) Quantitative analysis of cat retinal ganglion cell response to visual stimuli. Vision Res 5:583–601.

Rosenberg AF, Ariel M (1990) Visual-response properties of neurons in turtle basal optic nucleus in vitro. J Neurophysiol 63:1033-1045.

Rosenberg AF, Ariel M (1991) Electrophysiological evidence for a direct projection of direction-sensitive retinal ganglion cells to the turtle's accessory optic system. J Neurophysiol 65:1022-1033.

Reiner A (1994) Laminar distribution of the cells of origin of ascending and descending tectofugal pathways in turtles: implications for the evolution of tectal lamination. Brain Beh Evol 43: 254-292.

Sato H, Katsuyama N, Tamura H, Hata Y, Tsumoto T (1995) Mechanisms underlying direction selectivity of neurons in the primary visual cortex of the macaque. J Neurophysiol 74:1382-1394.

Schechter Pb, Ulinski PS (1979) Interactions between tectal radial cells in the red-eared turtle, Pseudemys scripta Elegans: An analysis of tectal modules. J Morph 162:17-36.

Sceniak MP, Ringach DL, Hawken MJ, Shapley R (1999) Contrast's effect on spatial summation by macaque V1 neurons. Nat Neurosci 2:733-739.

Sereno MI, Ulinski PS (1987) Caudal topographic nucleus isthmi and the rostral nontopographic nucleus isthmi in the turtle, Pseudemys scripta. J Comp Neurology 261:319-346.

Sillito AM, Jones HE (2002) Corticothalamic interactions in the transfer of visual information. Philos Trans R Soc Lond B Biol Sci 357:1739-1752.

Sorenson EM, Parkinson D, Dahl JL, Chiappinelli VA (1989) Immunohistochemical localization of choline acetyltransferase in the chicken mesencephalon. J Comp Neurol 281:641-657.

Sherk H (1978) Visual response properties and visual field topography in the cat's parabigeminal nucleus. Brain Res 145:375-379.

Sherk H (1979a) A comparison of visual-response properties in cat's parabigeminal nucleus and superior colliculus. J Neurophysiol 42:1640-1655.

Sherk H (1979b) Connections and visual field mapping in cat’s tectoparabigeminal circuit. J Neurophysiol 42:1656-1668.

Wang Y, Luksch H, Brecha NC, Karten HJ (2006) Columnar projections from the cholinergic nucleus isthmi to the optic tectum in chicks (Gallus gallus): A possible substrate for synchronizing tectal channels. J Comp Neurol 494:7-35.

Wang Y, Major DE, Karten HJ (2004) Morphology and connections of nucleus isthmi pars magnocellularis in chicks (Gallus gallus). J Comp Neurol 469:275-297.

Wang Y, Xiao J, Wang SR (2000) Excitatory and inhibitory receptive fields of tectal cells are differentially modified by magnocellular and parvocellular divisions of the pigeon nucleus isthmi. J Comp Physiol A 186:505-511.

Wang YC, Frost BJ (1991) Visual response characteristics of neurons in the nucleus isthmi magnocellularis and nucleus isthmi parvocellularis of pigeons. Exp Brain Res 87:624-633.

Wang SR (2003) The nucleus isthmi and dual modulation of the receptive field of tectal neurons in non-mammals. Brain Res Brain Res Rev 41:13-25.

Wang SR, Wang YC, Frost BJ (1995) Magnocellular and parvocellular divisions of pigeon nucleus isthmi differentially modulate visual responses in the tectum. Exp Brain Res 104:376-384.

Wiggers W, Roth G (1991) Anatomy, neurophysiology and functional aspects of the nucleus isthmi in salamanders of the family Plethodontidae. J Comp Physiol A 169:165-176.

Winkowski DE, Gruberg ER (2002) The representation of the ipsilateral eye in nucleus isthmi of the leopard frog, Rana pipiens. Vis Neurosci 19:669-679.

Yan K, Wang SR (1986) Visual responses of neurons in the avian nucleus isthmi. Neurosci Lett 64:340-344.

Chapter 6

LATERAL INTERACTIONS BETWEEN VISUAL STIMULI IN TURTLE NUCLEUS ISTHMI

6.1 Abstract

In a complex visual world, when multiple stimuli occur at different locations, neuronal mechanisms compete to propagate the most salient feature of the stimuli to higher visual centers. The superior colliculus (optic tectum in turtle) plays a key role in the stimulus selection and spatial attention observed in mammals. In this study, the turtle isthmotectal system is investigated to study the role of the nucleus isthmi (homolog of the parabigeminal nucleus in mammals) in stimulus competition. To conduct the lateral interaction investigations, a small moving black spot on white background was chosen as the preferred stimulus. The selection was made from a pool of different static and dynamic stimuli as the Ipc neurons responded strongest to a small moving black spot. To test the effects of competing stimuli, two black spots were moved through the visual field with or without delays between them. Competition was tested for a secondary stimuli located outside the excitatory receptive field of the Ipc neuron. In some cases, the Ipc responses to a small moving stimulus inside the excitatory receptive field (ERF) is suppressed by a secondary stimuli moving outside the ERF. Intracellular recordings from the Ipc neurons in response to multiple stationary flashes produce non-linear responses.

6.2 Introduction

Competitive interaction between spatiotemporal neural representations of a cluttered scene leads to shifts in space or feature-based attention (Desimone and Duncan 1995; Motter 1998; Itti and Koch 2001), which in turn, causes spatio-temporal modulation of responses in the earlier stages of the visual pathway (Kastner and Ungerleider 2000; Schroeder et al. 2001; Assad 2003; Yantis and Serences 2003; Reynolds and Chelazzi 2004; Sarter et al. 2005; Boynton 2005; Maunsell and Treue 2006). The ability to shift attention towards relevant locations or features in a complex scene has evolutionary significance because it allows the organism to detect quickly possible prey, mates, or predators. Consequently, a mechanistic understanding of shifts in attention in terms of the neurobiological components, biophysical mechanisms, and systems dynamics represents a major goal in neuroscience (Niebur et al. 2002; Brandt and Wessel 2007; Knudsen 2007).

The turtle isthmotectal complex is an ideal system to study the lateral interactions between different stimuli for three reasons. First, the anatomy of the turtle isthmotectal connections (Fig. 4.1) provides framework for the possibility of competing visually triggered isthmi pars parvocellularis (Ipc) activities at two different loci via long-distance suppressive interactions mediated by the isthmi pars magnocellularis (Imc) neurons (Sereno and Ulinski 1987). Second, the competitive interaction and spatial shifts of activity in response to novel stimuli have been demonstrated in the homologous isthmotectal system of bird (Marin et

al. 2007), which includes both Ipc and Imc neurons (Wang et al. 2004, 2006). Third, model simulations predict such spatial shifts of activity to occur in the turtle isthmotectal system as well (Wessel et al. 2008).

Here, using extracellular recordings, we study the single-unit activity of Ipc neurons in response to two small moving black spots, one inside and the other outside the excitatory receptive field (ERF) of an Ipc neuron. In some cases, the Ipc response to a moving black spot inside the ERF decreased due to a parallel spot moving outside its receptive field (Fig. 6.1). We have also recorded the intracellular Ipc activity to local flash of lights, which are spatially and temporally separated. Here also, we have found that the combined Ipc response to two flashes is not the linear summation of the responses to individual flashes (Fig. 6.3).

6.3 Methods

6.3.1 Extracellular experiments

Extracellular recordings were achieved from an eye-attached whole-brain preparation as mentioned in Chapter 2 (see SECTION 2.1, 2.4). After aligning the eye-cup of the preparation and the image on the projection screen (see SECTION 2.5.1), responsive area in the Ipc nucleus was determined using the search stimulus (see SECTION 2.5.2). The stimulation coordinate, which covers about twice the excitatory receptive field of the Ipc neuron, was set-up as described in SECTION 2.5.3. To test the effect of lateral interaction in the Ipc

neurons due to multiple stimuli in visual field, two small black spots of same dimensions and speeds were used. One spot was moved through the center of the excitatory receptive field of the lpc neuron and the other spot was moved outside the ERF parallel to the central spot. The two spots were either moved simultaneously or with some delay. The voltage traces were filtered using 300 - 5000 Hz analog band pass filter, sampled at 10 kHz and saved for further analysis. Single-units were isolated from the recorded voltage trace using *waveclus*, a spike-sorting algorithm based on spike detection and sorting using wavelets and superparamagnetic clustering (Quiroga et al. 2004).

6.3.2 Intracellular experiments

Whole-cell blind-patch recordings were achieved from the eye-attached whole-brain preparations as described in SECTION 2.2. To test the lpc responses to two spatially separated light spots in contralateral retina, computer-controlled LEDs (white) were used. The light spots were projected to the two locations on the retina via two optic fibers each with 200 µm diameter, which generated light spots of similar dimensions. The temporal delay between two flashes was varied. For each configuration of the stimulus, at least 3 trials were conducted. An inter-trial interval of 30 s was maintained for all experiments.

6.4 Results

To test the hypothesis that a stimulus outside the ERF of an lpc neuron could modulate the lpc responses to a stimulus inside the ERF, we used two small dark

moving spots on white background as stimulus. One spot was moved through the center of the Ipc ERF while the other spot was moved outside the excitatory receptive field. First, to detect the direction that elicited maximum response, one black spot was moved through the center of the Ipc ERF along 8 directions with 45^{o} separation between paths (stimulus S1, see SECTION 5.3.2). The lateral interaction experiments were performed along the direction that generated strongest response and aligns best with the center of the Ipc ERF (e.g. 90^{o} for Fig. 6.1, 6.2). One spot moved along the center of the ERF while the other spot moved outside of the ERF, parallel to the path of central spot. Both the spots started outside the ERF and covered about twice the length of the ERF in a linear sweep. The contrast, dimension, and speed were kept same for both the spots. In one unit, when single spot was moved along the center of the ERF, the unit responded with bursts of spikes (Fig. 6.1a). For a spot moving outside the ERF, the response was around zero (Fig. 6.1 inset, Spot 2). The unit's response to the centrally moving spot decreased (Fig. 6.1, inset) due to simultaneous movement of a second spot outside the ERF (Fig. 6.1b) indicating lateral interactions in the Ipc neurons due to presence of multiple stimuli.

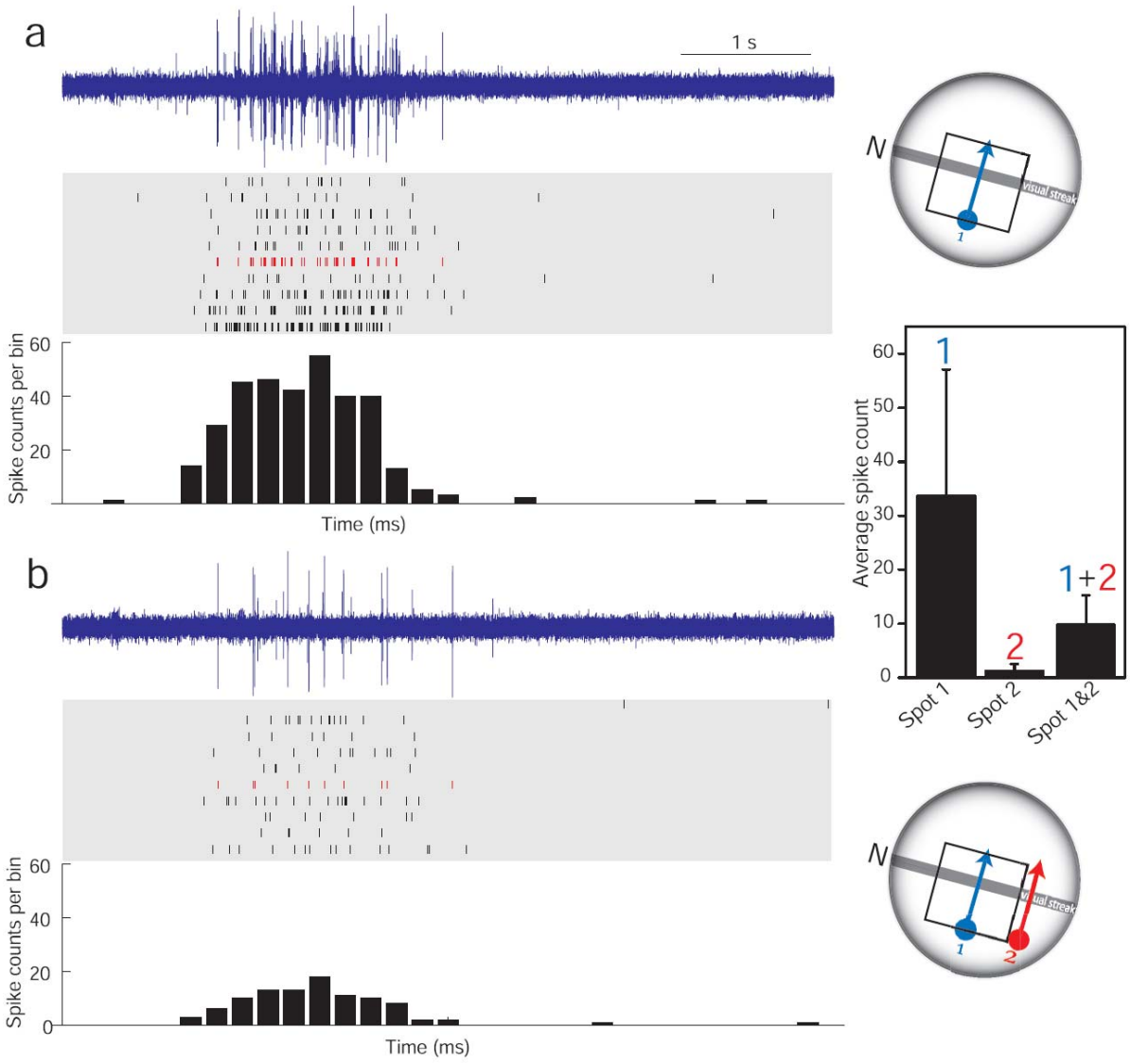

Figure 6.1 Lateral interactions In the lpc neuron due to two small moving black spots. (a) Response on an lpc neuron to a small (diameter 6°) black spot moving (speed 5 °/s) through the estimated center of the excitatory receptive field (ERF) of the lpc neuron. The spot moves perpendicular to the visual streak. From top to bottom, raw voltage trace of one lpc single-unit during the movement of the spot, raster of 10 trials, and peristimulus time histogram (bin-size 200 ms) of total spike count for all 10 trials over

the duration of the stimulus movement (6 s). The red raster corresponds to the voltage trace shown at the top. Right, the schematic of the spot (#1, blue) location in the eye-cup. The black square indicates the stimulation coordinate system (see SECTION 2.5.3), which is about twice the size of lpc ERF. The nasal retina is indicated by *N*. (b) The same unit's response to two small black spots, moving simultaneously, one (spot # 1, blue) at the center of the ERF while the other(spot # 2, red) at the outside of the ERF (18^{o} apart in visual angle). The results are displayed in the same way as in (a). Right, schematic showing the locations of the two spots on the eye-cup. Inset, average spike counts due to individual spot movements and their simultaneous movement. The error-bars indicate SDs.

In another unit studied for lateral interaction, we used two spots with a temporal delay between them. The first spot (blue, Fig. 6.2a) moved through the center of the ERF and the second spot (red, Fig. 6.2b) moved outside the ERF. We recorded the lpc responses to the two spots when a delay of 3 s was introduced between the movement of the spots (Fig. 6.2c, d). We found the average spike counts over the duration of the spot movement remain approximately unchanged between single spot trough the center and combined movement of the two spots (Fig. 6.2 inset).

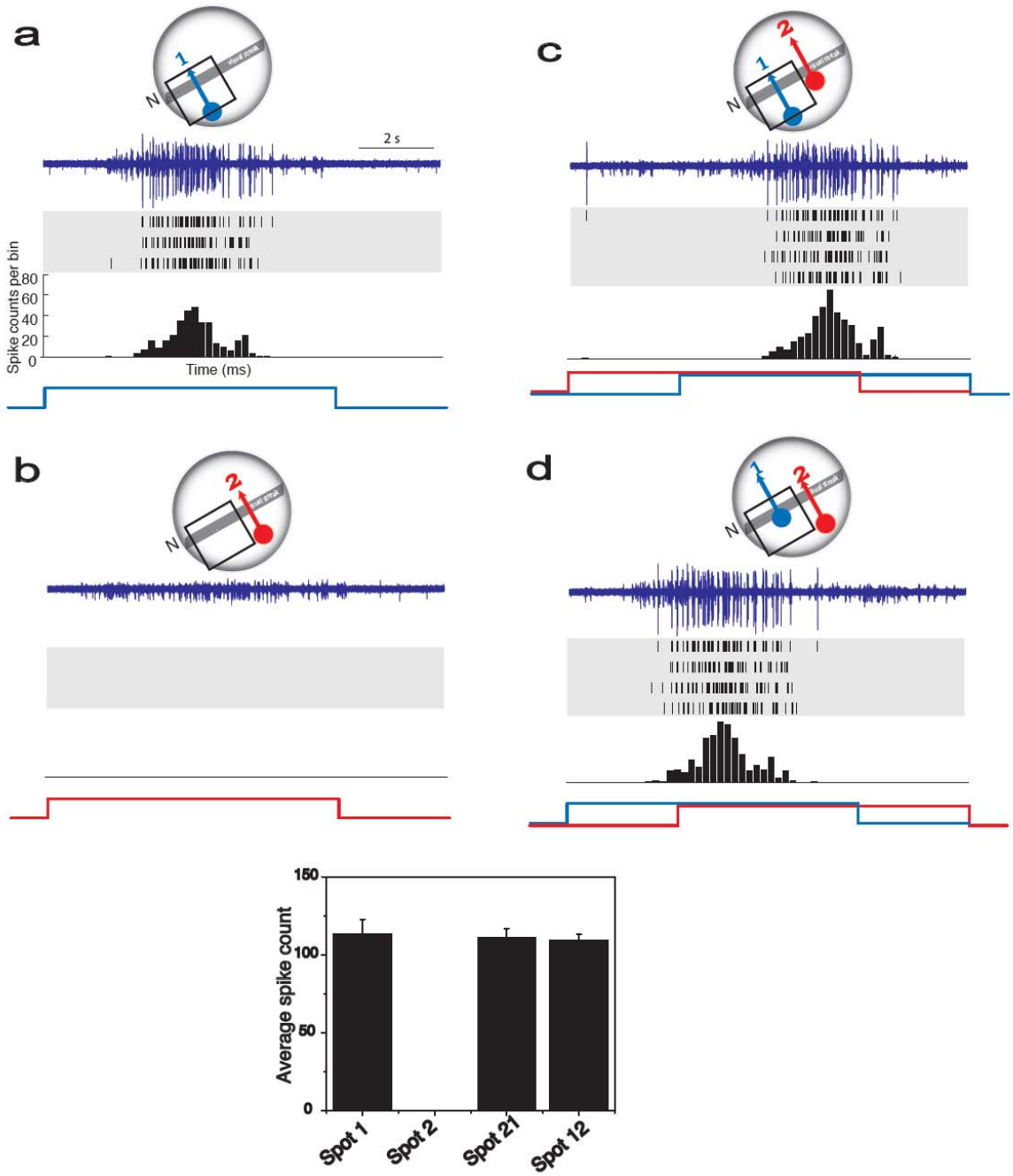

Figure 6.2 The lpc neuron's responses to spatially separated moving black spots with a delay. The schematic above each figure indicates the locations and directions of movement of the spots on the eye-cup (blue, Spot 1; red, Spot 2). (a) Response of an lpc neuron to a small (diameter 6°) moving (speed 4°/s) black spot through the center of the ERF. From top to bottom,

raw voltage trace of an lpc single-unit, raster of 3 trials, peristimulus time histogram (bin-size 200 ms) of total spike count for all 3 trials over the duration of the stimulus movement (8 s), and the duration of the stimulus movement (blue line). (b) The same unit's response to a moving spot of same dimension and speed, separated by 18^{o} in visual angle from Spot # 1. The results is displayed in the same way as in (a). (c) The unit's responses to two moving spots (Spot 21), when the spot outside the ERF (Spot 2) moves 3 s ahead of the central spot (Spot 1). (d) The same unit's response to the stimulus configuration (Spot 12), where the Spot 1 moves 3 s ahead of the Spot 2. Inset, the average spike count for individual spot movements (as in (a), (b)) and delayed movement of two spots (as in (c), (d)). Error-bar represents SD.

Our preliminary intracellular studies on lateral interactions illustrate the complexity of the turtle lpc response when the novel stimulus is just a local flash of light (Fig. 6.3). Two light spots were positioned without spatial overlap within the excitatory receptive field of the recorded lpc neuron, i.e., each individual 500 ms flash of light caused a delayed excitatory response, which lasted for a few hundred milliseconds. When one flash was followed by a second flash delivered 900 ms after the onset of the first flash, the lpc response to the first flash was unchanged, as expected. However, the response to the second flash was advanced in time and increased in amplitude compared to the isolated-flash response. Furthermore, when the second flash was delivered 200 ms after the

onset of the first flash, the combined Ipc response to the two flashes was advanced in time, reduced in overall amplitude, and followed by a temporally structured and long-lasting response. In conclusion, the combined Ipc response to two flashes is not the linear summation of the responses to individual flashes.

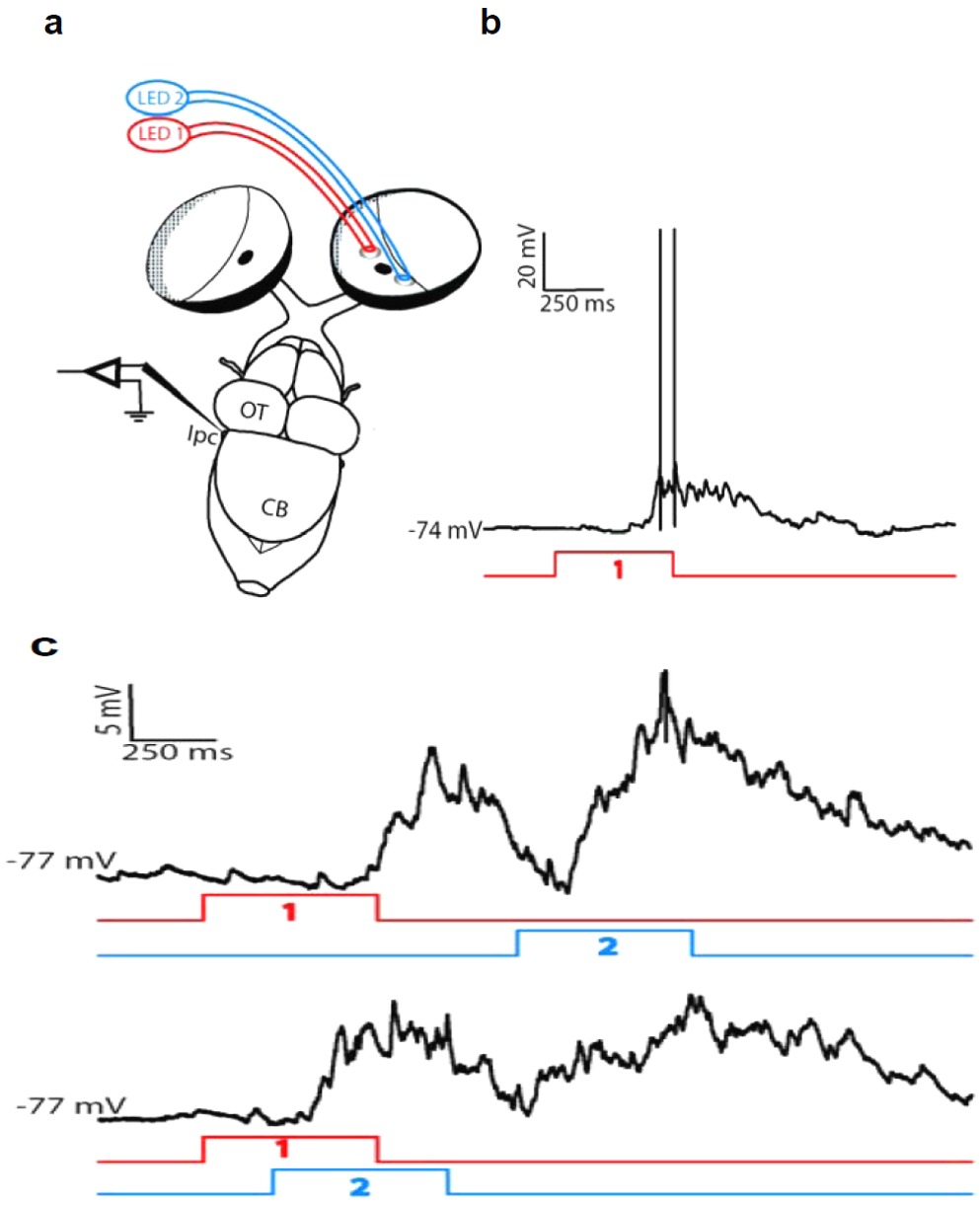

Figure 6.3 Ipc responses to spatiotemporal visual stimulation. (a) Schematic of a dorsal view of the turtle whole-brain preparation with the

attached eye-cup and whole-cell recording electrode in lpc nucleus. Two flashes of light of 500 ms duration are generated with computer-controlled LEDs. The light is projected to specific location on the retina via fiber optics of 200 μm diameter which generates a spot of light of similar dimension. (b) A 500-ms flash of light (#1) causes an excitatory response in the recorded lpc neuron. The response to flash #2 is similar in amplitude and time course (data not shown). (c) Top: Flash #2 is delivered 900 ms after the onset of flash #1. Bottom: Flash #2 is delivered 200 ms after the onset of flash #1. The traces are averages of 3 trials, with spikes clipped before averaging.

6.5 Discussion

We have found evidence of lateral interaction in some lpc neurons due to presence of multiple stimuli in the visual field. Although inconclusive, our extracellular recordings show that for some units the response to a spot moving through the center of ERF decreases, when another spot moves simultaneously outside the ERF. Our intracellular recordings also show non-linear changes in subthreshold membrane potential of an lpc neuron due to spatially separated, localized light flashes, when the delay between the two flashed are varied.

Inside the turtle isthmotectal circuitry (Fig. 4.1d), both the SGP and the lpc projections are local and topographic without documented evidence for lateral interaction (Sereno and Ulinski 1987). Thus the GABAergic Imc neurons with

their broad projections to both, the tectum and the Ipc nucleus, are the prime candidate to mediate the lateral interactions in the Ipc. We have already shown that the Imc to Ipc synaptic connection is inhibitory (CHAPTER 4, Fig. 4.7). The mechanism of lateral interaction mediated by the Imc is the following. Retinal inputs impinging on multiple locations of tectum (black arrows, Fig. 6.4) activate both Ipc and Imc neurons along that pathway. The GABAergic Imc neurons project back to the tectum and to the Ipc nucleus in a nontopographic manner. The activity of one Imc neuron could modulate all tectal neurons in the SGP layer and Ipc neurons, thus generating competition between multiple tectal loci. This would in turn, generate competition between corresponding activated Ipc neurons receiving retinal inputs.

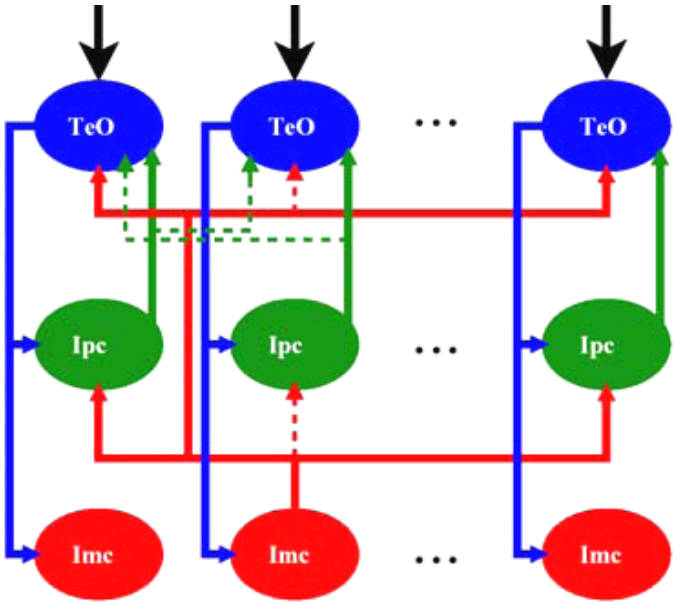

Figure 6.4 Diagrammatic representation of the synaptic connections in the turtle isthmotectal system. The black arrows indicate retinal inputs into tectal neurons. The tecto-isthmic projections are local. Strong isthmotectal projections are shown by solid lines and weak projections are shown by

dashed lines. For clarity, the projection from only one Imc neuron is shown. The figure is adapted from Wessel et al. 2008.

In birds, it has been shown, when a second visual stimulus is presented far away from the first, the Ipc feedback to the first tectal location is diminished while the feedback to the second location is initiated (Marin et al. 2007). The Imc neurons are implicated to mediate this long-range suppressive interaction in birds. Competitive interaction provides a mechanism for selecting and attending to one visual stimulus from the complex visual scenes. The spatial attention enhances visual processing at one location while suppressing response to unattended locations in several interconnected visual processing areas (Posner 1980; Desimone and Duncan 1995; Maunsell and Cook 2002; Marin et al. 2007). Local facilitations and wide-field competitive interactions are implicated to play integral role in the gating effect of spatial attention (Deco et al. 2002). In mammals, activity increases in parts of superior colliculus (SC) that attend to a target location during saccade preparation (Glimcher and Sparks 1992; Kustov and Robinson 1996; Basso and Wurtz 1998) while no long-range inhibitory connection has been found in SC (Lee and Hall 2006). It is speculated that the parabigeminal nucleus (PBN), mammalian homolog of Ipc (Graybiel 1978; Sherk 1979b; Hall et al. 1989), along with GABAergic neurons medial to PBN that project to SC (Wang et al. 2004; Lee and Hall 2006), mediate the SC activity in a spatially restricted manner (Marin et al. 2007).

In conclusion, our investigation of lateral interaction in turtle Ipc neurons show mixed results. In one case, we find clear suppression in Ipc response due to movement of a second spot while in the other case we have found almost no change in Ipc response when the second spot is introduced. This suggests a possibility of context dependent lateral interaction, which is specific to the locations of two competing stimuli in the visual field. Similar observations are found in birds when the amount of suppression in Ipc changes depending on the location (superior or inferior) of the second stimulus in the visual field (Marin et al. 2007). We have speculated the role of long-rage Imc inhibition creating the framework for the lateral interactions in Ipc. There are also possibilities of tectal and retinal long-rage inhibitions that might contribute to the lateral interaction properties of the Ipc neurons.

6.6 References

Assad JA (2003) Neural coding of behavioral relevance in parietal cortex. Current Opinion in Neurobiology 13: 194-197.

Basso MA, Wurtz RH (1998) Modulation of neuronal activity in superior colliculus by changes in target probability. J Neurosci 18: 7519 –7534.

Boynton GM (2005) Attention and visual perception. Current Opinion in Neurobiology 15: 465-469.

Brandt SF, Wessel R (2007) Winner-take-all selection in a neural system with delayed feedback. Biol Cybernetics 97: 221-228.

Deco G, Pollatos O, Zihl J (2002) The time course of selective visual attention: theory and experiments. Vision Res 42: 2925–2945.

Desimone R, Duncan J (1995) Neural mechanisms of selective visual attention. Annu Rev Neurosci 18: 193-222.

Glimcher PW, Sparks DL (1992) Movement selection in advance of action in the superior colliculus. Nature 355: 542–545.

Graybiel AM (1978) A satellite system of the superior colliculus: the parabigeminal nucleus and its projection to the superficial collicular layers. Brain Res 145: 365-374.

Hall WC, Fitzpatrcik D, Klatt LL, Raczkowski D (1989) Cholinergic innervation of the superior colliculus in the cat. J Comp Neurol 287: 495-514.

Itti L, Koch C (2001) Computational modeling of visual attention. Nature Reviews Neuroscience 2: 194-203.

Kastner S, Ungerleider LG (2000) Mechanisms of visual attention in the human cortex. Annu Rev Neurosci 23: 315-341.

Knudsen EI (2007) Fundamental components of attention. Annu Rev Neurosci 30: 57-78.

Kustov AA, Robinson DL (1996) Shared neural control of attentional shifts and eye movements. Nature 384: 74 –77.

Lee P, Hall WC (2006) An *in vitro* study of horizontal connections in the intermediate layer of the superior colliculus. J Neurosci 26: 4763– 4768.

Marín G, Salas C, Sentis E, Rojas X, Letelier JC, Mpodozis JA (2007) cholinergic gating mechanism controlled by competitive interactions in the optic tectum of the pigeon. J Neurosci 27: 8112-8121.

Maunsell JH, Cook EP (2002) The role of attention in visual processing. Philos Trans R Soc Lond B Biol Sci 357: 1063–1072.

Maunsell JHR, Treue S (2006) Feature-based attention in visual cortex. TINS 29: 317-322.

Motter BC (1998) Inside and outside the focus of attention. Neuron 21: 951-953.

Niebur E, Hsiao SS, Johnson KO (2002) Synchrony: a neuronal mechanism for attentional selection? Current Opinion in Neurobiology 12: 190-194.

Posner MI (1980) Orienting of attention. Q J Exp Psychol 32: 3–25.

Quiroga RQ, Nadasdy Z, Ben-Shaul Y (2004) Unsupervised spike detection and sorting with wavelets and superparamagnetic clustering. Neural Comput 16: 1661-1687.

Reynolds JH, Chelazzi L (2004) Attentional modulation of visual processing. Annu Rev Neurosci 27: 611-647.

Sarter M, Hasselmo ME, Bruno JP, Givens B (2005) Unraveling the attentional functions of cortical cholinergic inputs: interactions between signal-driven and cognitive modulation of signal detection. Brain Res Rev 48: 98-111.

Sereno MI, Ulinski PS (1987) Caudal topographic nucleus isthmi and the rostral nontopographic nucleus isthmi in the turtle, Pseudemys scripta. J Comp Neurology 261: 319-346.

Schroeder CE, Mehta AD, Foxe JJ (2001) Determinants and mechanisms of attentional modulation of neural processing. Frontiers in Biosciences 6: 672-684.

Sherk H (1979b) Connections and visual field mapping in cat's tectoparabigeminal circuit. J Neurophysiol 42: 1656-1668.

Wang Y, Luksch H, Brecha NC, Karten HJ (2006) Columnar projections from the cholinergic nucleus isthmi to the optic tectum in chicks (Gallus gallus): A possible substrate for synchronizing tectal channels. J Comp Neurol 494: 7-35.

Wang Y, Major DE, Karten HJ (2004) Morphology and connections of nucleus isthmi pars magnocellularis in chicks (Gallus gallus). J Comp Neurol 469: 275-297.

Wessel R, Brandt SF, Lai D (2008) The isthmo-tectal feedback loop as a winner-take-all and novelty-detection circuit. SfN Abstract.

Yantis S, Serences JT (2003) Cortical mechanisms of space-based and object-based attentional control. Current Opinion in Neurobiology 13: 187-193.

Chapter 7

OSCILLATORY BURSTING IN TURTLE ISTHMIC NEURONS IN RESPONSE TO VISUAL STIMULATION

7.1 Abstract

Oscillatory bursts (OBs) are repetitive high-frequency neuronal discharges observed in various sensory systems. The long-standing hypotheses of the functional roles of these bursts include reliable signal transfer and stimulus-specific coding. Here, we test some of these hypotheses by investigating the bursting properties of turtle nucleus isthmi pars parvocellularis (Ipc) neurons in response to a wide range of computer-generated visual stimuli. All recordings were made extracellularly from the Ipc neurons in an eye-attached whole-brain preparation while showing visual stimuli in the contralateral eye. We found that oscillatory bursts in Ipc are present for all localized spatiotemporally changing stimuli. However, the amount of OBs compared to isolated spikes, quantified by a burst-index, is highest for small dark moving or flashing spot stimulus. The average interburst interval is shortest for moving spot stimulus and larger for other stimuli. The burst frequency remained roughly constant (160 – 180 Hz) for different stimuli that generated OBs in Ipc. Furthermore, we used the burst-index to quantify differences in bursting responses for a moving spot at different speeds.

7.2 Introduction

Oscillatory bursts (OBs) are frequently observed in neurons of different sensory systems (Llinás and Jahnsen 1982; Steriade et al. 1993; Azouz et al. 1996; Metzner et al. 1998; Ramcharan et al. 2000, Marin et al. 2005). It has been postulated that high frequency bursting plays an important role in information transfer between different stages of sensory systems (Crick 1984). Various investigations have shown that the oscillatory bursts play a significant role in stimulus encoding (Gabbiani et al. 1996; Reinagel et al. 1999; Lesica and Stanley 2004; Oswald et al. 2004), in the communication between neurons (Lisman 1997; Sherman 2001; Izhikevich et al. 2003) and even in generation of epileptic seizure states (McCormick and Contreras 2001).

Oscillatory bursts due to visual stimulations are prominent in neurons in different layers of the avian optic tectum (Knudsen 1982; Neuenschwander and Varela 1993; Neuenschwander et al. 1996). A recent investigation shows that tectal OBs are manifestations of re-entrant signals from nucleus isthmi pars parvocellularis neurons (Ipc), which share reciprocal topographic connections with the optic tectum (Marin et al. 2005). We have observed visual stimulation-triggered repetitive busting discharges in the turtle Ipc neurons (Fig. 7.1), which are similar in both morphology and synaptic connectivity to avian Ipc neurons (Sereno and Ulinski 1987, Wang et al. 2004, 2006). Bursts of cholinergic Ipc neurons play an important role in the generation of large columnar ACh concentrations, which is a dynamic function of the rate of release and the rate of

removal via acetylcholinesterase. A jump in firing rate during a burst leads to a concurring jump in the rate of ACh release in tectum via Ipc axon's paintbrush terminals (Fig. 4.1b, d) and thus resulting in a temporary pulse in columnar ACh concentration. The Ipc oscillatory bursts to visual stimuli and resulting spatially restricted columnar ACh release in tectum is implicated as an attention mechanism in birds (Marin et al. 2005).

Here, we investigate the turtle Ipc neuron's oscillatory burst properties and its relation to visual stimuli. We have recorded extracellular responses from Ipc neurons responding to visual stimulations in an eye-attached whole-brain preparation (Fig. 2.1). Computer-generated visual stimuli, drawn from a large library, are applied to the eye-cup in search for stimulus features that generate oscillatory bursting in the Ipc nucleus. We have found that small moving stimuli or stationary flash; both generate OBs in Ipc neurons (Fig. 7.2). The Ipc neurons responded weakly to whole-field stimulations (see SECTION 5.4.1, Fig. 5.3) and we have found no evidence of bursting in the Ipc responses to these stimuli (Fig. 7.2). Among spatiotemporally changing stimuli, the burst frequency (~200 Hz) approximately remains unchanged but the interburst frequency is found to be higher for small black moving spot stimulus than to other stimuli tested.

7.3 Methods

Extracellular recordings from the Ipc neurons were achieved in an eye-attached whole-brain preparation (see SECTION 2.1, 2.4). 7 adult red-ear turtles

(Trachemys scripta elegans, 12-15 cm carapace length) were used in this study. First, the eye-cup and the stimulation monitor were aligned (see SECTION 2.5.1). The responsive area in the Ipc nucleus was found using a search stimulus (see SECTION 2.5.2) and the stimulation coordinates, which covers about twice the Ipc excitatory receptive field was set (SECTION 2.5.3). The same sets of visual stimuli were used as described in SECTION 5.3.2. The single-unit Ipc responses were extracted using *waveclus*, a spike-sorting algorithm based on spike detection and sorting using wavelets and superparamagnetic clustering (Quiroga et al. 2004). Only single-unit Ipc responses were analyzed in this study.

7.4 Results

A burst was defined as an event that consisted of at least two spikes less than 10 ms apart and occurred after at least 50 ms of inactivity. Similar criterion has been employed in previous studies (Cattaneo et al. 1981; Livingstone et al. 1996; Sillito and Jones 2002). The Ipc neurons responded with oscillatory bursts of spikes (burst frequency, 130 – 270 Hz; interburst frequency, 20 – 8 Hz) in response to a small (diameter 6^{o}) black spot on white background moving through the excitatory receptive field at a speed of 4^{o}/s (Fig. 7.1).

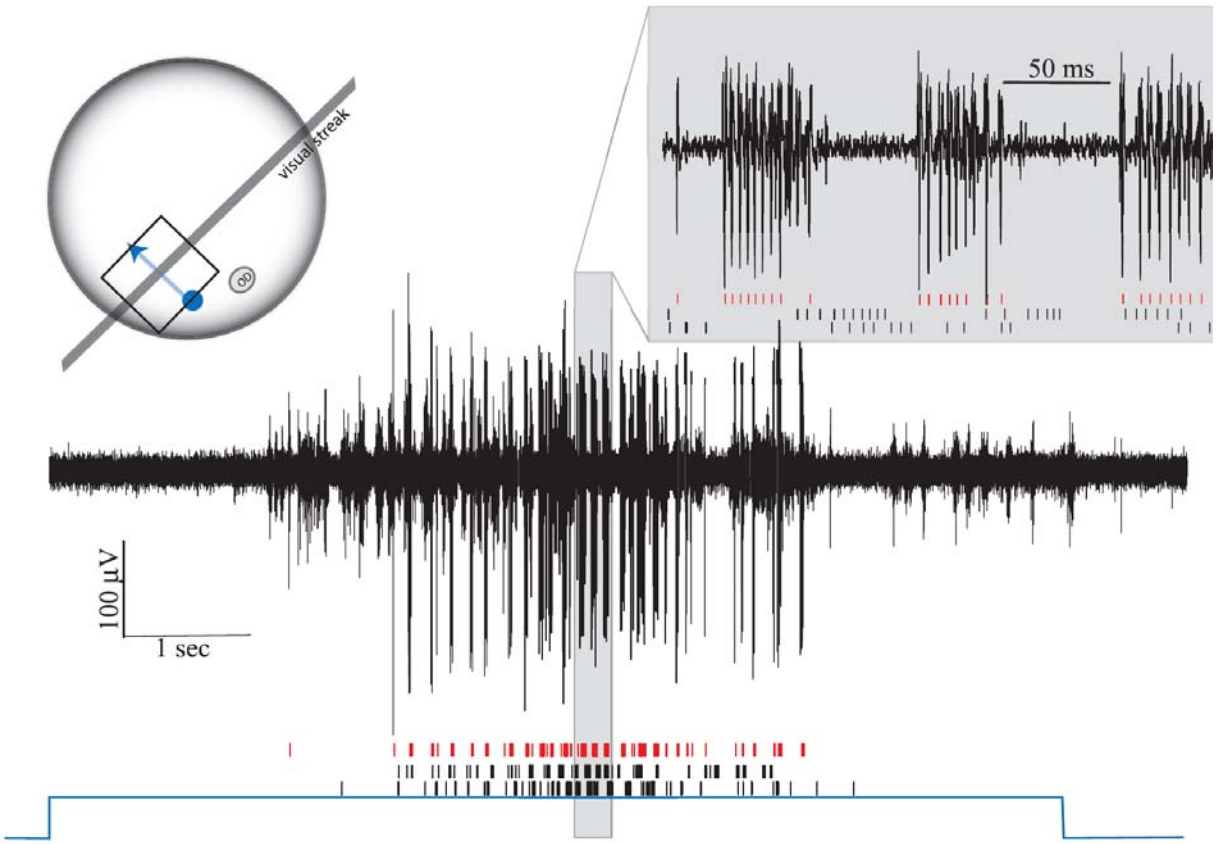

Figure 7.1 lpc oscillatory bursting in response to a black spot (blue in the graph, diameter 6°) on a white background moving (speed 4°/s) perpendicular to the visual streak and through the estimated center of the unit's excitatory receptive field. The black-square stimulation coordinate system represents twice the size of the receptive field. From the raw voltage trace of multiunit recording a single-unit is isolated with a spike-sorting algorithm. The single-unit responses for three repetitions are shown in the raster plots below. The red raster plot corresponds to the raw voltage trace. The blue line below the raster plots indicates 8 s window during which the spot was moving. The response during a short window of

time is enlarged (gray rectangle) for better visualization of the oscillatory bursts.

To quantify the bursting properties of Ipc neurons, we used a burst-index that was defined by the total numbers of spikes in all OBs divided by the total number of spikes (including spikes in bursts) elicited by the stimulation. The burst-index would be 1 if all the Ipc spikes were part of oscillatory bursts and would be 0 if all the spikes were isolated. The change in Ipc bursting properties were investigated using 7 different computer-generated stimuli (see details in SECTION 5.3.2). The same 5 Ipc single-units that were investigated for stimulus selectivity (SECTION 5.4.1) were analyzed for oscillatory bursting properties. Although there were large variation of burst-index from cell to cell and between stimulus classes, we found that the small black stimuli that elicited strong response also generated high OBs (Fig. 7.2). Although the moving spot (or the leading edge) stimulus generated more spiking response than flashing stimuli in Ipc (see Fig. 5.3 and 5.4), noticeably, the burst-indices for some units were relatively higher (Fig. 7.2, green and blue units) for small flashing stimulus than others. The burst-index turned out to be zero for whole-field stimuli, to which The Ipc neuron responded with very few spikes (average spike count; whole screen flash, 2, 0, 2, 5, 0; drifting sine grating, 1, 0, 1, 5, 1).

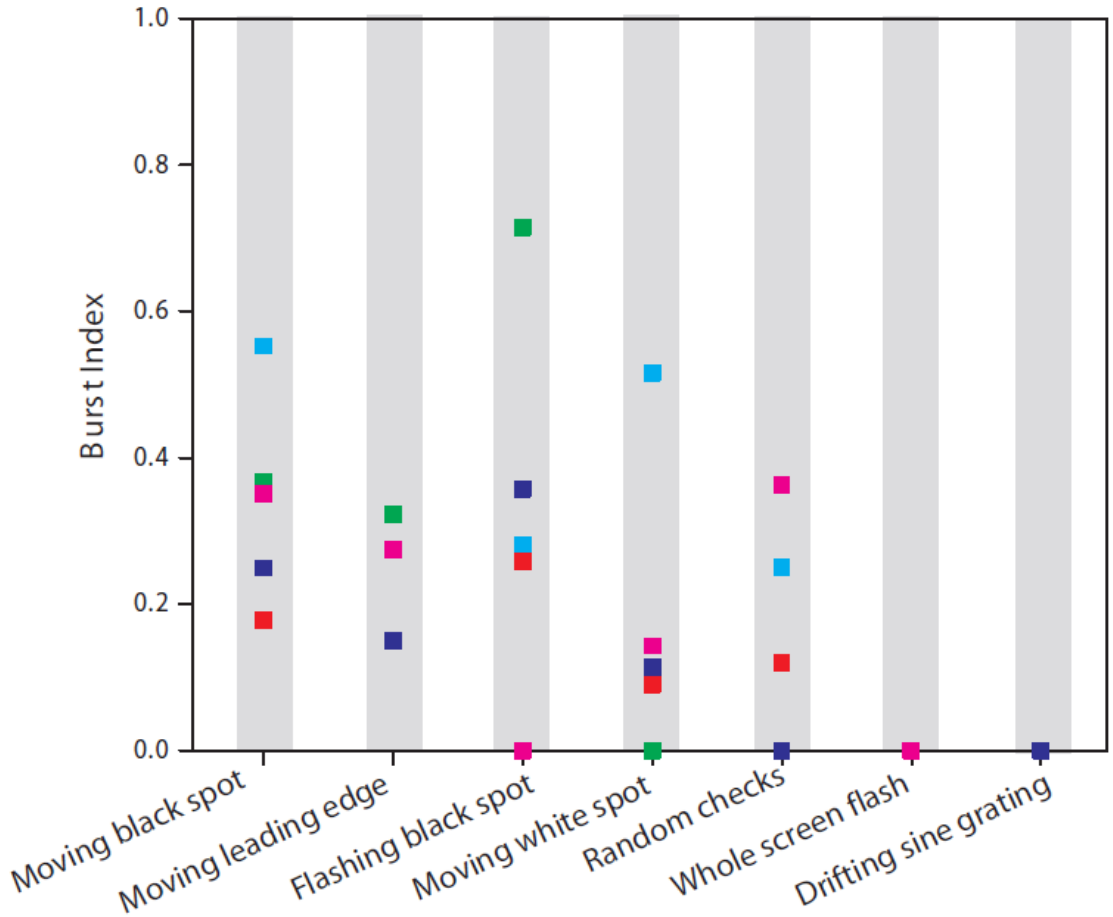

Figure 7.2 Amount of oscillatory bursts (OB) present in the lpc neuron's responses to different visual stimulations. The burst-index for any given stimulus is the ratio of total spikes in all OBs to total spikes generated (including OBs) by the stimulus. The burst-index for the same 5 units as in SECTION 5.4.1(see Fig. 5.3, 5.4) are shown in a column (gray bar) corresponding to each stimulus. Same color coding is used for the units. The cyan unit is not tested for the leading edge stimulus. Notice the large variation in burst-indices for flashing spot, which is partly because of widely different firing rates for different units (see Fig. 5.4). For whole field

stimuli (whole screen flash and drifting sine grating), the burst-index is zero. The burst index for a unit is averaged over 3 trials of each stimulus with some exceptions (trail, stimulus, unit; n = 2, white moving spot, blue and magenta; n = 2, flashing black spot, purple).

The OB frequency and the interburst frequency were investigated for different spatiotemporally changing stimuli (Fig. 7.3). The average interburst interval for a moving spot stimulus was lower (Fig. 7.3a) than other stimuli. For moving spot stimulus the average OB and interburst frequencies were 174 ± 17 Hz and 8 ± 2 Hz (mean ± SD, n = 5), respectively. For other stimuli (Fig. 7.3b, c, d), the interburst frequency was relatively lower (format: stimulus, mean ± SD; moving leading edge, 5 ± 2 Hz; flashing black spot, 6 ± 4 Hz; moving white spot, 4 ± 1 Hz). The burst frequency remained roughly similar for all stimulations (format: stimulus, mean ± SD; moving leading edge, 158 ± 14 Hz; flashing black spot, 185 ± 30 Hz; moving white spot, 170 ± 42 Hz).

The variation of the Ipc burst-index was analyzed for the small moving spot stimulus with different speeds (Fig. 7.4). For one unit (red, Fig. 7.4), the burst-index was lower for the highest speed. However, for another unit the tuning of burst-index to stimulus speed was not readily visible (black, Fig. 7.4).

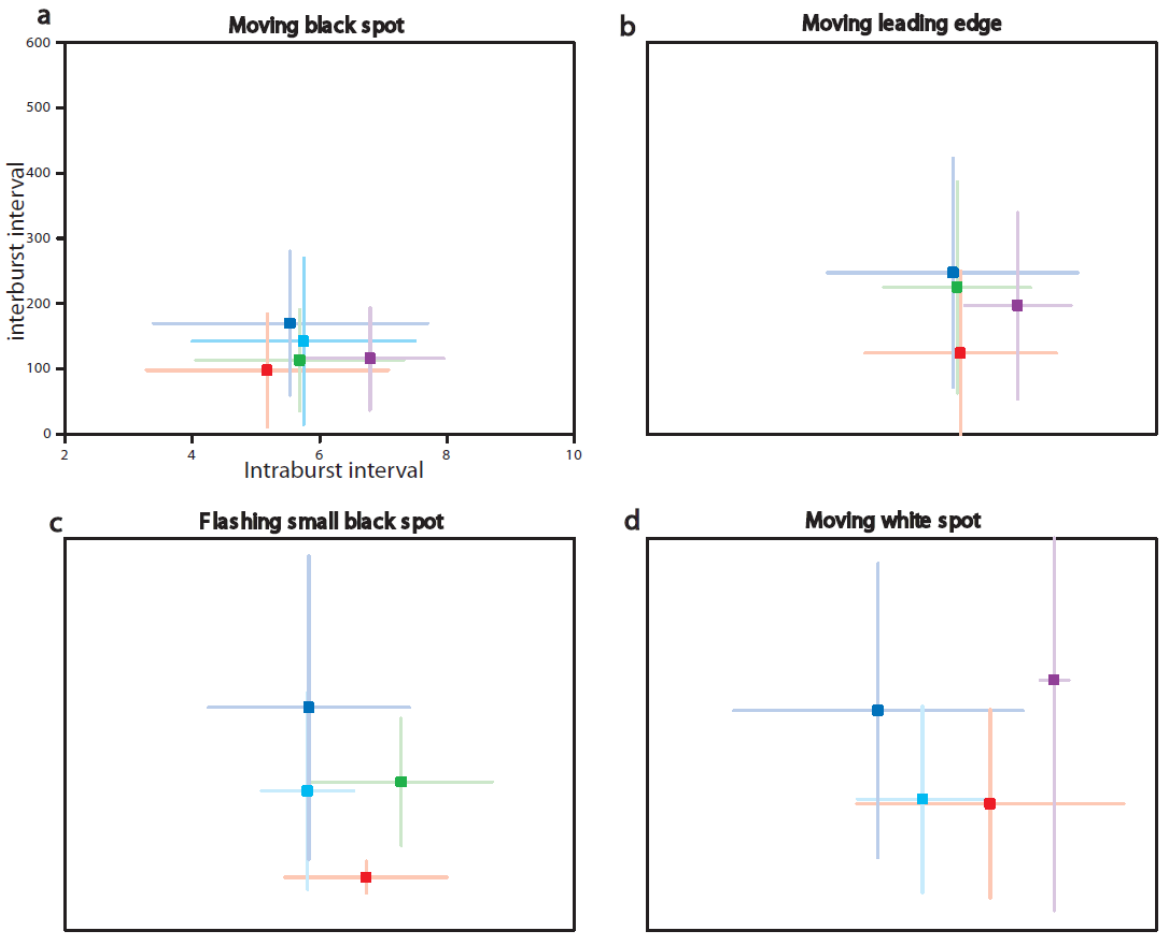

Figure 7.3 The average intraburst and interburst intervals for lpc neurons responding to different visual stimuli. The same units are presented as in Fig. 7.2 (same color coded). Burst is defined as an event that occurs after at least 50 ms of inactivity and contains at least two spikes separated by less than 10 ms. The error bars indicate standard deviations over multiple trials.

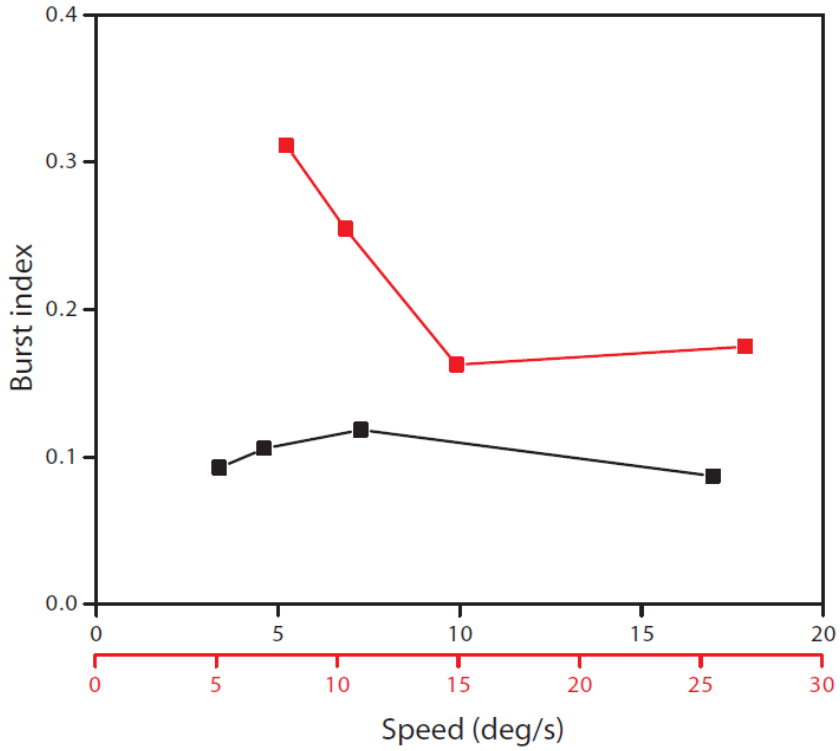

Figure 7.4 Burst-indices in Ipc neurons due to small moving black spot stimulus of different speeds. The two units and their corresponding stimulus speeds are shown in different colors.

7.5 Discussion

We have found that the Ipc neurons respond with oscillatory bursts of spikes to localized spatiotemporally changing stimuli. The burst-index, which represents the amount of OBs present in Ipc response, is the highest for small dark moving or flashing spot stimulus. Whole-field stimulations generate zero bursting response in the Ipc units. The interburst interval is found to be shortest for small moving spot stimulus. The variation of OBs with a stimulus feature is investigated by using different speeds of moving spot stimulus.

The interburst intervals of Ipc OBs correspond to the theta range (4 – 8 Hz) of brain oscillations, which has strong behavioral correlations. The theta-band activity has been implicated to play a role in stimulus encoding and retrieval of working memory (Givens 1996; Rizzuto et al. 2003). Variations of the Ipc bursting properties with stimulus classes (Fig. 7.2) may carry some stimulus-specific information (Cattaneo et al. 1981; Eggermont and Smith 1996; Livingstone et al. 1996). It has been also suggested that the time of burst onset represents the timing of a stimulus feature and the number of spikes in a burst discriminates between different stimulus features (Eyherabide et al. 2009). The Ipc neurons respond with regular spike trains, not bursts, to somatic current injections (see Fig. 3.2a, SECTION 3.4.1). Oscillatory burst generation can be mediated by network mechanisms that typically include delays, and excitatory and inhibitory connections (Traub et al. 2004; Buzsaki 2006). Thus oscillatory bursts in Ipc are likely the result of interactions within the isthmotectal microcircuitry (Shao et al. 2009).

Bursting has also been hypothesized as a possible mechanism of reliable signal transfer between different stages of a network (Allen and Stevens 1994; Thomson 1997; Lisman 1997). In the case of Ipc neurons, the OBs might act as a modulator of tectal neurons by spatially restricted columnar ACh release. It has been found that the cholinergic isthmic activity enhances calcium influx into the optic nerve fiber terminals in frog tectum (Dudkin and Gruberg 2003) and gates the ascending visual pathway to the nucleus rotundus in birds (Marin et al.

2007). Similarly, in turtle, the ACh release by Ipc OBs might also play an important role in the collothalamic visual pathway by modulating tectal broad-field SGC neurons that project to the nucleus rotundus (Reiner 1994; Belekhova et al. 2003).

7.6 References

Allen C, Stevens CF (1994) An evaluation of causes for unreliability of synaptic transmission. Proc. Natl Acad. Sci. USA 91: 10380–10383.

Azouz R, Jensen MS, Yaari Y (1996) Ionic basis for spike after-depolarization and burst generation in adult rat hippocampal CA1 pyramidal cells. J Physiol (Lond.) 492: 211–223.

Belekova M, Kenigfest N, Rio JP, Reperant J, Ward R, Vesselkin N, Karamian O (2003) Tectothalamic visual projections in turtles: Theirs cells of origin revealed by tracing methods. J Comp Neurology 457: 37-56.

Buzsaki G (2006) Rhythms of the brain. Oxford University Press.

Cattaneo A, Maffei L, Morrone C (1981) Patterns in the discharge of simple and complex visual cortical cells. Proc R Soc Lond B 212: 279–297.

Crick F (1984) Function of the thalamic reticular complex: the searchlight hypothesis. Proc Natl Acad Sci USA 81: 4586–4590.

Dudkin EA, Gruberg ER (2003) Nucleus isthmi enhances calcium influx into optic nerve fiber terminals in Rana pipiens. Brain Res 969: 44-52.

Eggermont JJ, Smith GM (1996) Burst-firing sharpens frequency-tuning in primary auditory cortex. Neuroreport 7: 753–757.

Eyherabide HG, Rokem A, Herz AVM, Samengo I (2009) Bursts generate a non-reducible spike-pattern code. Frontiers in Neuroscience 3: 8-14.

Gabbiani F, Metzner W, Wessel R, Koch C (1996) From stimulus encoding to feature extraction in weakly electric fish. Nature 384: 564-567.

Givens B (1996) Stimulus-evoked resetting of the dentate theta rhythm: relation to working memory. NeuroReport 8: 159 –163.

Izhikevich EM, Desai NS, Walcott EC, Hoppensteadt FC (2003) Bursts as a unit of neural information: selective communication via resonance. Trends in Neuroscience 26: 161-167.

Knudsen EI (1982) Auditory and visual maps of space in the optic tectum of the owl. J Neurosci 2: 1177–1194.

Lesica NA, Stanley GB (2004) Encoding of natural scene movies by tonic and burst spikes in the lateral geniculate nucleus. Journal of Neuroscience 24: 10731-10740.

Lisman J (1997) Bursts as a unit of neural information: making unreliable synapses reliable. Trends in Neuroscience 20: 38-43.

Livingstone MS, Freeman DC, Hubel DH (1996). Visual responses in V1 of freely viewing monkeys. Cold Spring Harb. Symp. Quant. Biol. 61: 27–37

Llinás RL, Jahnsen H (1982) Electrophysiology of mammalian thalamic neurons in vitro. Nature 297: 406–408.

Marín G, Salas C, Sentis E, Rojas X, Letelier JC, Mpodozis JA (2007) cholinergic gating mechanism controlled by competitive interactions in the optic tectum of the pigeon. J Neurosci 27: 8112-8121.

Marín G, Mpodozis J, Sentis E, Ossandón T, Letelier JC (2005) Oscillatory bursts in the optic tectum of birds represent re-entrant signals from the nucleus isthmi pars parvocellularis. J Neurosci 25: 7081-7089.

McCormick DA, Contreras D (2001) On the cellular and network bases of epileptic seizures. Annu Rev Physiol 63: 815–846.

Metzner W, Koch C, Wessel R, Gabbiani F (1998) Feature extraction by burst-like spike patterns in multiple sensory maps. J Neurosci 18: 2283–2300.

Neuenschwander S, Varela FJ (1993) Visually triggered neuronal oscillations in the pigeon: an autocorrelation study of tectal activity. Eur J Neurosci 5: 870–881.

Neuenschwander S, Engel AK, Konig P, Singer W, Varela FJ (1996) Synchronization of neuronal responses in the optic tectum of awake pigeons. Vis Neurosci 13: 575–584.

Oswald AM, Chacron MJ, Doiron B, Bastian J, Maler L (2004) Parallel processing of sensory input by bursts and isolated spikes. Journal of Neuroscience 24: 4351-4362.

Quiroga RQ, Nadasdy Z, Ben-Shaul Y (2004) Unsupervised spike detection and sorting with wavelets and superparamagnetic clustering. Neural Comput 16: 1661-1687.

Ramcharan EJ, Cox CL, Zhan XJ, Sherman SM, Gnadt JW (2000) Cellular mechanisms underlying activity patterns in the monkey thalamus during visual behavior. J Neurophysiol 84: 1982–1987.

Reinagel P, Godwin D, Sherman SM, Koch C (1999) Encoding of visual information by LGN bursts. Journal of Neurophysiology 81: 2558-2569.

Reiner A (1994) Laminar distribution of the cells of origin of ascending and descending tectofugal pathways in turtles: implications for the evolution of tectal lamination. Brain Beh Evol 43: 254-292.

Rizzuto DS, Madsen JR, Bromfield EB, Schulze-Bonhage A, Seelig D,Aschenbrenner-Scheibe R, Kahana MJ (2003) Reset of human neocorticaloscillations during a working memory task. Proc Natl Acad Sci USA 100: 7931–7936.

Sereno MI, Ulinski PS (1987) Caudal topographic nucleus isthmi and the rostral nontopographic nucleus isthmi in the turtle, Pseudemys scripta. J Comp Neurology 261: 319-346.

Shao J, Lai D, Meyer U, Luksch H, Wessel R (2009) Generating oscillatory bursts from a network of regular spiking neurons without inhibition. J Comput Neurosci 27: 591-606.

Sherman SM (2001) Tonic and burst firing: dual modes of thalamocortical relay. Trends in Neurosciences 24: 122-126.

Sillito AM, Jones HE (2002) Corticothalamic interactions in the transfer of visual information. Philos Trans R Soc Lond B Biol Sci B 357: 1739–1752.

Steriade M, McCormick DA, Sejnowski TJ (1993) Thalamocortical oscillations in the sleeping and aroused brain. Science 262: 679–685.

Thomson AM (1997) Activity-dependent properties of synaptic transmission at two classes of connections made by rat neocortical pyramidal axons in vitro. J. Physiol. (Lond.) 502: 131–147.

Traub RD, Bibbig A, LeBeau FEN, Buhl EH, Whittington MA (2004) Cellular mechanisms of neuronal population oscillations in the hippocampus in vitro. Annual Review of Neuroscience 27: 247-248.

Wang Y, Luksch H, Brecha NC, Karten HJ (2006) Columnar projections from the cholinergic nucleus isthmi to the optic tectum in chicks (Gallus gallus): A possible substrate for synchronizing tectal channels. J Comp Neurol 494: 7-35.

Wang Y, Major DE, Karten HJ (2004) Morphology and connections of nucleus isthmi pars magnocellularis in chicks (Gallus gallus). J Comp Neurol 469: 275-297.

Chapter 8

OPEN QUESTIONS AND FUTURE DIRECTIONS

8.1 Are the Ipc response properties stimulus-shape specific?

Similar to turtle Ipc neurons, the isthmic neurons in other species respond vigorously to small moving stimuli (Pigeon: Yan and Wang 1986; Wang and Frost 1991; Marin et al. 2005; Li et al. 2007; Marin et al. 2007; owl: Maczko et al. 2006; fish: Gallagher and Northmore 2006). Isthmic neurons also show some stimulus-size, direction and speed tuning (Wang and Frost 1991; Li et al. 2007; Sherk 1979a). However, stimulus shape-specific responses have not been reported before in the Ipc neurons (Fig. 8.1). We have observed changes in Ipc responses when a small moving spot stimulus (Fig. 8.1, left) is replaced by a square-shaped stimulus of the same size and holding all other stimulus parameters constant (Fig. 8.1, right).

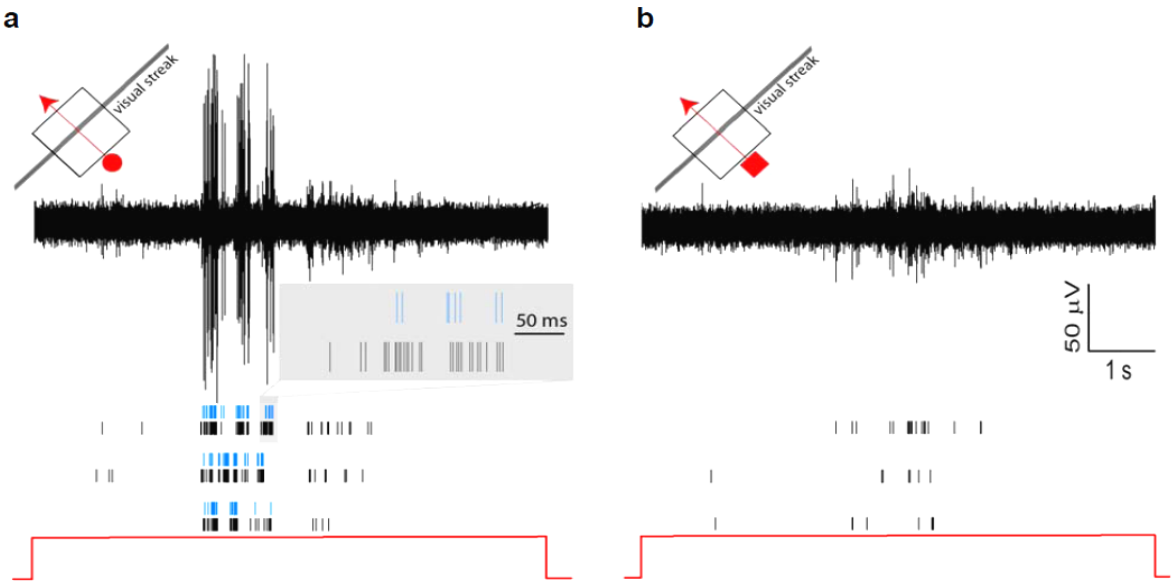

Figure 8.1 The lpc unit's responses to moving stimuli of different shapes. (a) A black spot (6^{o} diameter, red in the graph) moves (4^{o}/s) for 8 s (indicated by the red line below the raster plot) on a white background perpendicular to the visual streak and through the estimated center of the lpc recording site excitatory receptive field. From the raw voltage trace of multiunit recordings, two units were isolated with a spike-sorting algorithm and their spike timing is represented in the raster plot (blue and black). Three trials are shown. The raster plots in blue correspond to the large-amplitude spikes in the recording. Both units respond vigorously to the moving spot. The receptive field for one unit (black) is larger than for the other unit (blue). Since individual spikes can not be seen at this time scale, the raster plot during a short window of time for the first trial is enlarged (gray rectangle) for better visualization of the spikes. Note that the spikes from the two units are not synchronized. (b) When the black spot is replaced by a black square of the same dimension, the unit with the previously large-amplitude spikes (blue) does not respond, whereas the other unit continues to spike at a lower rate. The six trials in (a) and (b) were taken in a pseudo-random order. Neither unit responded to a moving bar (data not shown).

However, in another unit, we have found similar responses elicited by both spot and square stimulus (data not shown). These observations raise possibility of multiple functional communities specific to stimulus feature within the lpc

nucleus. The sophisticated turtle retina (Bowling 1980, Granda 1989) has the ability to send stimulus-specific information to tectum. Interestingly, shape recognition is generally observed in higher visual centers, e.g, V4 cortical area (Pasupathy and Connor 1999, 2001; Arcizet et al. 2009), whereas the broad consensus is that isthmic neurons contribute to spatial attention (Marin et al. 2005).

8.2 Do intracellular recordings reveal dual states of lpc neurons?

We have recorded from several lpc neurons in response to somatic current injections (CHAPTER 3). The resting membrane potential is between -50 to -60 mV and the lpc neurons respond with tonic firing (Fig. 8.2, left). In some cases (n = 5 cells), we have observed sudden change in resting membrane potential from -50 to around -70 mV. The neuron's firing responses are changed at this state and the neurons fire only one or two spikes to somatic current injections (Fig. 8.2, right). This change in firing property generally occurs after 30 – 50 min of patching. However, in some units this change happens only after few minutes of patching. We have also found that the lpc neurons (n = 5) never switch from the hyperpolarized state (Fig. 8.2, State 2) to the tonic-firing state (Fig. 8.2, State 1). This is in contrast to the membrane properties of the striatal spiny neurons and cortical pyramidal cells, which toggle between subthreshold depolarized (Up state) and hyperpolarized (Down state) membrane potential (Steriade et al. 1993; Wilson and Kawaguchi 1996; Stern et al. 1997)

.

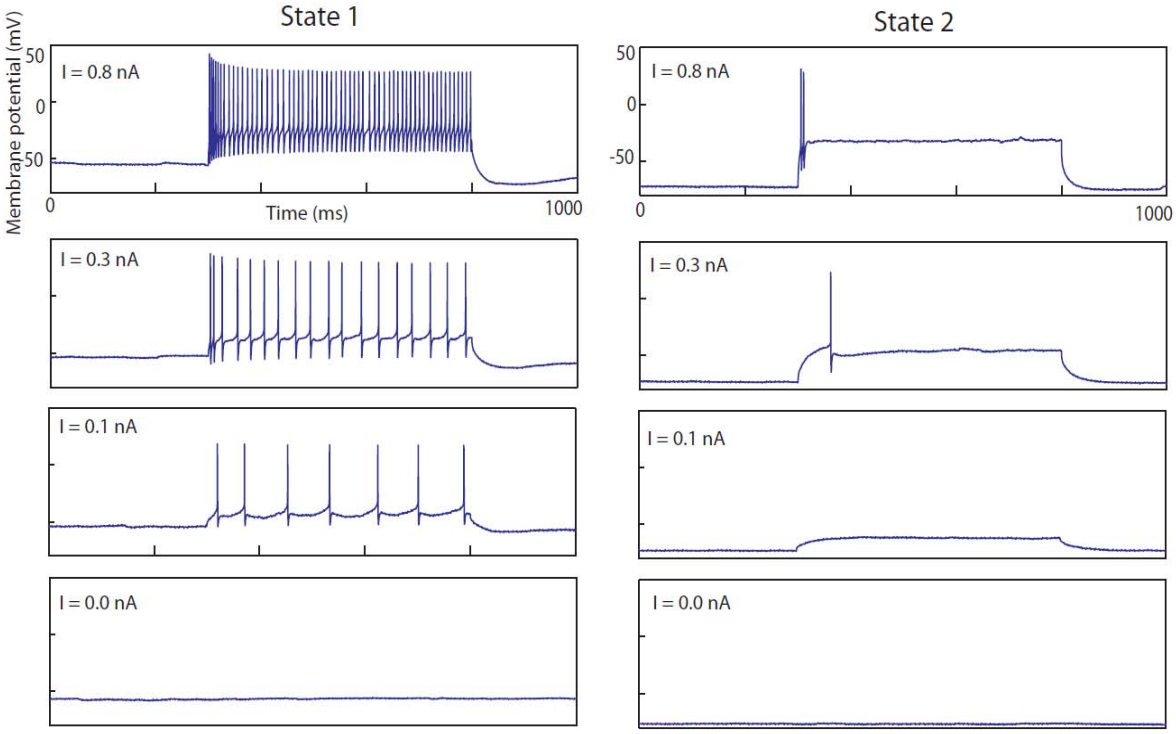

Figure 8.2 lpc neuron's responses to somatic current injections. The current injection starts at 300 ms and ends at 800 ms. The injection current amplitude is mentioned at the top left corner of each plot. Left (State 1), a typical lpc neuron's responses to somatic current injections. The neuron responds with tonic firing with resting membrane potential of about -50 mV. Right (State 2), after a sudden decrease in resting membrane potential to ~ -70 mV, the neuron's responses to similar somatic current injections. The spiking properties are changed and the neuron responds with only one or two spikes to higher current injections.

8.3 Fine structure of the lpc firing profile to small moving stimuli

The lpc neurons sometimes have a characteristic gap in firing pattern (e.g. Fig. 6.2a, c) in response to small moving stimuli. Although this period of inactivity is widely varying (200 – 500 ms), it is higher than the average interburst interval. There are several mechanisms that can generate this period of inactivity. The lpc receptive field may have some patchy structure, which is overlooked in our previous analysis (Fig. 5.5). This effect may also depend on the spatiotemporal structure of the lpc receptive field, which is not investigated in this work. This gap in firing pattern can be generated by the trailing edge of the stimulus. This can also be generated due to adaptation, which is prominent in lpc for flashing stimulus (Fig. 5.4). Systemic investigations are needed to quantify the fine structures of lpc response profile.

8.4 lpc responses to the leading edge stimulus of different sizes

We have investigated the lpc stimulus-size tuning with a black leading edge stimulus. The goal is to eliminate the trailing edge effect in stimulus-size tuning, which might have been introduced by the moving spot stimulus that we studied previously (SECTION 5.4.3, Fig. 5.6). In these experiments, the stimulus is moved along 8 directions through the lpc excitatory receptive field (ERF). All 8 directions produce responses for a smaller width of the edge (7^{o}, Fig. 8.3a) and the responses along all 8 directions are eliminated when the edge width is large (34^{o}, data not shown). However, for an edge of medium width (17^{o}), only first 3-4 directions elicit responses (Fig. 8.3b) while the rest of the directions elicit almost

no response. The lpc response property to the specific width of a leading edge stimulus (8.3b) can not be explained by linear sum of the presumed excitatory center and inhibitory surround structure (Fig. 5.6) of the lpc receptive field. There are evidences that the lpc neurons adapt to static stimuli (Fig. 5.4) but no effects of adaptation are readily visible for more salient stimuli, like, small moving spot. Clearly, adaptation plays a role in the lpc response properties to a leading edge stimulus, but the reason for its prominence to a specific width of the edge remains unclear.

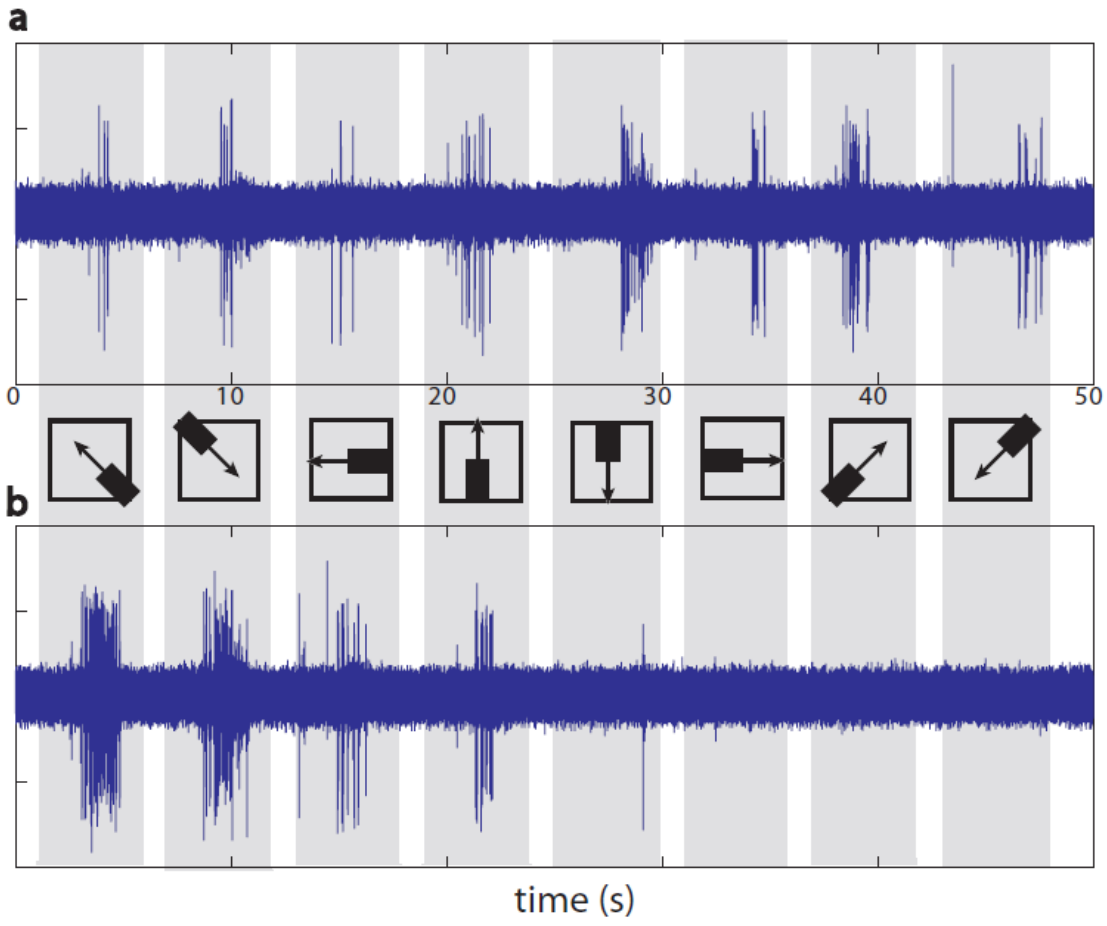

Figure 8.3 The lpc neuron's responses to a leading edge stimulus moving through the lpc ERF along 8 directions 45° apart. The edge starts (at 1s)

outside the lpc ERF and covers about twice the length of the ERF along each direction. The stimulus locations and directions of movement with respect to the stimulation coordinate system (black square, see SECTION 2.5.3) are shown at the middle. The shaded area represents the movement of the leading edge along a direction (5 s) and the white area represents the wait time between changing directions (1s). The directions from left to right are 135^o, 315^o, 180^o, 90^o, 270^o, 0^o, 45^o, and 225^o, respectively. (a) The lpc neuron's response to a leading edge stimulus of 7^o width and moving along 8 different directions through the lpc ERF at the speed of 7^o /s. The unit responds to all 8 directions. (b) The same unit's response to a leading edge of 17^o width. The lpc response abruptly stops after the stimulus movement along first 4 directions. One trial out of three characteristically similar trials for each size of the stimulus is shown.

8.5 Role of lmc neurons in generating lpc response properties

We have not performed intracellular or extracellular recordings from the lmc neurons, which presumably play an important role in generating lpc response properties. The lmc nucleus is a rostrocaudally elongated structure (1000 – 1500 μm long) with loosely grouped neurons (Sereno and Ulinski 1987). This, along with lmc nucleus's location underneath the tectum makes it difficult for blind-patch recordings (Fig. 8.4a). Only a few recordings have been obtained from the lmc neurons and the neurons are labeled using neurobiotin (Fig. 8.4b, result obtained by personal communications with Michael Ariel). To understand the

visual response properties and to explore cellular properties and synaptic connectivities of the Imc neurons, more experiments are needed. The tecto-isthmic fibers pass just medial to Imc nucleus (Sereno and Ulinski 1987) making it difficult to achieve extracellular recordings from the Imc neurons as well. We have tried to pharmacologically inactivate the GABAergic Imc neurons by using bath application of bicuculline (Fig. 4.7c) and intracellular application of picrotoxin (data not shown). Both of these investigations were inconclusive. As it has been shown in recent studies, local inactivation of the Imc neurons (Marin et al. 2005) is a possible way to proceed with the pharmacological manipulations of the Imc neurons.

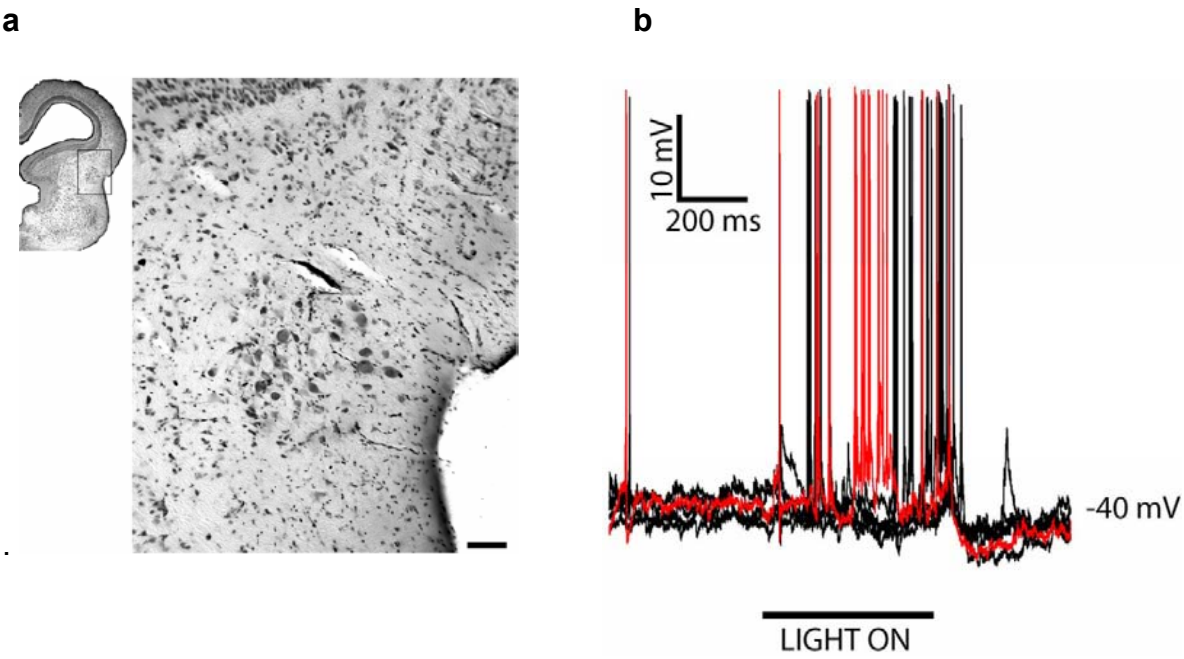

Figure 8.4 Location and response properties of Imc neurons. (a) Transverse section of a cresyl-violet-stained turtle brain. The Imc neurons are of large size (20 – 30 µm wide, 30 – 40 µm long) but are loosely packed (section thickness = 50 µm; scale bar = 100 µm). (b) Visual responses of

Imc neurons to a flash of diffuse whole-field illumination (LIGHT ON) of the contralateral eye-cup. The Imc neuron responded with an irregular sequence of spikes during a 500-ms flash of light. Multiple trials are shown.

8.6 The response properties of the tectal SGP neurons

The response properties of the tectal SGP neurons that project to Ipc and Imc have not been investigated in this study. Although very little is known about the structure of turtle tectum, there is evidence of gap junction between SGP neurons and dendrodendritic connections between SGP radial dendrites in SFGS layer (Schechter and Ulinski 1979). A recent study using voltage sensitive dye shows that the excitation in turtle tectum due to visual stimulation spreads along all directions over a period of about 80 ms (Brown and Ariel 2009). This spatial extent of response is correlated with strength of the stimulus. Similar optical imaging study and recordings using array of electrodes will help understand the role of tectal (SGP) neurons in turtle isthmotectal feedback system.

8.7 References

Arcizet F, Jouffrais C, Girard P (2009) Coding of shape from shading in area V4 of the macaque monkey. BMC Neurosci 10: 140.

Bowling DB (1980) Light responses of ganglion cells in the retina of the turtle. J Physiol 299: 173-196.

Brown ME, Ariel M (2009) Topography of visual responses in the optic tectum of the turtle. SFN abstract.

Gallagher SP, Northmore DP (2006) Responses of the teleostean nucleus isthmi to looming objects and other moving stimuli. Vis Neurosci 23: 209-219.

Granda AM, Fulbrook JE (1989) Classification of turtle retinal ganglion cells. J Neurophysiol 62: 723-737.

Li DP, Xiao Q, Wang SR (2007) Feedforward construction of the receptive field and orientation selectivity of visual neurons in the pigeon. Cereb Cortex 17: 885-893.

Maczko KA, Knudsen PF, Knudsen EI (2006) Auditory and visual space maps in the cholinergic nucleus isthmi pars parvocellularis of the barn owl. J Neurosci 26: 12799-12806.

Marín G, Salas C, Sentis E, Rojas X, Letelier JC, Mpodozis JA (2007) cholinergic gating mechanism controlled by competitive interactions in the optic tectum of the pigeon. J Neurosci 27: 8112-8121.

Marín G, Mpodozis J, Sentis E, Ossandón T, Letelier JC (2005) Oscillatory bursts in the optic tectum of birds represent re-entrant signals from the nucleus isthmi pars parvocellularis. J Neurosci 25: 7081-7089.

Pasupathy A, Connor CE (1999) Responses to contour features in macaque area V4. J Neurophysiol 82: 2490-2502.

Pasupathy A, Connor CE (2001) Shape representation in area V4: position-specific tuning for boundary conformation. J Neurophysiol, 86: 2505-2519.

Schechter Pb, Ulinski PS (1979) Interactions between tectal radial cells in the red-eared turtle, Pseudemys scripta Elegans: An analysis of tectal modules. J Morph 162: 17-36.

Sereno MI, Ulinski PS (1987) Caudal topographic nucleus isthmi and the rostral nontopographic nucleus isthmi in the turtle, Pseudemys scripta. J Comp Neurology 261: 319-346.

Sherk H (1979a) A comparison of visual-response properties in cat's parabigeminal nucleus and superior colliculus. J Neurophysiol 42:1640-1655.

Steriade M, Nunez A, and Amzica F (1993) A novel slow (<1 Hz) oscillation of neocortical neurons in vivo: depolarizing and hyperpolarizing components. J Neurosci 13: 2352–3265.

Stern EA, Kincaid AE, and Wilson CJ (1997) Spontaneous sub-threshold membrane potential fluctuations and action potential variability of rat corticostriatal and striatal neurons in vivo. J Neurophysiol 77: 1697–1715.

Wang YC, Frost BJ (1991) Visual response characteristics of neurons in the nucleus isthmi magnocellularis and nucleus isthmi parvocellularis of pigeons. Exp Brain Res 87: 624-633.

Wilson CJ, Kawaguchi Y (1996) The Origins of Two-State Spontaneous Membrane Potential Fluctuations of Neostriatal Spiny Neurons. J Neurosci 13: 2397-2410.

Yan K, Wang SR (1986) Visual responses of neurons in the avian nucleus isthmi. Neurosci Lett 64: 340-344.